

Declaration

I Usman Rana hereby declare that this thesis titled "Validation of Kinectic Model of Methane Oxidation at High Pressures" is a record of original work carried out by me under the guidance of Dr. Victor P. Zhukov, Jan van Schyndel, M.Sc. and Nikolaos Perakis, M.Sc.

I confirm that:

1. I have written this report without any external help and without the use of documents and aids other than those stated in the references.
2. This work was undertaken as a part of the curriculum to obtain a Master's degree in Aerospace Engineering, TU Munich.
3. There are no conflicts of interest associated with this thesis and that the outcome has not been influenced or altered based on hidden financial support
4. All the sources have been listed.

.....
Date, Sign

Acknowledgements

I would like to thank my supervisors Dr. Victor Zhukov, Nikolaos Perakis and Jan van Schyndel for their great support during this project. I appreciate the efforts and the time they invested in this project. In the last 6 months they were always keen to help me with their ideas, advice and discussions. This project was a great challenge. But thanks to the support from my supervisors, I was able to accomplish it successfully. Furthermore I am also grateful to Jan van Schyndel for his support and the fruitful discussions with him. In the last phase of this project he allowed me to use his computer for the CFD simulations. Otherwise I would not be able to accomplish this project in time. I wish him a very good and successful time for his PhD at DLR. Moreover I am also thankful to my colleague Darith Parikh, who helped me with the software installation on my computer.

Abstract

Within the framework of this thesis the newly developed CH₄/O₂ skeletal reaction mechanism Zhukov & Kong is validated against ignition delay times and premixed laminar flame speeds. Further frequently used reaction mechanisms for CH₄/O₂ combustion are also validated, and the results are compared. This comparison study is conducted using different kinds of reaction mechanisms for instance global chemistry based, skeletal and detailed reaction mechanisms. The reaction mechanisms show a pressure dependency, especially the skeletal and global chemistry based one are optimized for specific conditions (mostly for intermediate pressures and lean mixtures).

Zhukov & Kong delivers good results for ignition delay times, but it is unable to predict the other important validation parameter premixed laminar flame speeds. Zhukov & Kong produces a mean absolute percentage error of around 50 % for predicting laminar flame speeds. Furthermore, it cannot predict the typical profile of laminar flame speed, which increases until the stoichiometric equivalence ratio, and starts decreasing afterwards. Therefore a new skeletal reaction mechanism named NewMechanism is developed using Sensitivity analysis of premixed laminar flame speeds, Zhukov & Kong and RAMEC are used as the parent reaction mechanisms, this new reaction mechanism consists of 53 reactions and 26 species, for pure CH₄/O₂ combustion it can be reduced to 51 reactions and 23 species. NewMechanism is able to predict ignition delay times with a good accuracy for pressures ranging from 15 to 450 atm and equivalence ratio from 0.4 to 6. In case of premixed laminar flame speeds NewMechanism delivers very accurate validation results, which are comparable with the detailed reaction mechanisms C1-C4 Zhukov and RAMEC.

In the last part of this thesis a 2D simplified numerical simulation of LUMEN nozzle is conducted using NewMechanism. The flow is considered as inviscous, therefore turbulence, turbulence-chemistry interaction and boundary layer effects are neglected. Different chemistry models (frozen, equilibrium and finite rate) are applied to investigate the impact of the chemistry on the centerline reactive nozzle flow. All three chemistry models would predict a similar thrust, since the impact of the chemistry on the velocity and pressure is small. On the contrary in case of temperature distribution and the resulting heat flux in the nozzle equilibrium chemistry model would overpredict the temperature and heatflux, while frozen flow would underpredict it. Finite rate chemistry model predicts a temperature, which is between the equilibrium model's temperature and frozen flow's temperature.

Contents

List of figures	VI
List of tables	XI
1. Introduction	1
1.1. Methane, a new rocket fuel	1
1.2. Basics of chemical rocket engines	3
1.3. Thesis motivation	4
2. Theory	7
2.1. Chemical kinetics	7
2.2. Theory of premixed laminar flat flames	12
2.3. Counterflow diffusion flame	16
2.4. Computational fluid dynamics	19
3. Reaction mechanism	21
3.1. Reaction mechanism reduction methods	21
3.2. Thermodynamic data	26
3.3. Transport data	27
4. Ignition and laminar flame speed simulation	30
4.1. Cantera	30
4.2. Ignition simulation	31
4.3. Comparison of multicomponent and mixture-averaged model	34
5. Validation	36
5.1. Validation against ignition delay times	39
5.2. Validation against premixed laminar flame speed	43
6. Development of a new CH₄/O₂ reaction mechanism	47
6.1. Analysis of development process of Zhukov & Kong	47
6.2. Development of NewMechanism	50
6.3. Validation	56
6.4. Verification	63
7. 2D numerical simulation of the LUMEN nozzle	68
7.1. Simulation results	70

8. Conclusion and Outlook	77
A. Identified rate limiting reactions for premixed laminar flame speed	79
B. Comparison of initial and final version of NewMechanism	81
C. Radical induced Ignition	82
D. Influence of thermochemistry data	84
E. Validation results	85
E.1. Validation against ignition delay time	85
E.2. Validation against premixed laminar flame speed	98
F. Verification results	107
G. NewMechanism in CHEMKIN format	109
H. Westbrook & Dryer reaction mechanism in CHEMKIN format	113
I. Nomenclature	114
Bibliography	119

List of Figures

1.1. Specific impulse of various propellant combinations at ideal conditions [1].	2
1.2. Schematic of an ideal rocket engine [2].	3
1.3. Major partners of the SFB/TR-40 project [2].	5
2.1. Response of a reaction at equilibrium to increasing pressure [3].	8
2.2. Temperature dependence of reaction rate of halogen atoms with H ₂ [4].	10
2.3. Pressure-temperature dependency in fall-off region of reaction C ₂ H ₆ → CH ₃ +CH ₃ and experimental values [4].	11
2.4. Typical profile of a premixed busen burner laminar flame [5].	12
2.5. Schematic of counter flow diffusion flame [6].	16
2.6. Schematic diagram of a folded S-shape flame response [7].	18
3.1. Contribution of reactions to formation of species after reaction path analysis [4].	23
3.2. Relative sensitivity coefficients of k_{12} and k_{23} and their influence on formation of product $[S_3]/[S_1]_0$ [4].	25
3.3. Molar constant volume heat capacity dependence on temperature [4].	26
3.4. Thermodynamic data from Kee et al. 1987, Burcat 1984 [4] in polynomial form as used in CHEMKIN.	27
3.5. Data for transport properties from V. P. Zhukov, V. A. Sechenov and A. Yu Starikovskii [8] as used in CHEMKIN.	28
4.1. Schematics of the internal structure of Cantera [9].	30
4.2. Induction time (ignition delay time) in a chain-branching explosion [4].	31
4.3. Schematic of a batch reactor [10].	32
4.4. Temperature over time of stoichiometric compositions of CH ₄ /O ₂ at 1 bar.	32
4.5. Molar fraction of fuel CH ₄ and oxidizer O ₂	33
4.6. Molar fraction of H ₂ O and CO ₂ after ignition.	33
4.7. Autoignition limits of a stoichiometric methane-oxygen mixture.	34
4.8. Comparison of simulation results of premixed laminar flame speeds using different diffusion formulations with experimental values.	35
5.1. Comparison of simulation results of ignition delay time using different versions of Red.Slavinskaya with experimental values.	38
5.2. Comparison of simulation results of premixed laminar flame speeds using different versions of Red.Slavinskaya with experimental values.	38
5.3. Comparison of simulation results using different reaction mechanisms with experimental values at 50 atm.	40

5.4. Comparison of simulation results using different reaction mechanisms with experimental values at 450 atm.	41
5.5. Comparison of simulation results using different reaction mechanisms with experimental values at 170 atm.	41
5.6. Comparison of simulation results using different reaction mechanisms with experimental values at 70 atm.	42
5.7. Predicted premixed laminar flame speed by different reaction mechanisms and its comparison with experimental value at 10 atm	44
5.8. Predicted premixed laminar flame speed by different reaction mechanisms and its comparison with experimental value at 20 atm	44
5.9. Predicted premixed laminar flame speed by different reaction mechanisms and its comparison with experimental value at 40 atm	45
5.10. Predicted premixed laminar flame speed by different reaction mechanisms and its comparison with experimental value at 60 atm	45
6.1. Reactivity of carbon atoms [11].	47
6.2. Origin of Zhukov & Kong.	48
6.3. Maximum temperature profile of several CH ₄ /O ₂ reactions mechanism over mixture fraction at 80 bar.	49
6.4. Development strategy of NewMechanism.	50
6.5. Sensitivity analysis of premixed laminar flame speed at different conditions.	52
6.6. Comparison of predicted premixed laminar flame speed by NewMechanism and Zhukov & Kong with experimental values.	52
6.7. Predicted ignition delay time by the reaction mechanisms NewMechanism and Zhukov & Kong and its comparison with experimental values.	53
6.8. Multi-target reduction strategy applied in the reduction process of NewMechanism	54
6.9. Predicted ignition delay time by the reaction mechanism and its comparison with experimental values.	55
6.10. Predicted premixed laminar flame speed and its comparison with experimental vlaues.	56
6.11. Comparison of simulation results using different reaction mechanisms with experimental values at 100 atm.	59
6.12. Comparison of simulation results using different reaction mechanisms with experimental values at 25 atm from [12].	59
6.13. Predicted premixed laminar flame speed by different reaction mechanisms and its comparison with experimental value at 10 atm	61
6.14. Comparison of simulation results using different reaction mechanisms with experimental values at 60 atm.	62
6.15. Maximum temperature profile over mixture fraction at different scalar dissipation.	64
6.16. Comparison between theoretical equilibrium temperature with temperature profile of different reaction mechanisms at 60 bar over mixture fraction.	65

6.17. CH ₄ mass fraction over mixture fraction at different scalar dissipation [6].	66
6.18. CO ₂ mass fraction over mixture fraction at different scalar dissipation [6].	66
6.19. H ₂ O mass fraction over mixture fraction at different scalar dissipation [6].	67
7.1. Mesh of LUMEN nozzle.	70
7.2. Comparison of impact of different chemistry models on the centerline flow temperature of H ₂ /O ₂ (a) and CH ₄ /O ₂ (b).	71
7.3. CH ₄ /O ₂ flow temperature distribution in the LUMEN nozzle (upper equilibrium and bottom finite rate chemistry).	71
7.4. H ₂ /O ₂ flow temperature distribution in the LUMEN nozzle (upper equilibrium and bottom finite rate chemistry).	72
7.5. Impact of the chemistry model on the centerline pressure, H ₂ /O ₂ (a) and CH ₄ /O ₂ (b).	72
7.6. Impact of the chemistry model on the centerline velocity, H ₂ /O ₂ (a) and CH ₄ /O ₂ (b).	73
7.7. Impact of the chemistry model on the centerline Mach number, H ₂ /O ₂ (a) and CH ₄ /O ₂ (b).	73
7.8. Comparison of predicted centerline temperature by different CH ₄ /O ₂ reaction mechanism, finite rate chemistry model (a), equilibrium chemistry model (b). . .	74
7.9. Predicted centerline temperature by Jones–Lindestedt using finite rate chemistry model.	75
7.10. Predicted mass fraction of major species along the centerline by NewMechanism (a) and Westbrook & Dryer(b).	76
B.1. Comparison of simulation results using different versions of NewMechanism with experimental values at 50 atm.	81
B.2. Comparison of simulation results using different versions of NewMechanism with experimental values at 60 atm.	81
C.1. Massflow of H radical in PSR modified from [10].	82
C.2. Temperature over time of a stoichiometric composition of CH ₄ /O ₂ at 1 bar. . .	82
C.3. Molar fraction of fuel CH ₄ and oxidizer O ₂	83
C.4. Molar fraction of fuel H ₂ O and oxidizer CO ₂	83
D.1. Premixed laminar flame speed simulation using different thermochemistry data and its comparison with experimental data.	84
E.1. Comparison of simulation results using different reaction mechanisms with experimental values at 20 atm ($\phi = 0.5$).	85
E.2. Comparison of simulation results using different reaction mechanisms with experimental values at 50 atm ($\phi = 0.4$).	86
E.3. Comparison of simulation results using different reaction mechanisms with experimental values at 100 atm ($\phi = 0.4$).	87

E.4. Comparison of simulation results using different reaction mechanisms with experimental values at 150 atm($\phi = 0.4$)	88
E.5. Comparison of simulation results using different reaction mechanisms with experimental values at 150 atm ($\phi = 0.5$).	89
E.6. Comparison of simulation results using different reaction mechanisms with experimental values at 450 atm ($\phi = 0.5$).	90
E.7. Comparison of simulation results using different reaction mechanisms with experimental values at 15 atm ($\phi = 6$).	91
E.8. Comparison of simulation results using different reaction mechanisms with experimental values at 25 atm ($\phi = 2$) from [12].	92
E.9. Comparison of simulation results using different reaction mechanisms with experimental values at 40 atm ($\phi = 1$) from [13].	93
E.10. Comparison of simulation results using different reaction mechanisms with experimental values at 40 atm ($\phi = 1.3$) from [14].	94
E.11. Comparison of simulation results using different reaction mechanisms with experimental values at 70 atm ($\phi = 6$).	95
E.12. Comparison of simulation results using different reaction mechanisms with experimental values at 170 atm ($\phi = 3$).	96
E.13. Comparison of simulation results using different reaction mechanisms with experimental values at 260 atm ($\phi = 3$).	97
E.14. Predicted premixed laminar flame speed by different reaction mechanisms and its comparison with experimental value at 5 atm	98
E.15. Predicted premixed laminar flame speed by different reaction mechanisms and its comparison with experimental value at 10 atm from [15]	99
E.16. Predicted premixed laminar flame speed by different reaction mechanisms and its comparison with experimental value at 10 atm from [16]	100
E.17. Predicted premixed laminar flame speed by different reaction mechanisms and its comparison with experimental value at 10 atm	101
E.18. Predicted premixed laminar flame speed by different reaction mechanisms and its comparison with experimental value at 10 atm	102
E.19. Predicted premixed laminar flame speed by different reaction mechanisms and its comparison with experimental value at 20 atm	103
E.20. Predicted premixed laminar flame speed by different reaction mechanisms and its comparison with experimental value at 20 atm	104
E.21. Predicted premixed laminar flame speed by different reaction mechanisms and its comparison with experimental value at 40 atm	105
E.22. Predicted premixed laminar flame speed by different reaction mechanisms and its comparison with experimental value at 60 atm	106
F.1. Comparison between theoretical equilibrium temperature with temperature profile of different reaction mechanisms at 20 bar over mixture fraction.	107

F.2. Comparison between theoretical equilibrium temperature with temperature profile of different reaction mechanisms at 30 bar over mixture fraction.	107
F.3. Comparison between theoretical equilibrium temperature with temperature profile of different reaction mechanisms at 60 bar over mixture fraction.	108
F.4. Comparison between theoretical equilibrium temperature with temperature profile of different reaction mechanisms at 80 bar over mixture fraction.	108

List of Tables

1.1. CH ₄ /O ₂ reaction mechanisms	6
4.1. Deviation of simulation results from the experimental values	35
5.1. Absolute mean percentage error from experimental values of each reaction mechanism.	42
5.2. Absolute mean percentage error from experimental values of each reaction mechanism.	46
6.1. Absolute mean percentage error from experimental values of each reaction mechanism.	60
6.2. Absolute mean percentage error from experimental values of each reaction mechanism.	62
E.1. Absolute mean percentage error from experimental values of each reaction mechanism at 20 atm ($\phi = 0.5$).	85
E.2. Absolute mean percentage error from experimental values of each reaction mechanism at 50 atm ($\phi = 0.4$).	86
E.3. Absolute mean percentage error from experimental values of each reaction mechanism at 100 atm ($\phi = 0.4$).	87
E.4. Absolute mean percentage error from experimental values of each reaction mechanism at 150 atm ($\phi = 0.4$).	88
E.5. Absolute mean percentage error from experimental values of each reaction mechanism at 150 atm ($\phi = 0.5$).	89
E.6. Absolute mean percentage error from experimental values of each reaction mechanism at 450 atm ($\phi = 0.5$).	90
E.7. Absolute mean percentage error from experimental values of each reaction mechanism at 15 atm ($\phi = 6$).	91
E.8. Absolute mean percentage error from experimental values of each reaction mechanism at 25 atm ($\phi = 2$).	92
E.9. Absolute mean percentage error from experimental values of each reaction mechanism at 40 atm ($\phi = 1$) from [13].	93
E.10. Absolute mean percentage error from experimental values of each reaction mechanism atm 40 atm ($\phi = 1.3$).	94
E.11. Absolute mean percentage error from experimental values of each reaction mechanism atm 70 atm ($\phi = 6$).	95

E.12. Absolute mean percentage error from experimental values of each reaction mechanism at 170 atm ($\phi = 3$)	96
E.13. Absolute mean percentage error from experimental values of each reaction mechanism at 260 atm ($\phi = 3$)	97
E.14. Absolute mean percentage error from experimental values of each reaction mechanism at 5 atm.	98
E.15. Absolute mean percentage error from experimental values of each reaction mechanism at 10 atm.	99
E.16. Absolute mean percentage error from experimental values of each reaction mechanism at 10 atm.	100
E.17. Absolute mean percentage error from experimental values of each reaction mechanism at 10 atm.	101
E.18. Absolute mean percentage error from experimental values of each reaction mechanism at 10 atm.	102
E.19. Absolute mean percentage error from experimental values of each reaction mechanism at 20 atm.	103
E.20. Absolute mean percentage error from experimental values of each reaction mechanism at 20 atm.	104
E.21. Absolute mean percentage error from experimental values of each reaction mechanism at 40 atm.	105
E.22. Absolute mean percentage error from experimental values of each reaction mechanism at 60 atm.	106

1. Introduction

1.1. Methane, a new rocket fuel

In chemical rocket engines LOX/LH₂ and LOX/Kerosene (RP-1 or T(S)-1) are the most commonly used propellants. LOX/LH₂ is used in the Vulcain engine of Ariane 5, BE-3 of New Shepard, the first and second stage of Long March 5, while LOX/Kerosene is used in Soyuz, Falcon 9, first and second stage of Long March 6 [17]. Several other propellants, for instance N₂O₄/MMH, LOX/Methanol, LOX/Ethanol are also used in spacecraft engines. LOX/CH₄ is regarded as a top promising future propellant for chemical rocket engine, since methane has several advantages in comparison to commonly used propellants. Methane is a pure hydrocarbon, which is extracted from natural gas. It is non toxic and non corrosive. Furthermore its engineering is well known in pumps and valve industry.

In comparison to high hydrocarbons, the advantages of methane are higher specific impuls, superior cooling properties, low pressure drop in cooling channels, higher availability (LNG), higher coking limits and less soot depositon. Higher coking limits and less soot deposition makes methane especially important for reusable rocket engines [18]. Serveral companies for instance SpaceX, Blue Origin and ArianeGroup are working on reusable rocket engines to cut down the operational and manufacturing costs, which play a significant role in the aerospace industry. SpaceX and Blue Origin have successfully launched reusable rockets for example the first stage of Flacon 9 launcher and New Shepard. ESA is currently working on its reusable rocket engine named ProMetheus. Liquid oxygen/methane will be used in this engine.

Compared to liquid hydrogen fuel despite its lower specific impuls, methane has a higher density and a lower vapor pressure. From the launch vehicle design point of view LOX/CH₄ is much more attractive than LOX/LH₂. For LOX/CH₄ rocket engines smaller tanks can be used as compared to LOX/LH₂ engines, which would allow a simplified engine architecture. Furthermore, LOX/CH₄ are considered to be better suitable for reuse considering the lower stresses in the chamber wall as compared to LOX/LH₂ engines. Considering the turbompumps, LOX/CH₄ engine may allow a single shaft design due to smaller density difference between liquid oxygen and methane. The bulk density is 1141 kg/m³ for liquid oxygen and 830 kg/m³ for liquid methane, while liquid hydrogen has a bulk density of 70 kg/m³. Considering the boiling point, LOX/LH₂ requires a extensive tanks thermal protection, since hydrogen has a boling temperature of only 20 K. In case of LOX/CH₄ a simplified thermal tank protection could be used as result of higher boiling point, which is 110 K for

methane and 90 K for oxygen [19]. Furthermore instead of using helium, which is an expensive gas with a boiling point of 4 K for draining and pressurizing, gaseous nitrogen can be used as a purge gas for methane. Nitrogen starts to freeze under about 63 K at standard pressure, while hydrogen has a boiling point of 20 K. This means nitrogen cannot be used for pressurizing hydrogen, because it would start freezing considering the very low boiling point of hydrogen. On the contrary considering the boiling point of methane (110 K) even gaseous nitrogen (about 77 K) can be used.

In the study conducted by Haidn et al. [1] several commonly used propellants are taken into account, and their ideal specific impulse under vacuum conditions is compared. In Figure 1.1 the results of this study are shown. As previously mentioned, LOX/CH₄ produces higher specific impulse than LOX/Kerosene, but much lower than LOX/LH₂. Considering the mentioned advantages of LOX/CH₄ in comparison to LOX/LH₂, methane is still the more attractive future propellant than hydrogen considering the lower operational costs and reduced pollution of environment on ground (production facilities, test benches, launch sites), despite the lower specific impulse. Methane rocket engines have never flown, but extensive research is going on in many companies and research centers for instance LUMEN project from DLR, ProMetheus from ESA, BE-4 from Blue Origin and Raptor from SpaceX.

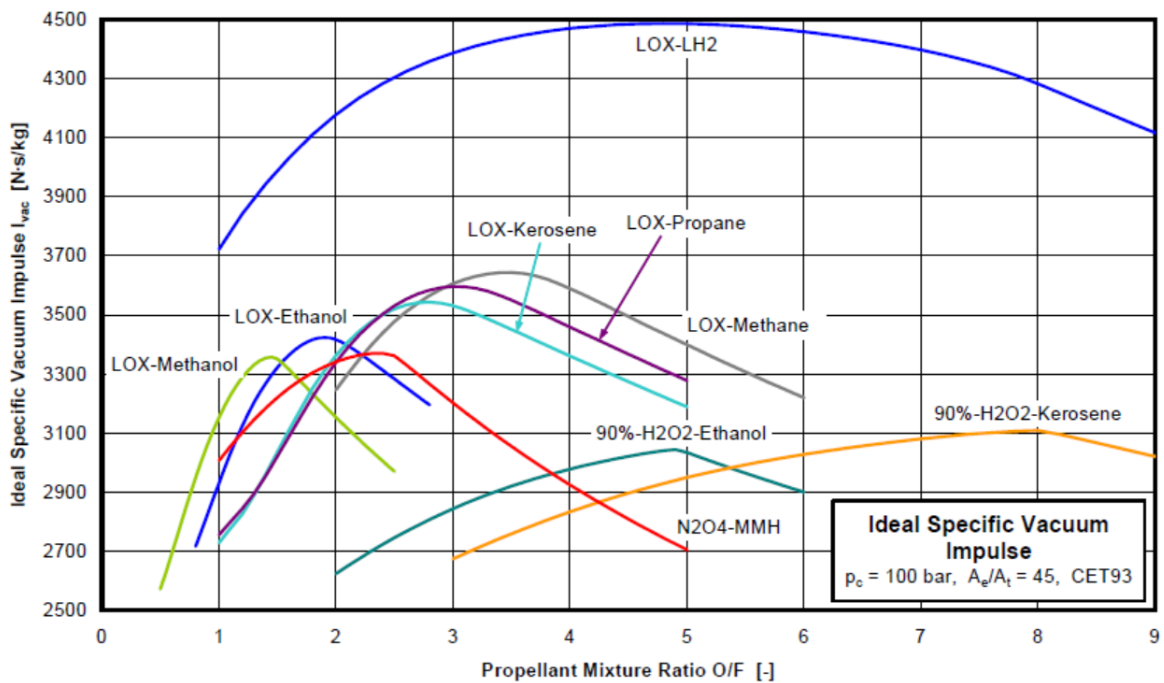


Figure 1.1.: Specific impulse of various propellant combinations at ideal conditions [1].

1.2. Basics of chemical rocket engines

A chemical rocket engine can work with a solid or liquid propellant. Besides this a combination of solid and liquid propellant can also be used. In this kind of rocket engines called hybrid rocket engines a liquid propellant is used mostly as an oxidizer and solid propellant as fuel for instance N₂O/HTPB in SpaceShipOne. In comparison to this, liquid rocket engines use either a mono-propellant or bi-propellant system. Mono-propellant engines use a single chemical as its propellant. It does not require a separate oxidizer. The power for propulsive reaction and resulting thrust is provided by the chemical decomposition of fuel. The needed energy is contained within the chemical bonds of the chemical molecules, which are involved in the reaction. The most commonly used mono-propellant in spacecraft engines is hydrazine. A monopropellant engine is basicly used in low thrust satellite propulsion system. Furthermore a monopropellant engine can also be pressure driven. On the contrary bi-propellant engines use an oxidizer and a fuel for instance LOX/LH₂, LOX/Kersone and LOX/Methane.

Chemical propulsion

In the combustion chamber of a chemical rocket engine internal energy of the propellant molecules is released through chemical reactions. The products of these reactions are accelerated in the nozzle, which results in a very high velocity of the flow in the nozzle. These accelerated gases in the nozzle produce thrust to propell the rocket according to momemtum conservation law [20] . In Figure 1.2 the concept of thrust according to momentum conservation law is illustrated. The rocket thrust Equation 1.1 is derived according to Konstantin Tsiolkovskiy. The subscript ("e") indicates the exit of the nozzle and ("a") the ambient.

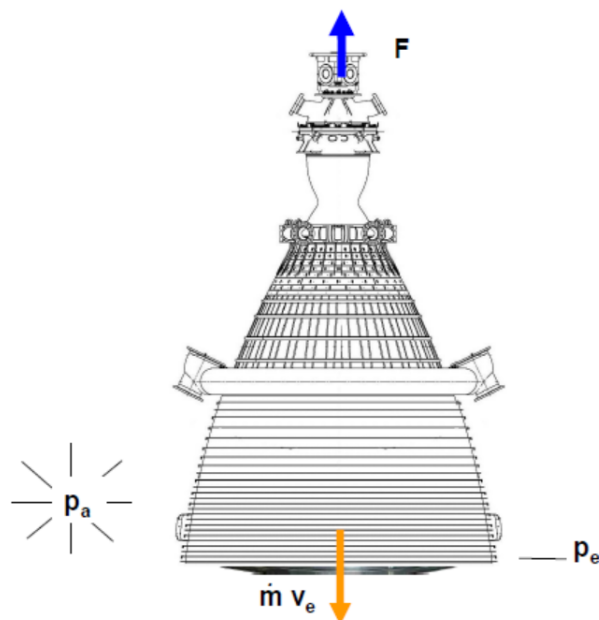


Figure 1.2.: Schematic of an ideal rocket engine [2].

$$F = \dot{m} \cdot v_e + (p_e - p_a)A_e \quad (1.1)$$

Specific impulse I_{sp} is an important parameter, which indicates the efficiency of a rocket engine. An engine with higher value of specific impuls is more efficient, because it produces more thrust for the same mass flow of propellant. Furthermore, it is used to determine the physcial size of an engine during the preliminary analysis. Dividing the thrust required by the specific impulse will indicate how large mass flow of propellants is necessary. The physcial size of engine is determined with this information. Specific impulse is calculated by using Equation 1.2.

$$I_{sp} = \frac{F}{\dot{m} \cdot g_o} = \frac{c_e}{g_o} \quad (1.2)$$

In Equation 1.2, F represents the thrust, \dot{m} the mass flow, g_o acceleartion due to gravity on the surface of earth and c_e the effective exit velocity, which is calculated by using Equation 1.3.

$$c_e = C_F \cdot c^* \quad (1.3)$$

Examining the thrust coefficient C_F and charactersitic velocity c^* in more detail one can get further important information about fluid properties and operational parameters of a rocket engine. The characteristic velocity is determined with Equation 1.4. It relates the combustion chamber pressure p_c to mass flow \dot{m} . Therefore it respresents the energy content of the propellant and the combustion efficiency.

$$c^* = \frac{p_c \cdot A_{th}}{\dot{m}} \quad (1.4)$$

Thrust coefficient C_F is another important coeffcient, which is used to evaluate the performance of a rocket engine. It indicates, how efficient the internal energy is converted into kinetic energy of the gas in the nozzle exit. The thrust coefficient is determined with Equation 1.5.

$$C_F = \frac{F}{p_c \cdot A_{th}} = \frac{F}{\dot{m} \cdot c^*} \quad (1.5)$$

1.3. Thesis motivation

As mentioned in Section 1.1 methane is considered to be a next generation rocket fuel. Hence extensive research is conducted by several companies, universities and resarch institutes to increase the Technology Readiness Level (TRL) of LOX/CH₄ combustion in rocket engines. Within the framework of this thesis the focus is put on the national resarch program Trans-regio SFB/TR-40 "Technological Foundation for the design of thermally and mechanically high loaded components of Future Space Transportation System" [22], which is financed by Deutsche Forschungsgesellschaft (DFG). The major partners of this project are shown in Figure 1.3.



Figure 1.3.: Major partners of the SFB/TR-40 project [2].

Some of the partners are conducting experimental work for instance Technical University of Munich (TUM) with its GOX-GCH₄ single element combustion chamber [23] and seven elements combustion chamber [24], while other contribute to this project through their numerical investigation of these combustion chambers for instance DLR, ArianeGroup, University of Stuttgart, and several others partners, which are shown in Figure 1.3. Further partners joined this project through their numerical work, which are Japan Aerospace Exploration Agency (JAXA) and Centre Européen de Recherche et de Formation Avancée en Calcul Scientifique (CERFACS).

The primary motivation of this thesis is to validate the newly developed reduced CH₄/O₂ reaction mechanism by Zhukov & Kong against a wide range of experiments of ignition delay times and premixed laminar flame speeds. Detailed information about the validation process can be found in Chapter 5. Furthermore other reaction mechanisms, which are either frequently used by the project partners for their numerical investigation or are well known shall also be validated. So that the accuracy of these reaction mechanisms at different conditions ranging from low pressure to high pressure can be compared. Following reaction mechanism (Table 1.1) are selected, which are either used by the project partners or are well known.

Table 1.1.: CH₄/O₂ reaction mechanisms

reaction mechanism	user or (well known)	reactions	species
Aramcomech 1.3 [25]	(well known)	2716	192
C1-C4 Zhukov [26]	(well known)	2329	207
GRI-Mech 3.0 [27]	TU Munich ArianeGroup UniBW CERFAS	325	52
RAMEC [28]	(well known)	190	38
Red.Slavinskaya [29]	DLR Stuttgart TU Munich JAXA	100	24
Zhukov & Kong [30]	DLR-Lampoldshausen	51	24
REDRAM [31]	(well known)	32	24
Tiafeng Lu [32]	TU Munich	73	17
Jones–Lindstedt (Frassoldati) [33]	(well known)	6	9
Westbrook & Dryer (Airbus DS) [34]	ArianeGroup	3	7

The secondary motivation of this thesis is to conduct a preliminary numerical simulation of LUMEN (Liquid Upper stage deMonstrator Engine), which is currently under development at DRL-Lampoldshausen. Within the frame of LUMEN project DLR is investing efforts in experimental and numerical work to obtain experience, so that the inhouse Technology Readiness Levels (TRL) of LOX/CH₄ rocket engines can be increased. Further Information regarding the LUMEN project can be found in [35]. The focus of this preliminary numerical simulation is to investigate the impact of various chemical models (frozen, equilibrium and finite rate) on reactive nozzle flow.

The reaction mechanisms except C1-C4 Zhukov and Aramcomech 1.3 (for higher hydrocarbons) from Table 1.1 are used in the CFD simulations for a further examination after the validation against ignition delay times and laminar flame speeds. Additional CFD simulation of nozzle flow is conducted with fozen, equilibrium and finite rate chemistry using LOX/LH₂ as propellants. The aim is to examine the impact of LOX/LH₂ and LOX/CH₄ chemistry on the nozzle flow.

2. Theory

2.1. Chemical kinetics

The oxidation of methane at temperature of several thousand degrees can be considered as a single stage process (Equation 2.45) with infinitely fast reaction rate. However, at moderate and low temperatures it is necessary to take the kinetics of the process into account, and to use the reaction mechanism for the modeling of methane oxidation.

In a chemical reaction the formation or consumption of species can be described by the rate law. A general form of rate law is given by Equation 2.1. The species A, B, and C represent the reactants of a chemical reaction and D, E, F are its products.



By using Equation 2.2 the consumption of a species for instance B in a chemical reaction can be determined. Here a , b and c denote the reaction order of species A, B and C.

$$\frac{\partial[B]}{\partial t} = -k[A]^a[B]^b[C]^c \quad (2.2)$$

Some chemical reactions are reversible. In this kind of reaction reactants form products that, in turn, react together to give reactants back. A general form of a reversible chemical reaction is given in Equation 2.3. Reversible reactions reach an equilibrium point, where the concentrations of the reactants and products will no longer change. At equilibrium state forward and backward reactions tend to have almost similar rate. As a result no net reaction seems to take place.



The state of equilibrium can be expressed by the so called equilibrium constant K_c , which relates the forward k_f and backward k_r reaction rate of a chemical reaction. K_c equals to one corresponds to the state of equilibrium.

$$K_c = \frac{k_f}{k_r} = \frac{[D]^d [E]^e [F]^f}{[A]^a [B]^b [C]^c} \quad (2.4)$$

The state of equilibrium is influenced by temperature and pressure according to Le Chatelier's principle [3]. It states, that a change in one of the variables, which determine a system at equilibrium, leads to a shift in the position of the equilibrium, that counteracts the effect of this change. In case of increasing temperature, a shift to endothermic direction occurs. On the

contrary, lowering temperature leads to shift of equilibrium to exothermic direction. Detailed information about the response of the equilibrium to temperature can be found in [3], since the topic of this thesis is the kinetics of methane oxidation at high pressures, the focus is put on the sensitivity of equilibrium in respect to pressure.

The response of equilibrium composition to a change in pressure is illustrated in Figure 2.1, where a system consisting of a gas mixture with a monoatomic component B and diatomic component A is compressed from initial stage (a) to stage (b).

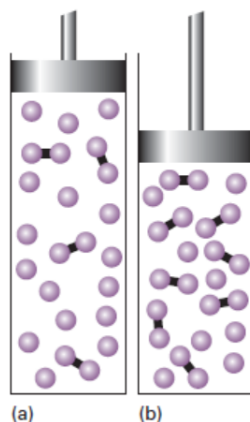


Figure 2.1.: Response of a reaction at equilibrium to increasing pressure [3].

Considering the system as a perfect gas equilibrium $A \rightleftharpoons 2B$ K_c can be expressed by Equation 2.5, where p_B refers to partial pressure of B, p_A to partial pressure of A and p^* to pressure at standard conditions 1 atm. By examining the Equation 2.5 it is evident, that K_c remains only constant, if the increase in p_A can counteract the increase in the square of p_B . Therefore a shift of equilibrium composition in favour of A and at the expense of B is required, which results in increase of number of A (diatomic component) and simultaneously decreasing the number of B (monoatomic component) as illustrated in Equation 2.6.

$$K_c = \frac{p_B^2}{p_A p^*} \quad (2.5)$$

Moreover the dependency of equilibrium composition on pressure can be described quantitatively by Equation 2.6, where α_{dis} denotes the extent of dissociation of A into 2B. It is assumed, that at equilibrium $(1 - \alpha_{dis})n$ is the amount of A and $2\alpha_{dis}$ the amount of B. Although K_c (equilibrium constant) is independent of pressure, but the equilibrium composition shows pressure dependency. According to Equation 2.6 an increase of pressure for instance through compression will result in decrease of α_{dis} , which will lead to higher number A and lower number of B in the system, stage (b) in Figure 2.1.

$$\alpha_{dis} = \left(\frac{1}{1 + 4p/Kp^*} \right)^{1/2} \quad (2.6)$$

Elementary reactions and non-elementary reactions

Elementary reactions occur on a molecular level in the same way, as described by the reaction equation. In the reaction Equation 2.7 an elementary reaction is illustrated, where hydroxyl radical reacts with molecular hydrogen to form H₂O and H directly without any intermediate reactions.



As compared to an elementary reaction, non-elementary reactions do not occur in the same way, as described by the reaction equation. The reaction in Equation 2.8 is a non-elementary reaction, also referred as global reaction or overall reaction. This kind of reaction (Equation 2.8) is composed of several intermediate reactions.



Elementary reactions have a constant reaction order, which is independent of time and of experimental conditions. It can be calculated by taking the molecularity of the reaction into account. There are three different types of molecularity Unimolecular, Bimolecular and Trimolecular. The rate law of Unimolecular reactions is of type first-order. Doubling the concentration of reaction partner A leads to doubling of reaction rate.



Bimolecular reactions have second-order rate law. In case of doubling the concentration of each reaction partner, the reaction rate is increased by factor four.



Trimolecular reactions have third-order rate law.



Generally speaking the order of an elementary reaction is equal to its molecularity. As a result for instance the rate law for the formation of species i in reaction r can be calculated by using Equation 2.12.

$$\left(\frac{\partial c_i}{\partial t} \right)_{\text{chem},r} = k_r (v_{ri}^{(p)} - v_{ri}^{(e)}) \prod_{s=1}^S c_s^{v_{rs}^{(e)}} \quad (2.12)$$

Reaction rate temperature dependency

In most of the cases at higher temperatures chemical reactions proceed faster than at low temperatures. It can be explained by examining the relationship of thermal energy to motion at the molecular level. If the temperature rises, molecules move faster and their collision intensity increases as well. This enhances the probability of bond cleavages and rearrangements as a

result. But some reactions lower their reaction with increasing temperature. The temperature dependency of rate coefficient is expressed by the Arrhenius Equation 2.13 , developed by the Swedish chemist Svante Arrhenius in 1899 [4].

$$k = A' \exp\left(\frac{-E_a'}{RT}\right) \quad (2.13)$$

According to the recent research a temperature dependence of preexponential factor A' is observed, which leads to a modified Arrhenius Equation 2.14

$$k = AT^b \exp\left(\frac{-E_a}{RT}\right) \quad (2.14)$$

In Figure 2.2 the temperature dependence of reaction of halogen atoms with molecular hydrogen is illustrated. The logarithms of the rate coefficients k versus the reciprocal temperature T are shown. As one can see, the reaction coefficient increases with higher temperature.

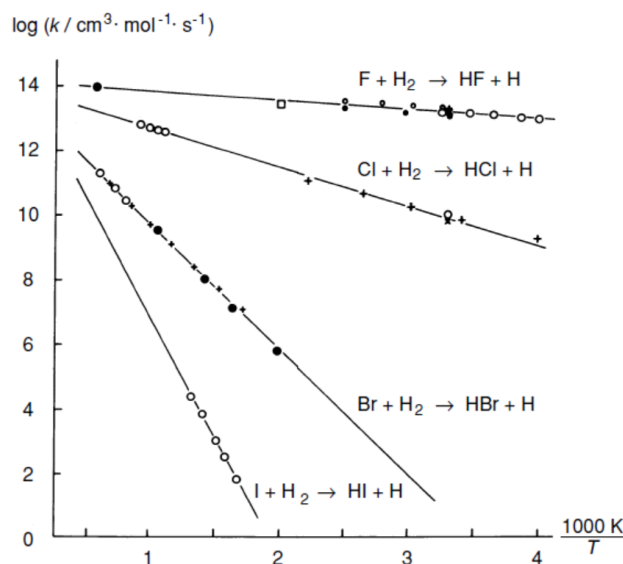


Figure 2.2: Temperature dependence of reaction rate of halogen atoms with H_2 [4].

Pressure dependent reactions

Some reactions show pressure dependency. Gas-phase kinetics delivers expressions, which are used to determine high- and low-pressure limiting reaction rates. The recombination of methyl is used to illustrate this. Under high pressure conditions the recombination reaction of methyl is described by the Equation 2.15, while at low-pressure limit the reaction rate depends on pressure, and it is described by Equation 2.16.



In the so called "fall-off region" a reaction happens at an intermediate state, which is between the high pressure and low pressure limits. For instance, the reaction rate of ethane C_2H_6 decomposition to methyl CH_3 depends on the fall-off region on pressure as well as temperature, as illustrated in Figure 2.3.

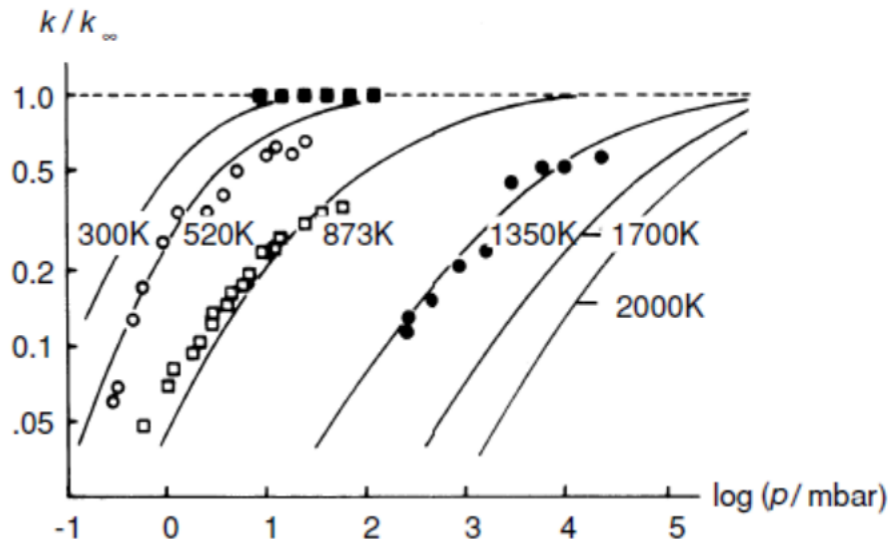


Figure 2.3.: Pressure-temperature dependency in fall-off region of reaction $C_2H_6 \rightarrow CH_3 + CH_3$ and experimental values [4].

The Arrhenius rate parameters k_0 Equation 2.17 is used for low pressure and the reaction rate k_∞ Equation 2.18 is used for high pressures.

$$k_o = A_o T^{b_o} \exp\left(\frac{-E_0}{R_c T}\right) \quad (2.17)$$

$$k_\infty = A_\infty T^{b_\infty} \exp\left(\frac{-E_\infty}{R_c T}\right) \quad (2.18)$$

Considering that the combustion happens at high temperature and pressures, an adequate treatment of reaction rate pressure dependency is very important. Different approaches are available to describe the reaction rate k in the fall-off region. One of the simplest methods is the Lindemann approach. It uses the Arrhenius rate parameters for the high pressure reaction rate (k_∞ Equation 2.18), the low pressure reaction rate (k_0 Equation 2.17) and relates them in a pressure-dependent rate expression (k Equation 2.19) [4].

$$k = k_\infty \left(\frac{p_r}{1 + p_r} \right) F \quad (2.19)$$

$$p_r = \frac{k_o[M]}{k_\infty} \quad (2.20)$$

In Equation 2.19 p_r denotes the reduced pressure, which depends on the concentration of the mixture $[M]$, containing the increased third-body efficiencies. If F from Equation 2.19 is one, this leads to the Lindemann form, otherwise F is described by Troe method, as follows.

$$F_{cent} = a \cdot \exp\left(\frac{T}{T_*}\right) + \exp\left(\frac{T}{T_{**}}\right) + (1-a) \cdot \exp\left(\frac{T}{T_{***}}\right) \quad (2.21)$$

$$\log F = \log F_{center} \left[1 + \left(\frac{\log p_r + c}{n - d \cdot (\log p_r + c)} \right)^2 \right]^{-1} \quad (2.22)$$

with $c = -0.4 - 0.67 \log F_{cent}$, $n = 0.75 - 1.27 \log F_{cent}$, $d = 0.14$

2.2. Theory of premixed laminar flat flames

A premixed laminar flame is self-sustaining propagation of a localized combustion zone typically at subsonic velocities due to molecular transport. Premixed laminar flames are described by their characteristic velocity, which is controlled by the diffusion of heat and active radicals. This characteristic laminar flame velocity will be used as a validation parameter of the reaction mechanisms in Chapter 5. A typical profile of a premixed busen burner laminar flame is shown in Figure 2.4.



Figure 2.4.: Typical profile of a premixed busen burner laminar flame [5].

Premixed laminar flames can be described sufficiently at each point in space and time by pressure, density, temperature, velocity of the flow, and concentration of each species. Convection, chemical reaction, molecular transport and radiation lead to spatial and temporal changes of fluid properties. These changes are mathematically described by the so called conservation equations. The general form of one-dimensional conservation equation is given by Equation 2.23. In this equation W denotes the density of the conserved variable, J the flux density of the conserved variable and Q a source or sink of the conserved variable. According to the conservation law a particular measurable property of a overall isolated physical system does not change as the system evolves over time. These properties are energy, mass and momentum. Conservation law is described through conservation equations such as continuity, energy and

momentum. Considering the assumption that the pressure is constant in this mathematical model of premixed laminar flat flame, description of momentum conservation equation is not necessary, since its change is negligible [4].

$$\frac{\partial W}{\partial t} + \frac{\partial J}{\partial z} = Q \quad (2.23)$$

Mass conservation

In an isolated physical system the conservation of mass of a mixture is given by the continuity Equation 2.24. In the notation used here, ρ represents the total mass density and ρv describes the flow flux. Since chemical reactions cannot create or destroy mass the source or sink term Q becomes zero.

$$\frac{\partial \rho}{\partial t} + \frac{\partial(\rho v)}{\partial z} = 0 \quad (2.24)$$

Conservation of species mass

In Equation 2.53 W from the general form of one-dimensional conservation equation is substituted by the partial density ρ_i of species i , the flux J is described by using the product of the partial density and the mass velocity v_i of the species. In comparison to the continuity Equation 2.24 this equation has a source term, since chemical reactions form or consume species i .

$$\frac{\partial \rho w_i}{\partial t} + \frac{\partial(\rho w_i v_i)}{\partial z} = M_i \frac{\partial c_i}{\partial t} \quad (2.25)$$

with

$$w_i = \frac{\rho_i}{\rho} \quad (2.26)$$

The mass velocity of v_i of the species i is determined by Equation 2.27. Where v represents the mean mass velocity of the center of mass of the mixture and V_i the diffusion velocity caused by molecular transport due to concentration gradients of the species i .

$$v_i = v + V_i \quad (2.27)$$

The diffusion velocity V_i can be calculated by Equation 2.28, where the symbol j_i denotes the diffusion flux of species i in the center of mass system.

$$V_i = \frac{j_i}{\rho_i} \quad (2.28)$$

Enthalpy conservation

The conservation of enthalpy of a mixture can be described by Equation 2.29. Here h_j represents the specific enthalpy of the species j , j_q a heat flux, which is caused by temperature gradients and thus leads to energy transport. The first and second term of Equation 2.29 denote the change of enthalpy h_j due to the flow of species. The transient form of enthalpy conversation is

given by Equation 2.30

$$\sum_j \frac{\partial(\rho v w_j h_j)}{\partial z} + \sum_j \frac{\partial(\rho V_j w_j h_j)}{\partial z} + \frac{\partial j_q}{\partial z} + \sum_j \frac{\partial(\rho w_j h_j)}{\partial t} = 0 \quad (2.29)$$

$$\rho v \sum_j w_j \frac{\partial h_j}{\partial z} + \rho \sum_j w_j \frac{\partial h_j}{\partial t} + \sum_j h_j r_j + \sum_j j_j \frac{\partial h_j}{\partial z} + \frac{\partial j_q}{\partial z} = 0 \quad (2.30)$$

The theoretical model of laminar premixed flat flame is still needs a closure. Further assumptions have to be made. As previously mentioned the temperature, pressure, the velocity, the partial densities or overall density and the independent mass fractions of the species have to be determined to describe the laminar premixed flat flame. By taking into account, that the pressure is assumed to be constant, the density can be calculated by using the ideal gas law Equation 2.31 with known temperature, pressure and mixture composition.

$$p = \rho \frac{R}{M} T \quad (2.31)$$

The velocity is determined with Equation 2.32. It is assumed that there are no temporal changes and thus the flame is stationary.

$$\frac{\partial(\rho v)}{\partial z} = 0 \quad (2.32)$$

In combination with the constraint that the mass fractions sum to unity, then the mass fractions w_i can be calculated by using Equation 2.53. The temperature is calculated with energy conservation equation by inserting heat flux j_q Equation 2.33.

$$j_q = -\lambda \frac{\partial T}{\partial z} \quad (2.33)$$

This leads to the following form of energy conservation Equation 2.34.

$$\rho c_p \frac{\partial T}{\partial t} = \frac{\partial}{\partial z} (\lambda \frac{\partial T}{\partial z}) - (\rho v c_p + \sum_j j_j c_{p,j}) \frac{\partial T}{\partial z} - \sum_j h_j r_j \quad (2.34)$$

Now the mathematical description of laminar premixed is complete and all the required equations are available, which are solved using numerical methods. Further details about numerical methods for solving partial differential equations can be found in [4].

Zeldovich's model of thermal propagation of flames

In Section 2.2 a mathematical model of laminar premixed flame is introduced. This model consists of partial differential equations, which are derived from conservation law of energy, mass and species. The solution of this problem can be only obtained with numerical methods. By making further simplifications of this model an analytical solution is possible, which is described by the model of thermal flame propagation by Zeldovich and Frank-Kamenetskii [64]. Following assumptions are made in this model [4].

1. one-step global reaction with first-order reaction rate as shown in Equation 2.35
2. constant thermal conductivity, heat capacity, product of the density and the diffusion coefficient ρD
3. neglecting the temperature change by different diffusion velocities of species with different specific heat capacities
4. Lewis number Le (Equation 2.36) is approximately unity.



$$Le = \frac{D}{\alpha} \quad (2.36)$$

These assumptions lead to simplification of species conservation Equation 2.53 and energy conversation Equation 2.34. Subsequently a simple differential equation system is obtained, as follows.

$$D \frac{\partial^2 w_F}{\partial z^2} - v \frac{\partial w_F}{\partial z} - w_F A \exp\left(-\frac{E}{RT}\right) = 0 \quad (2.37)$$

$$\frac{\lambda}{\rho c_p} \frac{\partial^2 T}{\partial z^2} - v \frac{\partial T}{\partial z} + w_F \frac{h_p - h_F}{c_p} A \exp\left(-\frac{E}{RT}\right) = 0 \quad (2.38)$$

Experimental data of premixed laminar flame allows further simplification, that the mass diffusivity D and thermal diffusivity $\lambda/\rho c_p$ are almost equal. After substituting the enthalpy by temperature via Equation 2.39, the species conservation Equation 2.37 and energy conservation Equation 2.38 can be replaced by Equation 2.40, which is valid for determining the mass fraction and temperature.

$$\delta = T_b - T = \left[\frac{(h_p - h_F)}{c_p} \right] w_F \quad (2.39)$$

$$\alpha \frac{\partial^2 \delta}{\partial z^2} - v \frac{\partial \delta}{\partial z} - \delta A \exp\left[-\frac{E}{R(T_b - \delta)}\right] = 0 \quad (2.40)$$

The analytical solution of Equation 2.40 is only possible, if v has a eigenvalue, which is designated as flame velocity v_L .

$$v_L = \sqrt{\frac{\alpha}{\tau}} \quad (2.41)$$

In Equation 2.41 τ denotes the charachteristic time of reation and α thermal diffusivity. According to the simplifications made in this model mass and thermal diffusion are the same. An analysis of Zedovich model shows, that the laminar flame velocity depends on the diffusivity and the chemical reaction timescale [4]. This leads to the assumption, that the chemical reactions create necessary gradients for the diffusive processes, which influences as a result the flame propagation.

2.3. Counterflow diffusion flame

In counterflow diffusion flame an oxidizer inlet and fuel inlet are located opposite to each other as illustrated in Figure 2.5. The oxidizer and fuel jet are decelerated at a stagnation plane, where they interact with each other. The location of the stagnation plane varies according to the mass flux of both fluid streams. The chemical reactions, which occur as a result of interaction between the oxidizer and fuel, lead to a stationary flame. The location of the flame does not have to be the same as the location of the stagnation plane.

The mixture fraction is a major variable used in the combustion modeling, especially in diffusion flames. Under a certain set of simplifying assumptions used in the non-premixed modeling approach the instantaneous thermochemical state of the fluids is related to a conserved scalar quantity known as the mixture fraction Z , which can be calculated using Equation 2.42, assuming equal diffusion coefficients for all species [65], where Z_i represents the elemental mass fraction for element i , $Z_{i,ox}$ the mass fraction at the oxidizer inlet and $Z_{i,fuel}$ the mass fraction at the fuel inlet.

$$Z = \frac{Z_i - Z_{i,ox}}{Z_{i,fuel} - Z_{i,ox}} \quad (2.42)$$

In case of combustion modeling of hydrocarbons the mixture fraction is determined by Equation 2.43 according to Bilge [67].

$$Z = \frac{\frac{Z_C}{mM_C} + \frac{Z_H}{nM_H} + \frac{2(Y_{O_2,ox} - Z_O)}{v_{O_2}M_{O_2}}}{\frac{Z_{C,fu}}{mM_C} + \frac{Z_{H,fu}}{nM_H} + \frac{2Y_{O_2,ox}}{v_{O_2}M_{O_2}}} \quad (2.43)$$

Where v_{O_2} represents the stoichiometric coefficient of oxygen with hydrocarbon in the one step chemical reaction according to Equation 2.44.

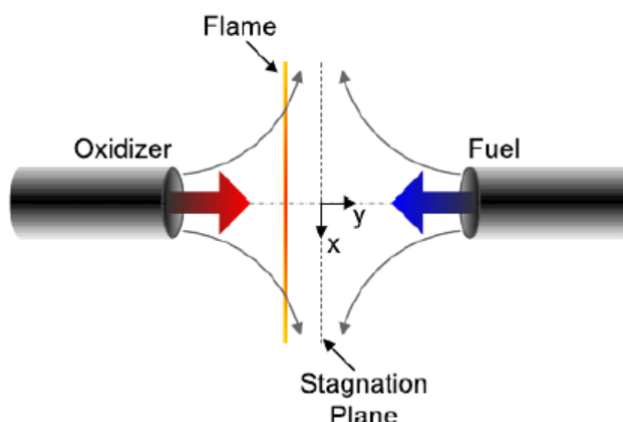


Figure 2.5.: Schematic of counter flow diffusion flame [6].

Combustion can be fuel-lean, fuel-rich or stoichiometric. In case of stoichiometric combustion the fuel and oxygen ratio is such, that all the fuel and all the oxygen is consumed in the combustion process to form the products, as shown in global methane-oxygen reaction (Equation 2.45). In the combustion process another parameter namely the equivalence ratio ϕ (Equation 2.46) is used to describe the ratio between the fuel and the oxidizer. This ratio is weighted against the stoichiometric ratio, to find out, whether the used mixture is lean, rich or stoichiometric. Equivalence ratio greater than 1 refers to rich mixture, smaller than 1 to lean mixture and equal to 1 to stoichiometric mixture.



$$\phi = \frac{\frac{X_{\text{fuel}}}{X_{\text{O}_2}}}{\frac{X_{\text{fuel,stoich}}}{X_{\text{O}_2,\text{stoich}}}} \quad (2.46)$$

Due to their geometrical simplicity, fundamental flame behavior and burning properties counterflow diffusion flames have been extensively studied under different flow and boundary conditions. A S-curve illustrates the relationship between flame temperature and Damkoehler number (Da) or any other variable, which measures the strength of external flow stretching for instance strain rate α (Equation 2.48) or scalar dissipation rate χ (Equation 2.49). Here the Damkoehler number represents the ratio of flow time scale to chemical time scale (Equation 2.47).

$$Da = \frac{\tau_f}{\tau_c} \quad (2.47)$$

As illustrated in Figure 2.6 a S-curve captures all the possible steady chemical states, which a reacting mixture is able to achieve. Furthermore, it shows the response of a reacting chemical state to changes in the local aerothermal condition in a flame zone. The S-curve characterizes the evolution of a flame in respect of continually varying flow conditions, which include ignition, extinction and instability. The chemical reaction rate increases with Damkoehler number along the weakly reacting flow branch. After reaching a certain Damkoehler number (Da_{ing}) ignition occurs, as result of heat generation exceedence over heat loss in a steady state. The flame temperature increases rapidly to the upper branch values. In case of decreasing Damkoehler number along the upper branch the flame gets extinguished at Da_{ext} . A unphysical behaviour occurs along the unstable middle branch, where the flame temperature decreases with increasing Damkoehler number. Such kind of unphysical behaviour exists only in the theory, therefore it is very unlikely to occur in most practical systems. Different counterflow diffusion flames are characterized by a variable named strain rate α . The inverse of strain rate represents the characteristic flow time (diffusion time). Several definitions are available in literature [68] [69] [70] for strain rate for instance mean strain rate, which refers to mean axial velocity gradient, maximum strain rate, which is the maximum axial velocity gradient and strain rate at stoichiometry, indicating the axial velocity gradient at stoichiometric point.

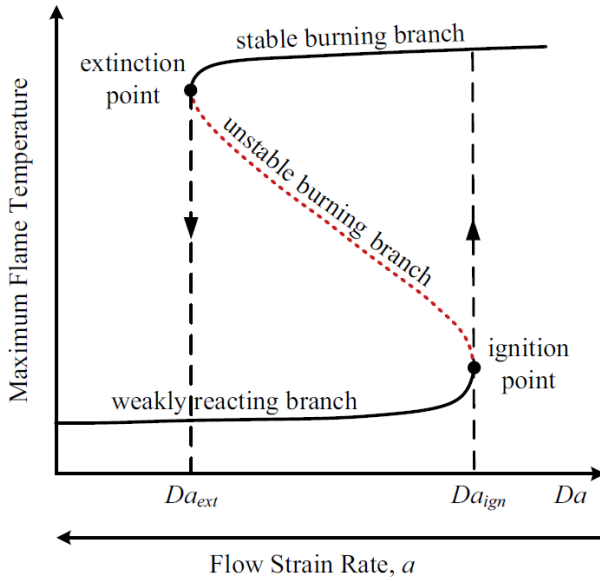


Figure 2.6.: Schematic diagram of a folded S-shape flame response [7].

The definition of strain rate at stoichiometry is used in this thesis (Equation 2.48). At higher strain rate chemical reactions can not occur fast enough to maintain a sufficient pool of reactive species against the flow of incoming reactants. This will lead to extinction of the flame as illustrated in Figure 2.6. The maximum temperature of the flame decreases slowly along the stable burning branch, as the strain rate increases. From a certain value of strain rate a drastic decrease of temperature occurs. This leads to the extinction of the flame, since chemical reactions are unable to produce enough heat to maintain the flame.

$$\alpha_{stoichiometric} = \left| \frac{\partial u}{\partial z} \right|_{\phi=1} \quad (2.48)$$

In counterflow diffusion flames, the mixture fraction Z equals to 0 at the oxidizer jet and 1 at the fuel jet. In this type of diffusion flames the species mass fraction and temperature along the axis can be converted from the physical space to mixture fraction space, since both of them can be uniquely described by the mixture fraction and the strain rate. By doing this the chemistry can be reduced and adequately described by the mixture fraction Z and strain rate α . The simplification of the chemistry allows the implementation of complex reaction mechanisms in combustion modeling, especially for the CH_4/O_2 combustion, where the reaction mechanisms can consist of hundreds or even thousands of reactions, for instance RAMEC (190 reactions and 38 species) from Petersen et al. [71] or $\text{C}_1\text{-}\text{C}_4$ reaction mechanism (2329 reactions and 207 species) from Zhukov et al. [26].

One of the major application of counterflow diffusion flames is the generation of flamelet tables, for further use in flamelet combustion model. In contrast to turbulent finite rate combustion model, non-equilibrium and finite rate effects are modeled without solving the mass fraction of the chemical species, which will result in high computational time. The departure from equilibrium is described by the variable scalar dissipation χ , which is proportional to

strain rate (Equation 2.49), where Z_{st} represents the stoichiometric mixture fraction and erf^{-1} the inverse complementary error function. A value of scalar dissipation χ equals to 0, refers to equilibrium and greater than 0 indicates the departure from equilibrium. The turbulent effects are captured with the variance of the mixture fraction Z''^2 . Only two further equations (mixture fraction Z and its variance Z''^2) are solved in flamelet combustion model instead of solving the equation of each species. A detailed description of flamelet and turbulent combustion model is out of the scope of this thesis. Further information regarding turbulent combustion modeling and flamelet model can be found in [66], [4].

$$\chi = \frac{\alpha \exp(-2[\text{erf}^{-1}(2Z_{st})]^2)}{\pi} \quad (2.49)$$

2.4. Computational fluid dynamics

Computational fluid dynamics (CFD) is used to analyze a system involving fluid flow, heat transfer and associated phenomena for instance chemical reactions. It is well known, that all flowing fluids obey the three laws of conservation. As a result the behaviour of a flow can be described by the Navier–Stokes equations [72].

1. Conservation of mass (Equation 2.50)
2. Conservation of momentum (Equation 2.51)
3. Conservation of energy (Equation 2.52)
4. Conservation of species mass (Equation 2.53)

$$\frac{\partial \rho}{\partial t} + \nabla \cdot (\rho, \vec{u}) = 0 \quad (2.50)$$

$$\frac{\partial \vec{u}}{\partial t} + \vec{u}(\vec{\nabla} \cdot \vec{u}) = \frac{1}{\rho} \sum_n \vec{F}_n \quad (2.51)$$

$$\frac{\partial(\rho E)}{\partial t} + \nabla(\vec{u}(\rho E + p)) = -\nabla(\sum_j h_j J_j) + S_h \quad (2.52)$$

$$\rho \frac{\partial Y_i}{\partial t} + \rho \vec{u} \cdot \nabla Y_i = \nabla \cdot (\rho D_i \nabla Y_i) + S_i \quad (2.53)$$

The Navier–Stokes equations are solved numerically using computers in a CFD simulation, since an analytical solution is not possible. There are several codes (commercial, open source and in-house), which are able to perform CFD simulations such as ANSYS Fluent, ANSYS CFX, OpenFOAM, TAU and Rocflam3. The methodology used in the most CFD approaches is, as follows

1. Definition of physical domain (geometry).
2. Division of the volume occupied by the fluid into discrete cells (mesh).

3. Selection of physical models such as radiation, reactions, multiphase flows and turbulence models.
4. Definition of boundary conditions (e.g inlet, outlet and wall) for solving the conservation equations.
5. Specifying the numerical procedures for instance selection of a discretization schemes e.g upwing schemes.
6. Selection of solution algorithm for example coupled vs. segregated solver.
7. Post processing (visualization and analysis of results).

Detailed information regarding the physical models and numerical procedures can be found in [72]. The Navier–Stokes equations are used to describe laminar and turbulent flows. For a flow at very high velocity for instance in a rocket nozzle viscous forces can be neglected, which results in description of the flow through Euler equations instead of Navier–Stockes equations. Through this simplification the flow can be treated as an inviscid flow and therefore no turbulence modeling is required [72]. In Chapter 7 a 2D CFD simulation of the LUMEN nozzle is conducted assuming inviscid flow, which is adequate description of the centerline flow. Since the wall region area and the capture of boundary layer is not the focus of this thesis.

3. Reaction mechanism

The combustion process of the propellants hydrogen and oxygen ($2\text{H}_2 + \text{O}_2 \rightarrow 2\text{H}_2\text{O}$) can be described by approximately 40 elementary reactions [4]. Petersen et al. [73] proposed a 18-step, 9-species mechanism for hydrogen-oxygen combustion, which produces satisfactory results for ignition delay time from 1 to 600 atm (1 atm = 1.01325 bar). Even further reduced hydrogen-oxygen reaction mechanisms exist for example the 8-step mechanism of Evans and Schexnayde [74]. But their application is limited to very high temperatures and low pressures, because several significant elementary reactions are not included in such over simplified reaction mechanisms [73]. Considering the 8-step mechanism of Evans and Schexnayder missing reactions with HO_2 or H_2O_2 in this mechanism could lead to unsatisfactory results at high pressures [73].

In case of hydrocarbons up to several thousand elementary reactions are required in the detailed chemical reaction mechanism for instance C1-C4 Zhukov [26]. In case of narrowing the range of conditions for instance high pressures and pure methane-oxygen mixtures, such detailed reaction mechanism (C1-C4 Zhukov) become strongly overdetermined. Therefore a detailed reaction mechanism can be reduced to reaction mechanism, which is customized for the required conditions.

3.1. Reaction mechanism reduction methods

Several methods can be applied to reduce a large chemical kinetics mechanism. Three of the mostly used reduction methods are as following.

1. global modeling
2. response modeling
3. detailed reduction

Several researchers use global modeling method to reduce detailed reaction mechanisms for instance Jones and Lindstedt [75], Hautman et al. [76] and Peters and Rogg [77]. In this method a quasi-steady partial equilibrium is assumed for reducing a detailed reaction mechanism. This leads to one, two, or more steps, which now represent algebraic combination of most significant steps and no longer the elementary reactions.

In the response modeling approach the full mechanism is tested for a wide range of temperatures, pressures, mixture ratios in order to examine the response of a specific selected parameter for instance ignition delay times. As a result a mathematical expression, which includes the response variable as a function of the parameter space replaces the full mechanism in the numerical flow solver. This leads to a massive reduction of the computation time. This method is used by Oran et al. [82] and Clifford et al. [83].

A full mechanism is reduced in the detailed reduction approach by neglecting reactions and species, which have minor influence on the selected variable. In comparison to the response modeling approach the elementary reaction format of full mechanism is not changed in the reduced mechanism. This kind of reduced mechanism is called as skeletal mechanism. This approach is used by Zhukov and Kong [30], Frenklach et al. [85], Wang et al. [86], and Yungster et al. [87]. Reaction path analysis and Sensitivity analysis are the most commonly used methods in the detailed reduction approach. These methods are used to eliminate unimportant reactions to obtain a simplified reaction mechanism.

Reaction path analysis

In reaction path analysis important reactions paths can be identified. A threshold value of net element flux is typically defined and only reactions, which contribute at this threshold value to the formation or consumption of the chemical species are included in the reduced reaction mechanism. A reaction mechanism consisting of reactions $r(r=1,\dots,R)$ and species $s(s=1,\dots,S)$ is taken into account for a brief explanation of reaction path analysis. Detailed explanation can be found in [4].

As shown in Figure 3.1 different reactions will contribute to different extent to the formation of the species. If species 1 is considered to be an important one, then reaction $R-1$ will have the biggest impact on the formation of species 1, while the reactions 2,3 and R have negligible influence and therefore these reactions can be removed from the reactions mechanism, if the defined threshold value for the species formation is greater than 5%. On the contrary reaction 3 has the greatest impact on the formation of species $S-1$ (100%) and S (90%). Therefore if species $S-1$ and S are also considered to be important, then reaction 3 can not be removed, where reactions 2 and R do not contribute to the defined threshold value of 5% to the formation of any species. As a result the reaction mechanism can be simplified by removing the reactions 2 and R .

Reaction ↓	Species ⇒					
	1	2	3	S-1	S
1	20%	3%	0	0	0
2	0	0	0	0	0
3	2%	5%	0	100%	90%
.
.
.
R-1	78%	90%	100%	0	5%
R	0	2%	0	0	0

Figure 3.1.: Contribution of reactions to formation of species after reaction path analysis [4].

Sensitivity analysis

After narrowing the application conditions for example to high pressures, several reactions in a detailed reaction mechanism become negligible, since they have minor influence on the parameter of interest, which can be ignition delay times, premixed laminar flame speeds or the concentration of specific species. These negligible reactions are called non rate-limiting reactions. Sensitivity analysis is applied to determine those non rate-limiting reaction to simplify a reaction mechanism. This method is used in this thesis to develope a updated version of the reaction mechanism Zhukov & Kong. Therefore it is dicussed in detail using an example of impact of specific reactions on the concentration of selected species.

The rate laws for a chemical reaction mechanism composed of R reactions with S species can be described by Equation 3.1a in form of first order ordinary differential equation [4].

$$\frac{\partial c_i}{\partial t} = F_i(c_1, \dots, c_s; k_1, \dots, k_R) \quad (3.1a)$$

$$i = 1, 2, \dots, s \quad (3.1b)$$

Where k is the parameter of the system, representing rate coefficients of the chemical reactions, c_i is the concentration of species i and a dependent variable, while the time t is an independent variable. The solution of Equation 3.1a depends on the initial conditions and on the parameters of the system k . So how does the soultion of Equation 3.1a change in respect to a change in the system parameter k , here as rate coefficent of the chemical reaction? To answer this question, one has to know, that a large chemical reaction mechanism consists of hundreds or even thousands of elementary reactions, some of them have almost no effect on time dependent solution of Equation 3.1a. This type of elemantary reactions are called non-rate limiting reactions, while the elementary reactions with a greater influence on the solution of Equation 3.1a are called as rate-limiting reactions. Therefore even if non-rate limiting reactions are included in the reaction

mechanism, their rate coefficient does not have to be very accurate. As a result experimental resources can be concentrated on determining an accurate rate of such elementary reaction with a greater influence on the rate law Equation 3.1a (concentration of a specific species). The dependence of solution of Equation 3.1a on the system parameter k is called sensitivity. There are two types of sensitivity, relative sensitivity Equation 3.3 and absolute sensitivity Equation 3.2.

$$E_{i,r} = \frac{\partial c_i}{\partial k_r} \quad (3.2)$$

$$E_{i,r}^{rel} = \frac{k_r}{c_i} \frac{\partial c_i}{\partial k_r} = \frac{\partial \ln c_i}{\partial \ln k_r} \quad (3.3)$$

The following two step reaction mechanism (Equation 3.4) will be examined using sensitivity analysis to determine the impact of rate coefficients k_{12} and k_{23} on the rate of formation of the final product S_3 of the reaction sequence.



with the rate laws for the species (concentration) S_1 , S_2 and S_3

$$\frac{\partial [S_1]}{\partial t} = -k_{12}[S_1] \quad (3.5)$$

$$\frac{\partial [S_2]}{\partial t} = k_{12}[S_1] - k_{23}[S_2] \quad (3.6)$$

$$\frac{\partial [S_3]}{\partial t} = k_{23}[S_2] \quad (3.7)$$

An analytic solution of Equation 3.5 - Equation 3.7 can be obtained by assuming, that only the compound S_1 is present at the initial time ($t=0$).

$$[S_1] = [S_1]_o \exp(-k_{12}t) \quad (3.8)$$

$$[S_2] = [S_1]_o \frac{k_{12}}{k_{12} - k_{23}} [\exp(-k_{23}t) - \exp(-k_{12}t)] \quad (3.9)$$

$$[S_3] = [S_1]_o \left[1 - \frac{k_{12}}{k_{12} - k_{23}} \exp(-k_{23}t) + \frac{k_{23}}{k_{12} - k_{23}} \exp(-k_{12}t) \right] \quad (3.10)$$

Now the sensitivity coefficients can be determined by forming the partial derivative of S_3 in Equation 3.10, assuming constant time.

$$E_{S_3,k_{12}}(t) = \frac{\partial [S_3]}{\partial k_{12}} = [S_1]_o \frac{k_{23}}{(k_{12} - k_{23})^2} [(k_{23}t - k_{12}t - 1) \exp(-k_{12}t) + \exp(-k_{23}t)] \quad (3.11)$$

$$E_{S_3,k_{23}}(t) = \frac{\partial [S_3]}{\partial k_{23}} = [S_1]_o \frac{k_{12}}{(k_{12} - k_{23})^2} [\exp(-k_{12}t) + (k_{12}t - k_{23}t - 1) \exp(-k_{23}t)] \quad (3.12)$$

The relative sensitivity coefficients ($\frac{\partial [S_3]}{\partial k_{12}}$ to $\frac{k_{12}}{[S_3]}$) can be calculated with Equation 3.13 and Equation 3.14.

$$E_{S_3,k_{12}}^{\text{rel}}(t) = \frac{k_{12}}{[S_3]} E_{S_3,k_{12}}(t) \quad (3.13)$$

$$E_{S_3,k_{23}}^{\text{rel}}(t) = \frac{k_{23}}{[S_3]} E_{S_3,k_{23}}(t) \quad (3.14)$$

In Figure 3.2 the time behavoir of relative sensitivity coefficients and the demensionless form of concentration of the final product S_3 is illustrated. As one can see, the reaction 23 has neglegible impact on the the formation of S_3 . Since its relative sensitivity coefficient $E_{S_3,k_{23}}^{\text{rel}}$ tends to zero immediately. On the other hand the slow reaction 12 ($E_{S_3,k_{12}}^{\text{rel}}$) has a greater influence on the formation of S_3 , which means, that the reaction 12 can be considered as a rate-limiting. Because the formation rate of S_3 is highly sensitive in respect to reaction 12. Sensitivity analysis is a powerful tool to determine, whether a reaction is significant for the selected parameter (such as ignition delay time or flame speed) or if it can be neglected, since it has no influence on the overall process.

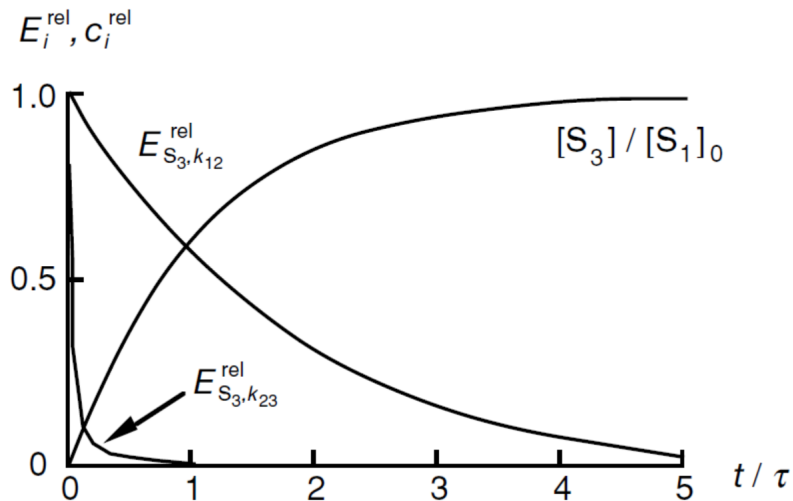


Figure 3.2.: Relative sensitivity coefficients of k_{12} and k_{23} and their influence on formation of product $[S_3]/[S_1]_0$ [4].

For instance in a combustion process some reactions are too fast and their influence on the overall combustion process is negligible. Such reactions can be found by the sensitivity analysis. These reactions with a minor effect on the combustion process can be removed from the detailed reaction mechanism to decrease the computational time of numerical simulation (CFD). Several software packages are available, which can be used for a sensitivity analysis such as CHEMKIN, Cantera or FlameMaster. Cantera is used in this study, since it is a open source software tool and it allows a greater flexibility than the commercial software for instance CHEMKIN. Cantera requires besides the reaction mechanism file in .inp format also a thermodynamic data and a transport data file of the species to create a reaction mechanism file in the cantera format .cti , which can be used to solve several chemical kinetics problems such as autoignition time, laminar flame speed, counter flow diffusion flame simulations. A brief

description of Cantera will be given in Section 4.1.

3.2. Thermodynamic data

Thermodynamics properties of species for instance specific heat capacity, enthalpy and entropie are computed as a function of temperature. In Figure 3.3 the temperature dependence of molar heat capacities of species H, H₂, N₂ and H₂O is illustrated. In the lower temperature range (e.g below 50 K) only translation degrees of freedom are active for the monoatomic, diatomic and polyatomic species. The translational excitation leads to a molar heat capacity of about 3/2 R for all three types of species. At higher temperature (50 - 150 K) further degree of freedom (rotation) are activated for diatomic and polyatomic species, which increases the molar heat capacities of diatomic and polyatomic species to 5/2. A continuous increase in temperature results in 7/2 R (diatomic species) caused by vibrational excitation for instance for H₂O up to about 300K .

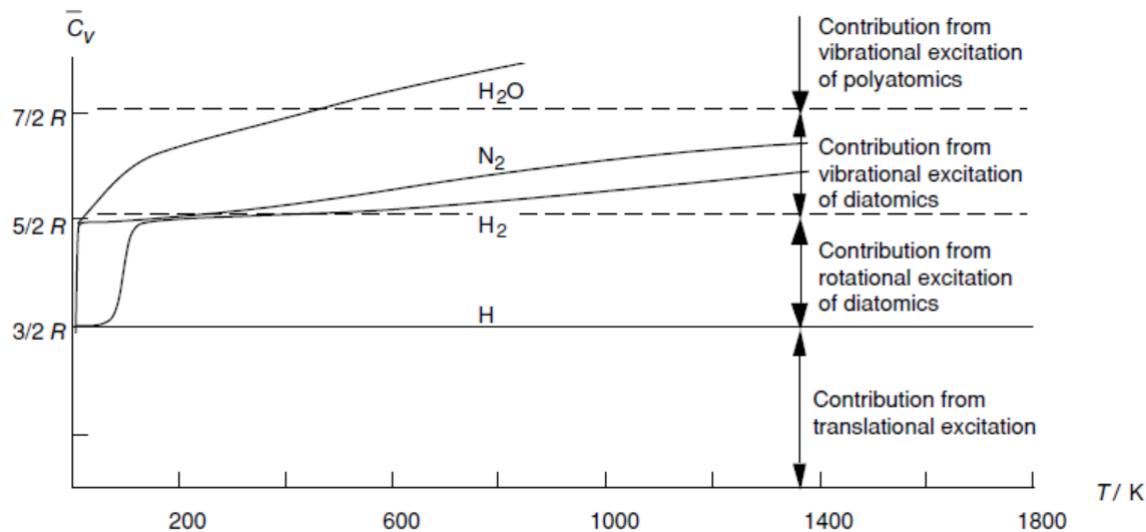


Figure 3.3.: Molar constant volume heat capacity dependence on temperature [4].

NASA-polynomials are used to approximate the specific heat, enthalpy and entropie as a function of temperature as shown in the following equations. The reference for computing the thermodynamic properties is the standard condition of 298 K and 1 bar.

$$\frac{\bar{C}_p^0}{R} = a_1 + a_2 T + a_3 T^2 + a_4 T^3 + a_5 T^4 \quad (3.15)$$

$$\frac{\bar{H}_T^0(T)}{R} = a_6 + a_1 T + \frac{a_2}{2} T^2 + \frac{a_3}{3} T^3 + \frac{a_4}{4} T^4 + \frac{a_5}{5} T^5 \quad (3.16)$$

$$\frac{\bar{S}_T^0(T)}{R} = a_7 + a_1 \ln T + a_2 T + \frac{a_3}{2} T^2 + \frac{a_4}{3} T^3 + \frac{a_5}{4} T^4 + \frac{a_5}{5} T^5 \quad (3.17)$$

In a combustion process temperatures vary from very low temperatures to very high temperatures. Therefore, two different set of polynomial coefficient are used to get the accurate approximation over a large temperature range. In Figure 3.4 the thermodynamic date in polynomial form is shown. This format is used in Cantera. In the first row information about the species (N_2 , CO, CO_2), date of generation, state, lowest temperature of validity and highest temperature of validity is given. The coefficients (a_1-a_7) required to determine the thermodynamic properties such as specific heat, enthalpy and entropie are given in lines 2-4. The first set of seven coefficients in lines 2-3 are used for high temperature ranges ($T>1000K$). The second set of other seven cofficients are used for low temperature ranges ($T<1000K$). Typically a temperature of 1000 K is used to switch between the lower and higher temperature ranges.

N2	J 3/77	G	300.000	5000.000	1
0.28532899E+01	0.16022128E-02	-0.62936893E-06	0.11441022E-09	-0.78057465E-14	2
-0.89008093E+03	0.63964897E+01	0.37044177E+01	-0.14218753E-02	0.28670392E-05	3
-0.12028885E-08	-0.13954677E-13	-0.10640795E+04	0.22336285E+01		4
CO	J 9/65	G	300.000	5000.000	1
0.29840696E+01	0.14891390E-02	-0.57899684E-06	0.10364577E-09	-0.69353550E-14	2
-0.14245228E+05	0.63479156E+01	0.37100928E+01	-0.16190964E-02	0.36923594E-05	3
-0.20319674E-08	0.23953344E-12	-0.14356310E+05	0.29555351E+01		4
CO_2	J 9/65	G	300.000	5000.000	1
0.44608041E+01	0.30981719E-02	-0.12392571E-05	0.22741325E-09	-0.15525954E-13	2
-0.48961442E+05	-0.98635982E+00	0.24007797E+01	0.87350957E-02	-0.66070878E-05	3
0.20021861E-08	0.63274039E-15	-0.48377527E+05	0.96951457E+01		4

Figure 3.4.: Thermodynamic data from Kee et al. 1987, Burcat 1984 [4] in polynomial form as used in CHEMKIN.

3.3. Transport data

The movement of molecules in a gas transports the corresponding physical properties of molecular transport processes for instance diffusion, heat conduction and viscosity [4]. Diffusion refers to mass transport caused by the concentration gradients. The velocity gradients cause momentum transport (viscosity) and a temperature gradient leads to energy transport (heat conduction). In addition to this, there exist also other pheomena for instance mass transport as a result of temperature gradients, called thermal diffusion or Soret effect and energy tranport caused by concentration gradients called Dufour effect [91].

In chemically reacting flows, chemical production and destruction are often balanced by the molecular transport processes. Diffusion coefficients, viscosities and thermal conductivities are required to characterize the molecular transport of species, momentum, and energy in a multicomponent gaseous mixture. Kinetic theory expressions are applied to determine the pure species properties, which can be used to compute the gas mixture properties by using certain approximate mixtue averaging rules according to Bird et al. [92]. In some cases these approximate mixture averaging rules may not be accurate enough. But the multicomponent mixing rule is considered to be more accurate for calculating the transport properties. In

a study Zhukov and Paetz compared different formulas based on multicomponent, mass averaging and mole averaging mixing rule for the calculation of thermal conductivity of gas mixtures in CFD simulations of rocket combustion chamber. They found out, that the best results can be achieved using the multicomponent mixing rule. Detailed information about this study can be found in [93]. A study is undertaken in Section 4.3 to evaluate both transport properties models (Mixture-averaged and Multicomponent) in consideration of computational cost and accuracy for predicting the selected validation parameter premixed laminar flame speed.

Mixture-averaged transport properties model

The mixture-averaged method is used to calculate diffusion for instance in premixed laminar flame. The transport properties are calculated from the individual species properties such as viscosity μ_k , thermal conductivity λ_k and binary diffusion coefficients D_{jk} .

Individual species transport properties

Cantera requires a molecular data file as illustrated in Figure 3.5 to compute the pure species transport properties. The first column of the transport data file contains the name of each species such as H, H₂ etc. In the second column information about the geometrical configuration of each individual species is given for instance 0 refers to a single atomic species (H), 1 to a linear molecule (H₂), 2 to a nonlinear molecule (H₂O). The Lennard-Jones potential well depth ε/k_B is given in the third column and the collision diameter σ in the fourth column. The next column contains $\bar{\mu}$, which is the dipole moment of each species. In the last two columns the polarizability $\bar{\alpha}$ and the rotational relaxation collision number Z_{rot} are given.

H	0	145.000	2.050	0.000	0.000	0.000
H ₂	1	38.000	2.920	0.000	0.790	280.000
O	0	80.000	2.750	0.000	0.000	0.000
O ₂	1	107.400	3.458	0.000	1.600	3.800
OH	1	80.000	2.750	0.000	0.000	0.000
H ₂ O	2	572.400	2.605	1.844	0.000	4.000
HO ₂	2	107.400	3.458	0.000	0.000	1.000
H ₂ O ₂	2	107.400	3.458	0.000	0.000	3.800

Figure 3.5.: Data for transport properties from V. P. Zhukov, V. A. Sechenov and A. Yu Starikovskii [8] as used in CHEMKIN.

The pure species thermal conductivity λ_k , binary Diffusion coefficient D_{jk} and viscosity μ_k are calculated by applying the following equations. The translational $f_{trans.}$, rotational $f_{rot.}$ and vibrational $f_{vib.}$ contributions in Equation 3.18 are determined according to [95].

$$\lambda_k = \frac{\mu_k}{W_k} (f_{trans.} C_{v,trans.} + f_{rot.} C_{v,rot.} + f_{vib.} C_{v,vib.}) \quad (3.18)$$

$$D_{jk} = \frac{3}{16} \frac{\sqrt{2\pi k_B^3 T^3 / m_{jk}}}{p \pi \sigma_{jk}^2 \Omega^{(1,1)*}} \quad (3.19)$$

$$\mu_K = \frac{5\sqrt{\pi m_k K_B T}}{16\pi\sigma_k^2 \Omega^{(2,2)*}} \quad (3.20)$$

The collision integrals $\Omega^{(1,1)*}$ and $\Omega^{(2,2)*}$ are computed by a quadratic interpolation of the tables based on Stockmayer potentials according to Monchick and Manson [96]. Now the mixture averaged transport properties μ , λ and D_{km} can be computed by using the pure species transport properties μ_k , λ_k and D_{jk} .

$$\mu = \sum_{k=1}^K \frac{X_k \mu_k}{\sum_{j=k}^K X_j \Phi_{kj}} \quad (3.21)$$

with

$$\Phi_{kj} = \frac{1}{\sqrt{8}} \left(1 + \frac{W_k}{W_j} \right)^{-\frac{1}{2}} \left(1 + \left(\frac{\mu_k}{\eta_j} \right)^{\frac{1}{2}} \left(\frac{W_j}{W_k} \right)^{\frac{1}{4}} \right)^2 \quad (3.22)$$

$$\lambda = \frac{1}{2} \left(\sum_{k=1}^K X_k \lambda_k + \frac{1}{\sum_{k=1}^K \frac{X_k}{\lambda_k}} \right) \quad (3.23)$$

$$D_{km} = - \frac{\sum_{j \neq k}^K W_j D_{k,j} d_j}{\bar{W} d_k} \quad (3.24)$$

Multicomponent transport properties model

The multicomponent approach is the other method to calculate diffusion, this method is considered to be more accurate as compared to the mixture-averaging method. The reason behind this is, that the mixture averaging rules are only adequate in some special cases for instance in systems, where the diffusion velocity of all species except one species is almost the same [92]. Another adequate application of mixture averaging method is binary mixtures. Furthermore in multicomponent method mass conservation is applied while solving the species continuity equations. On the contrary in the mixture-averaged method some ad-hoc correction procedure [97] is utilized as a compensation for not applying the mass conservation for species continuity equations. A major disadvantage of multicomponent method is computational cost, since more equations have to be solved as compared to mixture-averaged method. Since a detailed description of the equations needed in the multicomponent transport properties model would require several pages. There references for detailed information about the multicomponent transport properties model are Dixon-Lewis [94] or [95].

4. Ignition and laminar flame speed simulation

4.1. Cantera

Cantera is used within in Python-Interface in this thesis, it is a open-source software, which is able to solve problems of chemical kinetics, thermodynamics, and transport processes. It was developed by David G. Goodwin at California Institute of Technology [9]. Cantera can be also used within Matlab or codes written in Fortran and C++. In Figure 4.1 the internal structure of Cantera is shown.

Cantera requires a input file either in .xml or .cti format, which is generated by using the thermodynamic data, transport data files and a .inp file, which contains the reaction mechanism. This .cti or .xml files can be used to solve several thermochemistry problems such as one-dimensional premixed or non premixed flames, chemical equilibrium, reaction path diagrams, sensitivity analysis or reactor networks.

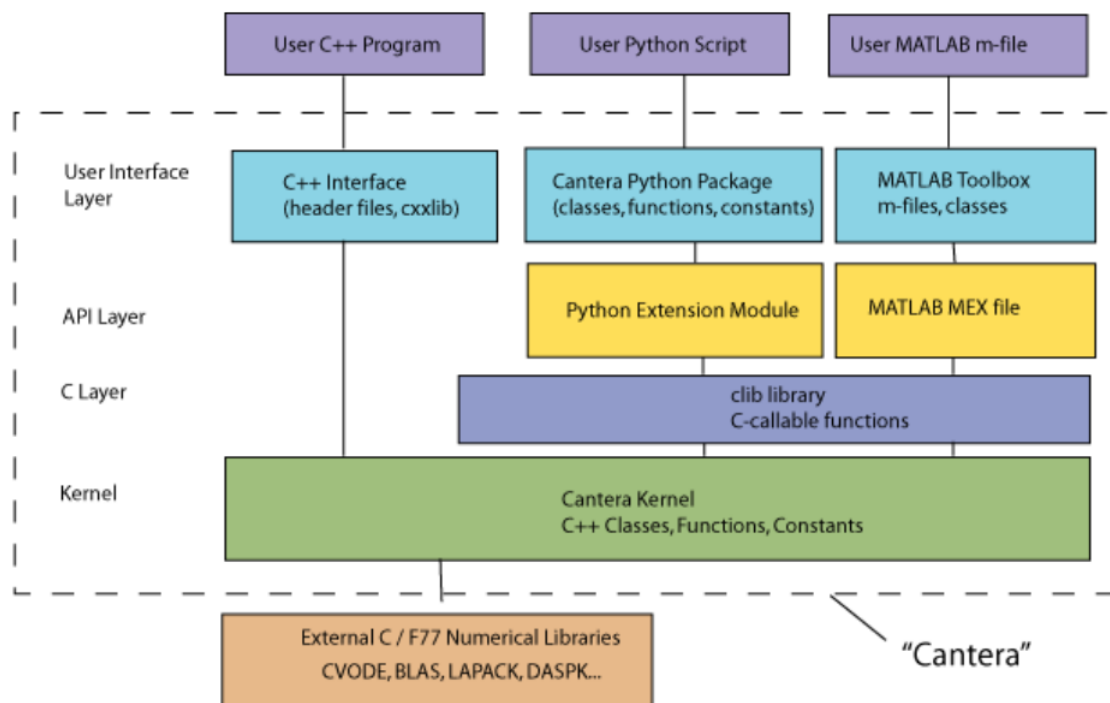


Figure 4.1.: Schematics of the internal structure of Cantera [9].

4.2. Ignition simulation

Ignition can be initiated through a spark or chemical kinetics (autoignition and radical-induced ignition). In a spark ignition process a mixture is ignited by a spark through a spark plug. This type of ignition process is typically used in internal combustion engines. On the contrary autoignition is controlled by temperature, pressure and mixture composition. For instance, for a methane-oxygen mixture a spontaneous explosion will occur at a certain value of temperature and pressure after an ignition delay time (τ_{ing}) or induction time (τ_{ind}), which is characteristic for radical-chain explosions, since ignition is controlled by chain-branching mechanism. Such chain-branching reactions lead to rapid production of radicals during the ignition delay period. After a certain time the radical pool is large enough to consume a significant fraction of the fuel, which results in rapid temperature increase and leads to ignition as shown in Figure 4.2.

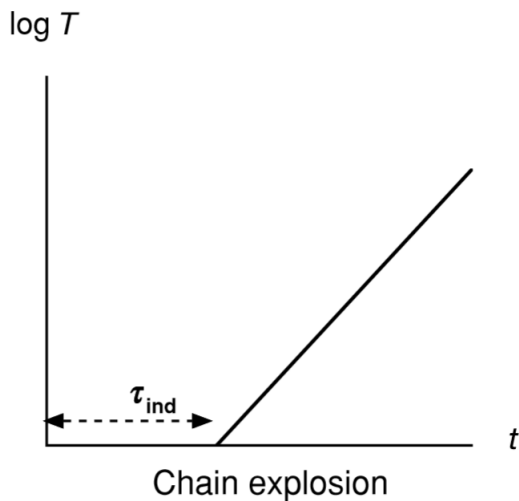


Figure 4.2.: Induction time (ignition delay time) in a chain-branching explosion [4].

But at lower temperature and pressure the reaction would proceed very slow, so that no autoignition occurs. As a result an important question has to be answered for safety consideration and ignition process in an engine. At which temperature, pressure and composition does autoignition occur? To answer this question, an ideal gas adiabatic constant pressure batch reactor simulation is conducted in Cantera. A batch reactor represents the simplest form of a chemically reacting system. It has no inlet or outlet and it consists of a tank and an agitor, which is used to create a perfectly stirred homogenous chemical composition. The schematic of a batch reactor is illustrated in Figure 4.3.

The homogeneous chemical composition inside the reactor changes in respect to time. In a batch reactor simulation cantera solves governing equations of species and energy conservation using a hybrid damped Newton iteration algorithm. Further information regarding this algorithm and the solution procedure can be found in [98]. Several criterion are used in literature to define autoignition for instance consumption of fuel or increase of temperature

in an adiabatic vessel. In this thesis the autoignition temperature is defined as an increase of initial temperature T_i by 500 K within 0.5 s [95]. A stoichiometric gas composition of methane oxygen in a batch reactor with adiabatic wall assumption is used to determine the autoignition temperature at 1 bar. The simulation is conducted using different initial temperatures ranging from 600 K to 950 K. The methane oxygen reaction mechanism from Zhukov et al. [26], which is validated for alkane oxidation from methane to n-heptane, is utilized in this autoignition study.

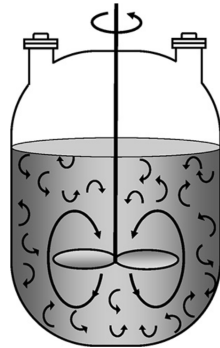


Figure 4.3.: Schematic of a batch reactor [10].

As previously mentioned several initial temperatures are used in this study. Two cases from the study one case with an initial temperature of 900 K and other with an initial temperature of 850 K are selected and compared. As one can see in Figure 4.4 the initial temperature of 850 K is not enough to ignite the used gas composition. Since no significant temperature increase or consumption of fuel and oxidizer is observed in Figure 4.4 and Figure 4.5. On the contrary 900 K is sufficient to initiate chemistry, which leads to a rapid temperature increase (see Figure 4.4), fuel CH₄ and oxidizer O₂ consumption (see Figure 4.5) and formation of product species CO₂ and H₂O (see Figure 4.6) according to the global reaction of methane combustion as shown in Equation 2.45.

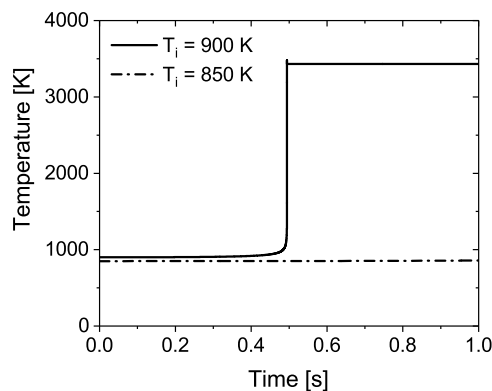


Figure 4.4.: Temperature over time of stoichiometric compositions of CH₄/O₂ at 1 bar.

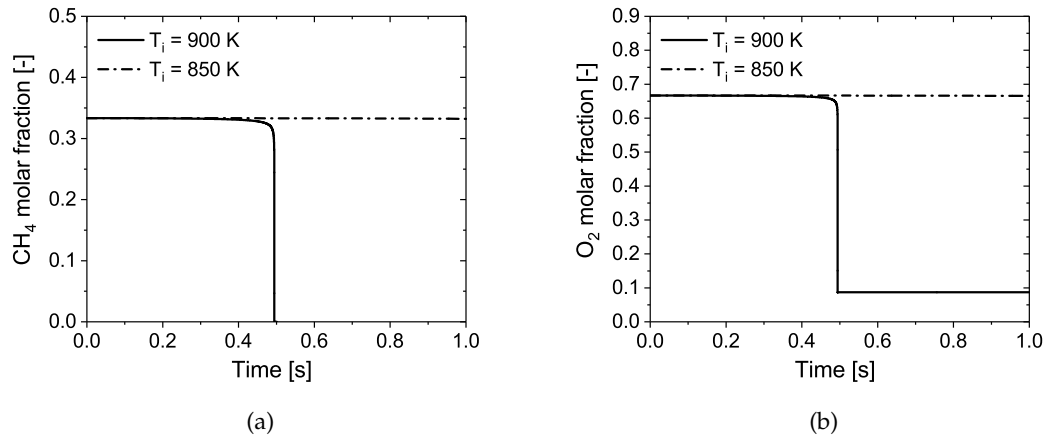


Figure 4.5.: Molar fraction of fuel CH₄ and oxidizer O₂.

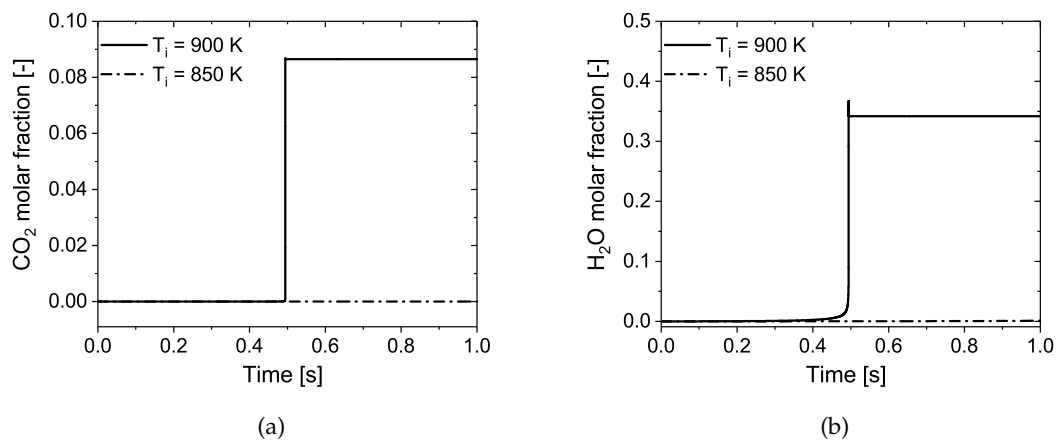


Figure 4.6.: Molar fraction of H₂O and CO₂ after ignition.

One of the reason, why the mixture does not autoignite at 850 K and 1 bar could be, that at this temperature not enough amount of radicals (H, OH) are produced to consume a significant fraction of fuel, which results in rapid temperature increase, and initiates ignition. An other option to ignite the mixture at 850 K and 1 bar is to bombard the mixture with a reactive species for instance H radical, which will lead to fast chemistry, rapid temperature increase, and autoignition of the mixture. This study can be found in Appendix C.

A further study is conducted to investigate the effect of increasing pressure on the minimum required initial temperature for autoignition. The required initial temperature for autoignition decreases with increasing pressure. The reason behind this is, that at elevated pressures some chain-branching reactions for instance $\text{CH}_3\text{O}_2 + \text{CH}_3 \rightarrow \text{CH}_3\text{O}$ and $\text{H}_2\text{O}_2 + \text{M} \rightarrow \text{OH} + \text{M}$ become very dominant. These reactions enhance the formation of H and OH radicals, which leads to lower initial temperatures required for autoignition at higher

pressures. The autoignition limits of a stoichiometric methane-oxygen mixture are shown in Figure 4.7. The region, where the reactions are slow are separated from the region, where ignition takes place by a curve.

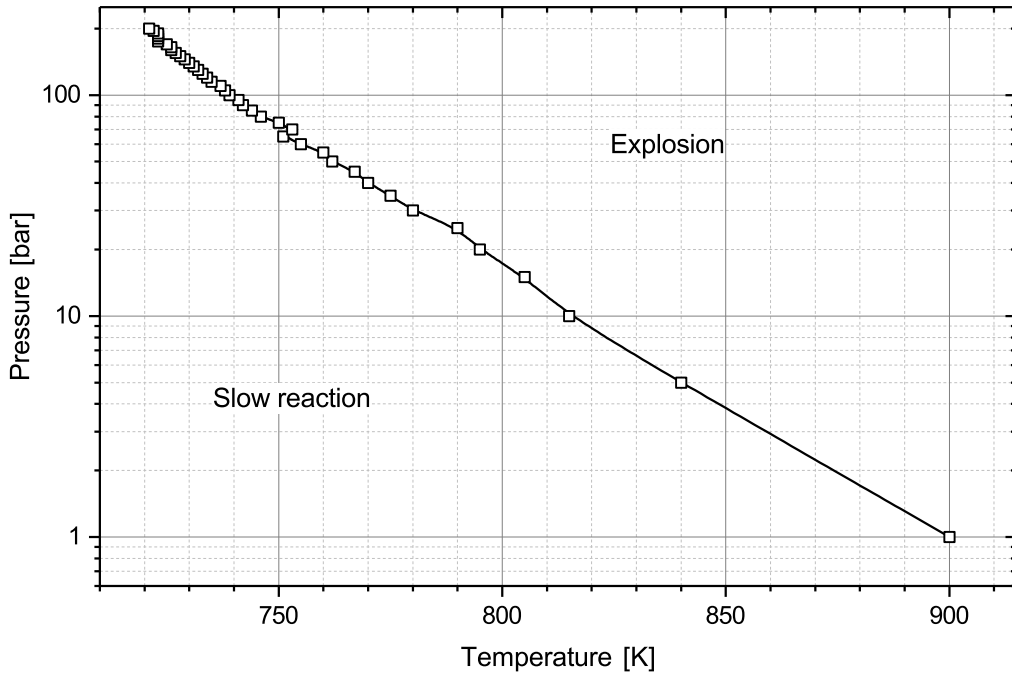


Figure 4.7.: Autoignition limits of a stoichiometric methane-oxygen mixture.

4.3. Comparison of multicomponent and mixture-averaged model

As previously mentioned in Section 3.3, two different models are used to calculate the transport properties of species for instance diffusion, heat conduction and viscosity. Therefore a study is undertaken using the reaction mechanism from Zhukov et al. [26] to select a model, which will be used in the validation simulation of laminar flame speed in Chapter 5. The accuracy and required computational time of each model are taken into account, where accuracy is the more important factor than the computational time, since premixed laminar flame simulations last only several minutes in Cantera. To determine the accuracy of each model the simulation results are compared with experiments conducted by Rozenchan et al. [99]. Considering the combustion conditions in rocket chamber two experiments conducted at elevated pressures of 40 atm and 60 atm are chosen. As expected both models predict different laminar flame velocity. The calculated values by the multicomponent model are closer to experimental values as shown in Figure 4.8.

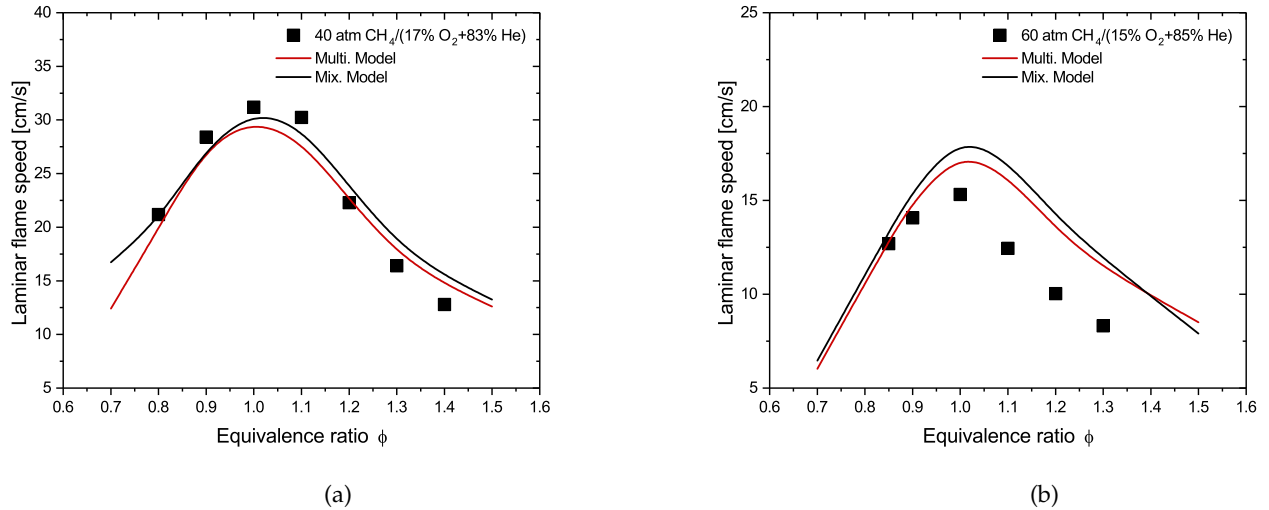


Figure 4.8.: Comparison of simulation results of premixed laminar flame speeds using different diffusion formulations with experimental values.

The mean absolute percentage error (MAPE) as shown in Equation 4.1 is used to determine the deviation of calculated results (*calc*) of each model from the experimental values (*exp*). The MAPE of both models is given in Table 4.1.

$$\text{MAPE} = \left(\frac{1}{n} \sum \frac{|exp - calc|}{|exp|} \right) \cdot 100 \quad (4.1)$$

Table 4.1.: Deviation of simulation results from the experimental values

Model	MAPE (40 atm)	MAPE (60 atm)
Multi. Model	6.1 %	20.4 %
Mix. Model	7.3 %	26.6 %

As compared to the mixture-averaged model the multicomponent model is slightly more accurate considering the 40 atm case. But the deviation between the both models is negligible. For the 60 atm case a significant difference between the both models is evident. The higher accuracy at elevated pressure could result from decreasing diffusivity at high pressure, which leads to lower flame velocity, since flame velocity is a function of diffusivity. The effect of decreasing diffusion at high pressures is not captured by the mixture-averaged model adequately. Considering the better accuracy of the multicomponent model and negligible difference between the both models regarding the computational time, which stays in range of 1-1.5 minutes for mixture-averaged and around 2 minutes for the multicomponent model for each simulation load point, the multicomponent model will be used in the validation simulation.

5. Validation

Ignition delay time and laminar flame speed are chosen as validation criteria for the validation of newly developed CH₄/O₂ skeletal reaction mechanism by Zhukov & Kong [30]. Several researchers used ignition delay times and laminar flame speeds for the validation of reaction mechanisms for instance, Petersen et al. [28], [31] used ignition delay times for the validation of the detailed reaction mechanism RAMEC, as well for the reduced reaction mechanism REDRAM. Slavinskaya et al. [29] used ignition delay times and laminar flame speeds for the validation of their reduced reaction mechanism. The reaction mechanism designed to model natural gas combustion GRI-Mech 3.0 [27] is also validated against ignition delay times and laminar flame speeds.

Calculated ignition delay times and flame speeds do not only depend on chemical reaction, but also on the thermodynamic and transport data. In order to isolate the impact of kinetics from the impact of the thermodynamic properties, the same thermodynamic and transport data from [25] is used for all reactions mechanisms in this thesis. The influence of using different thermochemistry is examined in a premixed laminar flame speed study, which can be found in Appendix D, before the validation process using Zhukov & Kong with two different thermochemistry data from C1-C4 Zhukov et al. [26] and Aramcomech 1.3 [25]. Using different thermochemistry data within the same reaction mechanisms leads to different predicted premixed laminar flame speed as shown in Appendix D. Therefore, the thermochemistry data from Aramcomech 1.3 is used for all reaction mechanisms, since this thermochemistry data is based on the latest researches.

The predicted results for ignition delay times and laminar flame speeds by Zhukov & Kong are compared with other well known or frequently used CH₄/O₂ reaction mechanisms:

1. C₁-C₄ Zhukov [26]
2. RAMEC [28]
3. Skeletal mechanism by Slavinskaya et al. [29] (further referred as Red.Slavinskaya)
4. REDRAM [31]
5. Aramcomech 1.3 [25]
6. Tiafeng Lu [32]
7. Westbrook & Dryer (version from Airbus DS) [34]

8. Jones–Lindstedt (version by Frassoldati) [33]

9. GRI-Mech 3.0 [27]

Petersen et al. reported in [28], that within the experimental accuracy ignition delay times were found to be independent of the bath gas used in the experiment. A study is carried out to confirm, whether the bath gas influences the simulation results for ignition delay times and laminar flame speeds. If an independency of the predicted simulation results can be confirmed, it will allow a more correct comparison between the reactions mechanisms, because some of the reaction mechanisms, which are based on global chemistry for instance Westbrook & Dryer (Airbus DS) and Jones-Lindstedt (Frassoldati) do not contain any reactions with commonly used bath gases in the experiments for example argon or nitrogen.

This study is conducted using the reaction mechanism Red.Slavinskaya, because it contains reactions with all commoly used bath gases (N_2 , Ar and He). Furthermore it has been validated against ignition delay time and laminar flame speed. Two different versions of Red.Slavinskaya are utilized to investigate the impact of the bath gas on the simulation results. One version (version 1) contains all reactions with N_2 , Ar and He , while in the other version (version 2) all reactions with N_2 , Ar and He are removed. The aim is to investigate whether both versions predict the identical ignition delay times.

The predicted results of both reaction mechanism versions are compared with the experimental data from Petersen et al. [100]. The data set are following experiments chosen for this study to capture any influence of the bath gas at serveral pressures, equivalence ratios and bath gases.

1. Test case 1: $p = 50$ atm, $\phi = 0.4$, mixture = $CH_4/(O_2+Ar)$
2. Test case 2: $p = 170$ atm, $\phi = 3$, mixture = $CH_4/(O_2+N_2)$

The simulation is conducted with both reaction mechanism versions utilizing an adiabatic constant volume batch reactor in Cantera with the same boundary conditions and mixtures as used in the experiment. As one can see in Figure 5.1 the deviation of predicted ignition delay times by both versions from the experimental data is almost identical for test case 1 and test case 2. One of the reasons of independency of ignition from bath gas could be, that the ignition is governed by so called chain-branching reactions. These kind of reactions produce radicals, which initiate ignition. This would mean, that ignition is independent of reactions with N_2 or Ar. Only these chain-branching reactions lead to ignition.

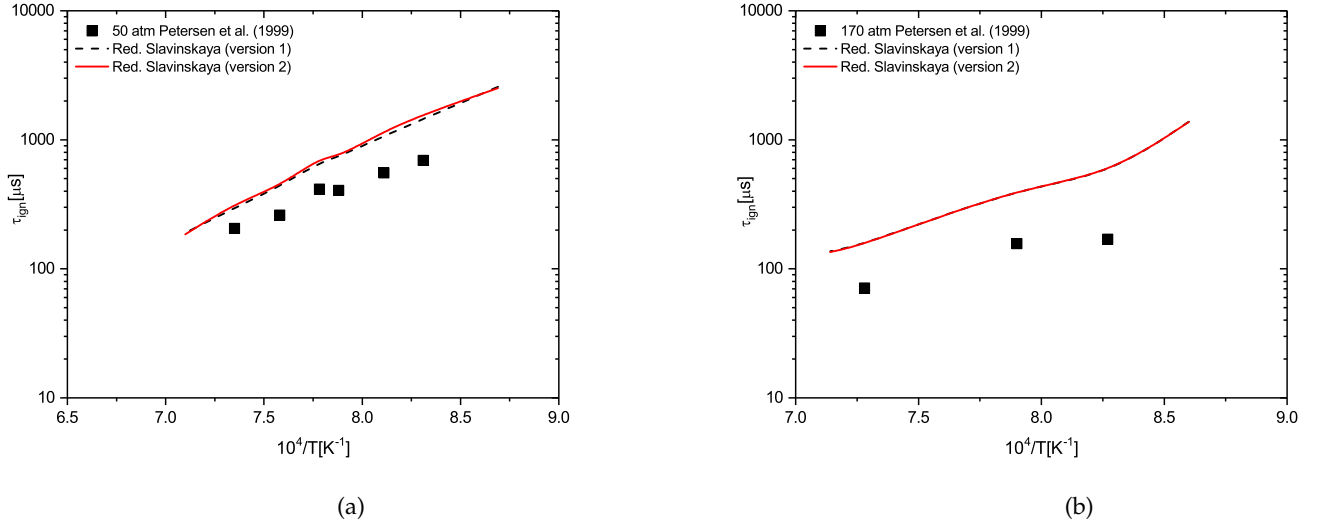


Figure 5.1.: Comparison of simulation results of ignition delay time using different versions of Red.Slavinskaya with experimental values.

Following experiments are chosen from Rozencan et al. [101] to examine the influence of bath gas on the laminar flame speed, which is also a widely used validation criteria as aforementioned.

1. Test case 1: $p = 10$ atm, $T_u = 298$ K, mixture = CH₄/(Air)
2. Test case 2: $p = 60$ atm, $T_u = 298$ K, mixture = CH₄/(15%O₂ + 85%He)

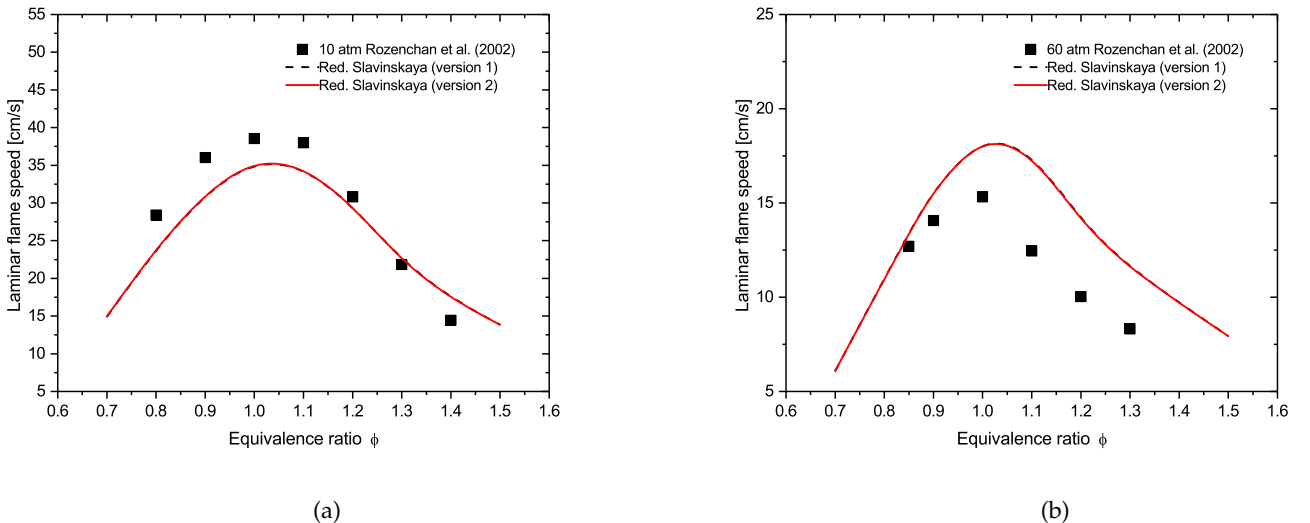


Figure 5.2.: Comparison of simulation results of premixed laminar flame speeds using different versions of Red.Slavinskaya with experimental values.

As shown in Figure 5.2 both versions (version 1 and version 2) deliver the same results for both test cases. This study confirms Petersen et al. [28] report of independency of ignition delay time results from the bath gas. Furthermore the simulation results of laminar flame speeds are also independent of used diluent gas.

5.1. Validation against ignition delay times

Experimental ignition delay time data ranging from lean mixture to rich mixtures, pressures from 50 atm to 450 atm are chosen from Petersen et al. [100] and Zhukov et al. [8] to validate the reaction mechanism Zhukov & Kong. Moreover it is compared with other well known or frequently used reaction mechanisms from summer program 2015 SFB/TR-40 project.

The deviation produced by each reaction mechanism from the experimental values is determined using Equation 4.1. The results are shown in Table 4.1. RAMEC and its derivative reaction mechanisms REDRAM, C1-C4 Zhukov and Zhukov & Kong are able to predict the ignition delay time with an error of 13 - 18% for lean mixture at 50 - 450 atm. Red.Slavinskaya produces an error of about 76 - 112% for test 1 (50 atm) and test 2 (450 atm). The reason behind this is, that Red.Slavinskaya has not been optimized for elevated pressures as demonstrated by Slavinskaya et al. in [29]. GRI-Mech 3.0 is also capable of predicting the ignition delay time for test 1 and test 2 with an error of 26 - 27%, which is higher than RAMEC, C1-C4 Zhukov, REDRAM and Zhukov & Kong, but still acceptable. The reaction mechanism by Tiafeng Lu produces an error of up to 1000% for all test cases (test1 - test4), since this reaction mechanism is not suitable for high pressure conditions.

Aramcomech 1.3 has an error of 25 - 50% for the test 1 and test 2. As expected the reaction Jones-Lindstedt (Frassoldatti), which is based on global chemistry, produces an error much higher than 100% (error up to 1000%). On the contrary the other global chemistry based reaction mechanism Westbrook & Dryer (Airbus DS) delivers unexpectedly better results with an error of 69 - 92% (test 1, test 2). The reason behind this could be the modification of Westbrook & Dryer by Riedmann et al. [34] by adding the reaction as shown in Equation 5.1, which captures water dissociation and recombination effects occurring due to the elevated temperatures. This reaction is a major reaction for CH₄/O₂ combustion, as shown in the sensitivity analysis in Section 6. Although Jones-Lindstedt (Frassoldatti) also contains this reaction, but it is not able to deliver acceptable error. A reason behind this could be a conflict between chain-branching and chain-termination reactions. Chain-branching reactions produce reactive species for further reaction and leads to ignition, whereas chain-termination reactions consume reactive species. Further details about chain-branching and chain-termination reactions are given in Section 6, Petersen et al. reported in [28] a similar problem of accuracy of predicted ignition delay time by a reaction mechanism, if it contains a higher amount of chain-branching reaction, which leads to an accelerated ignition and as a result smaller ignition delay time, as predicted by Jones-Lindstedt. It has to be mentioned at this stage, that it is only

an assumption. Further investigations need to be done, so that a statement can be made.



For rich mixtures ($\phi = 3$ in test 3 and $\phi = 6$ in test 4) Zhukov & Kong delivers an error of 9% for test 3 and 42% for test 2. RAMEC, REDRAM and C1-C4 Zhukov produce smaller error as compared to Zhukov & Kong for test 3 test 4 ranging from 5% to 27%. The error produced by GRI-Mech 3.0 is also in the similar range 42% for test 3 and 14% for test 4. As expected the accuracy of predicted ignition delay time by Red.Slavinskaya sinks at higher pressures and rich mixtures. For test 3 it produces an error of 165% and 86% for test 4 respectively. Westbrook & Dryer (Airbus DS) achieves a similar accuracy in test 3 and 4 as in test 1 and test 2 (Table 5.1). For rich mixtrue tests (test 3 and test 4) it delivers an error of 87% for test 3 and 96% for test 4. Jones–Lindstedt (Frassoldalti) delivers a error up to 1000% for both rich mixture test cases (test 3 and test 4).

Test 1: $\phi = 0.4$, $p = 50$ atm, mixture = $\text{CH}_4/(\text{O}_2+\text{Ar})$

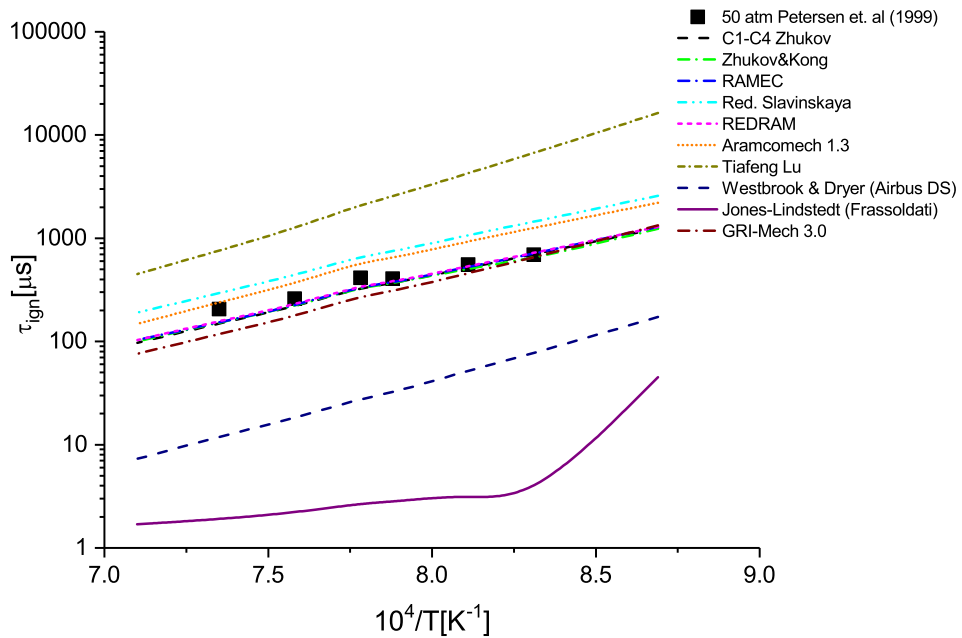


Figure 5.3.: Comparison of simulation results using different reaction mechanisms with experimental values at 50 atm.

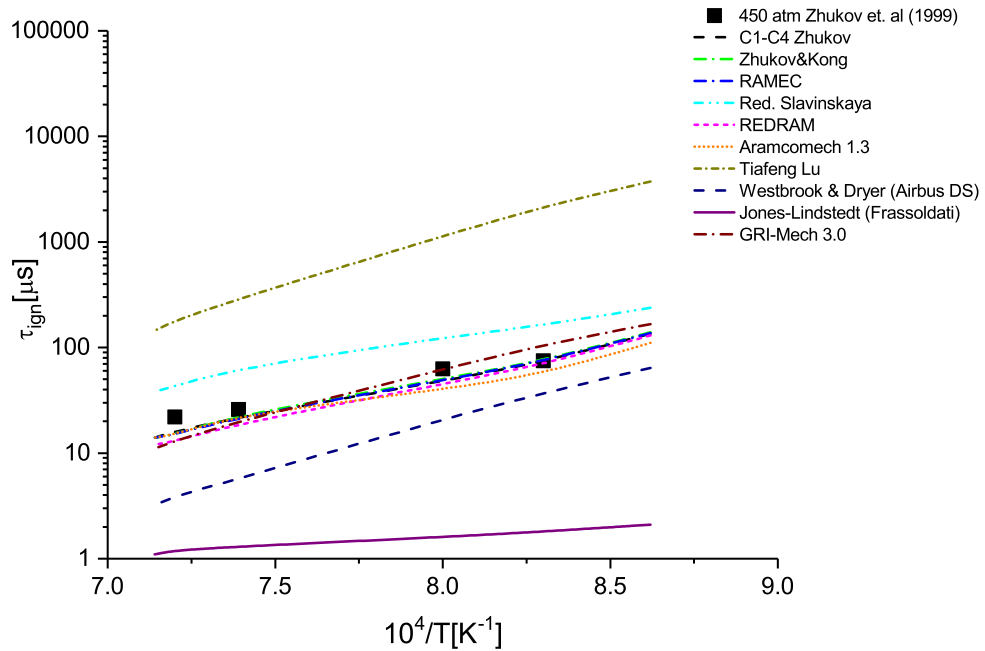
Test 2: $\phi = 0.5$, $p = 450$ atm, mixture = CH₄/(Air)


Figure 5.4.: Comparison of simulation results using different reaction mechanisms with experimental values at 450 atm.

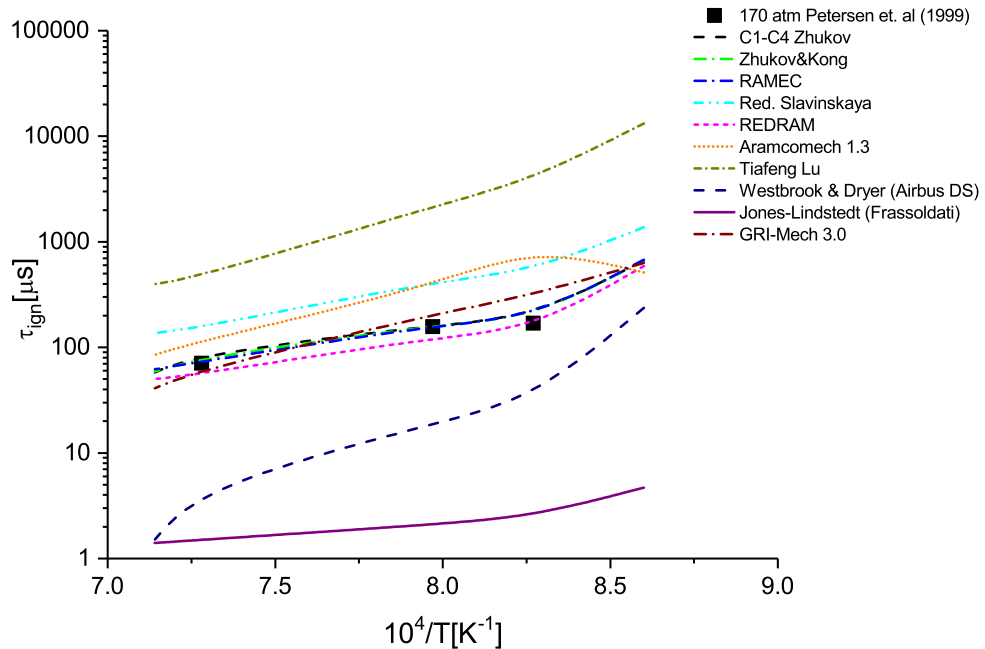
Test 3: $\phi = 3$, $p = 170$ atm, mixture = CH₄/(O₂+N₂)


Figure 5.5.: Comparison of simulation results using different reaction mechanisms with experimental values at 170 atm.

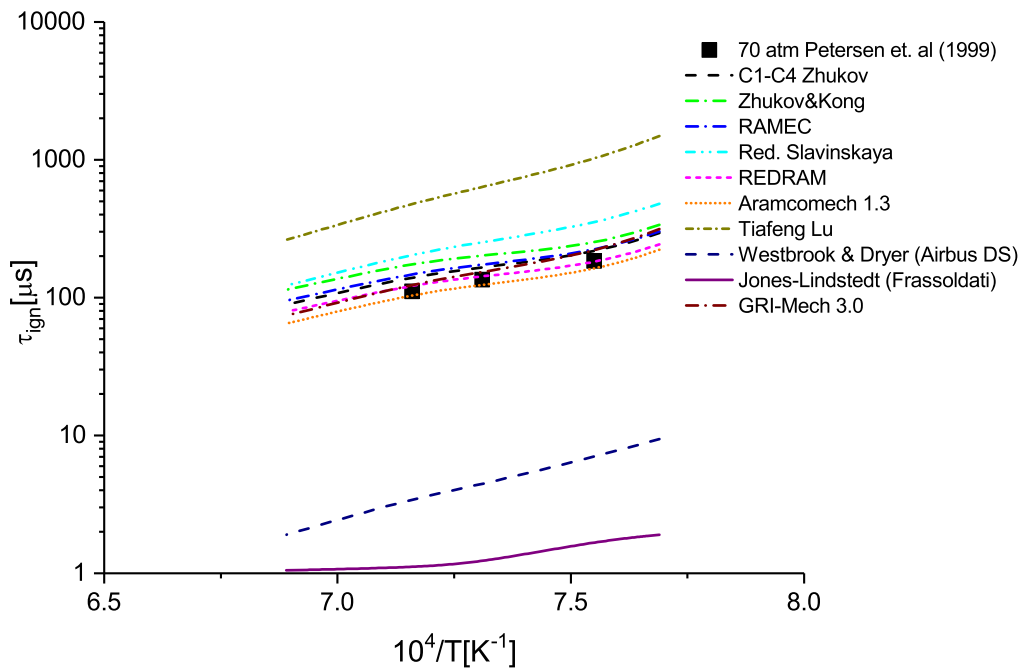
Test 4: $\phi = 6$, $p = 70$ atm, mixture = $\text{CH}_4/(\text{O}_2+\text{He})$


Figure 5.6.: Comparison of simulation results using different reaction mechanisms with experimental values at 70 atm.

Table 5.1.: Absolute mean percentage error from experimental values of each reaction mechanism.

Reaction mechanism	MAPE (test 1)	MAPE (test 2)	MAPE (test 3)	MAPE (test 4)
C1-C4 Zhukov	13%	18%	12%	21%
Zhukov & Kong	13%	18%	9%	47%
RAMEC	12%	18%	5%	27%
Red.Slavinskaya	76%	112%	165%	86%
REDRAM	11%	25%	18%	8%
Aramcomech 1.3	50%	26%	131%	10%
Tiafeng Lu	>1000%	>1000%	>1000%	>1000%
Westbrook & Dryer (Airbus DS)	92%	69%	87%	96%
Jones–Lindstedt (Frassoldalti)	>1000%	>1000%	>1000%	>1000%
GRI-Mech 3.0	26%	27%	42%	14%

Before a further validation of the reaction mechanisms against ignition delay time experiments can be conducted at several different conditions regarding pressure, equivalence ratio and temperatures, it is decided to validate Zhukov & Kong against the other widely used validation criteria laminar flame speed experiments. Several experiments are chosen for the validation from Rozenchan et al. [101] ranging from 10 atm to 60 atm.

5.2. Validation against premixed laminar flame speed

As compared to ignition delay times validation results, where Zhukov & Kong delivers very accurate results, which are comparable with its parent reaction mecahnisms RAMEC and C1-C4 Zhukov as shown in Table 4.1, Zhukov & Kong produces a higher error ranging from 42 - 48% for predicting the premixed laminar flame speeds. Furthermore it can not predict the typical profile of a premixed laminar flame speed, which increases till the stoichiometric equivalence ratio and then starts decreasing. All other reaction mechanisms except REDRAM and the global chemistry based reaction mechanisms Westbrook & Dryer (Airbus DS) and Jonses–Lindstedt (Frassoldalti) are capable of predicting the typical premixed laminar flame speed profile. Red.Slavinskaya has a very low error of around 9 - 14% for test1-test 3, but for higher pressures (test 4, 60 atm) the error increases to 27%. The reason behind this is as aforementioned, that this reaction mechanism has not been optimized for higher pressures as demonstrated by Slavinskaya et al. in [29].

REDRAM is able to predict the ignition delay time with an error of 8 - 25%, which is comparable with its parent reaction mechanism RAMEC. But it also fails to predict the typical profile of a premixed laminar flame speed as Zhukov & Kong. In contrast to the error produced by Tiafeng Lu for predicting the ignition delay time, which is up to 1000% as shown in Table 4.1. Now for the premixed laminar flame speed it delivers better results with an error of 23 - 28% (test 1- test 4). Moreover, it is capable of predicting the typical premixed laminar flame velocity profile. Similar to Red.Slavinskaya GRI-Mech 3.0 has a low error of 8 - 14% for test 1 - test 3, but for test 4 with a higher pressure of 60 atm the error increase to 51%. The same reason as for Red.Slavinskaya can be given for this behavoir. GRI-Mech 3.0 is not optimized for higher pressures. The best results are produced by the detailed reaction mechanisms RAMEC, C1-C4 Zhukov and Aramcomech 1.3 as shown in Table 5.2. They have an error of around 2 - 20%. Since premixed laminar flame speed is an important validation criteria for a reaction mechanism, as demonstrated by serveral researchers for instance Slavinskaya et al. [29], G. Smith et al.[27] (GRI-Mech 3.0), W. Metcalfe et al. [25] (Aramcomech 1.3) [25]. It is decided to examine, why Zhukov & Kong does not deliver acceptable results for the validation against premixed laminar flame speeds. In contranst to this the accuracy of Zhukov & Kong for predicting ignition delay times is comparable with its parent reaction mechanisms RAMEC and C1-C4 Zhukov. Furthermore, if needed a new reduced reaction mechanism should be developed, which is able to deliver better results against both validtion parameters ignition delay times and premixed laminar flame speeds.

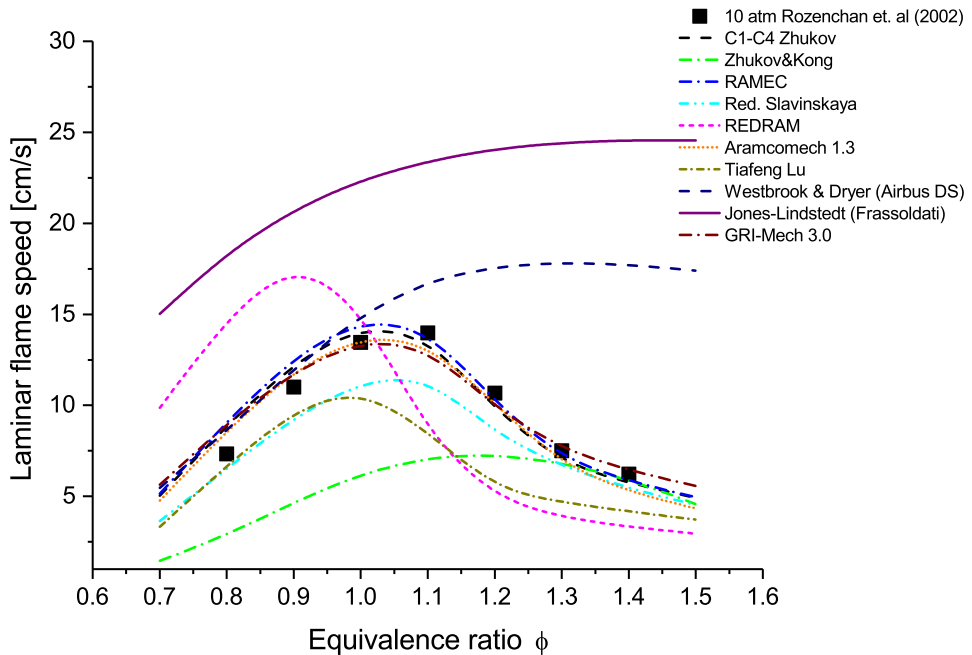
Test 1: $p = 10 \text{ atm}$, $T_u = 298 \text{ K}$, mixture = $\text{CH}_4/\text{(Air)}$


Figure 5.7.: Predicted premixed laminar flame speed by different reaction mechanisms and its comparison with experimental value at 10 atm

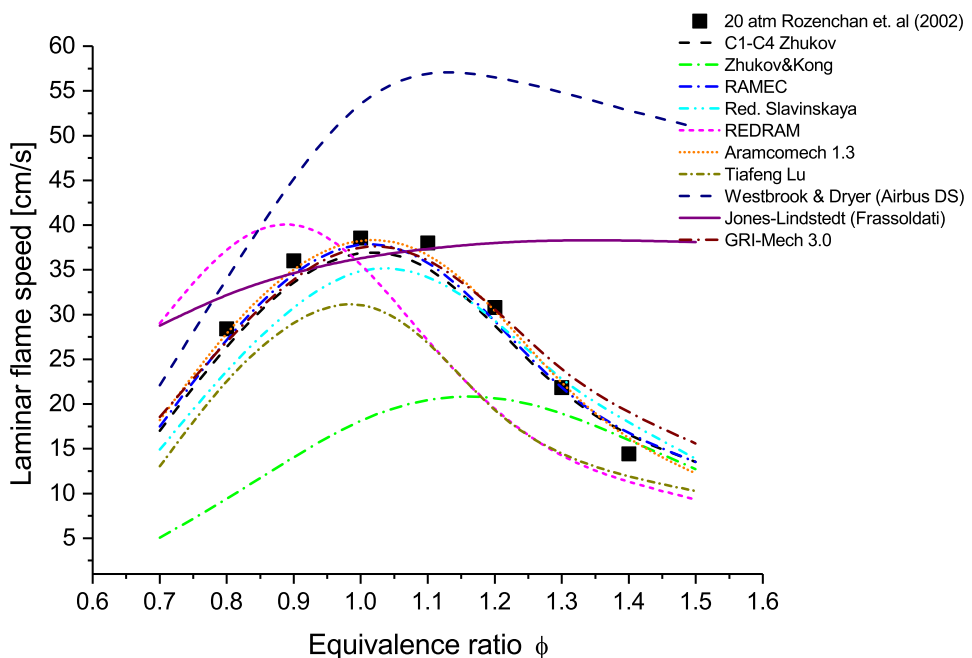
Test 2: $p = 20 \text{ atm}$, $T_u = 298 \text{ K}$, mixture = $\text{CH}_4/(\text{O}_2+\text{He})$


Figure 5.8.: Predicted premixed laminar flame speed by different reaction mechanisms and its comparison with experimental value at 20 atm

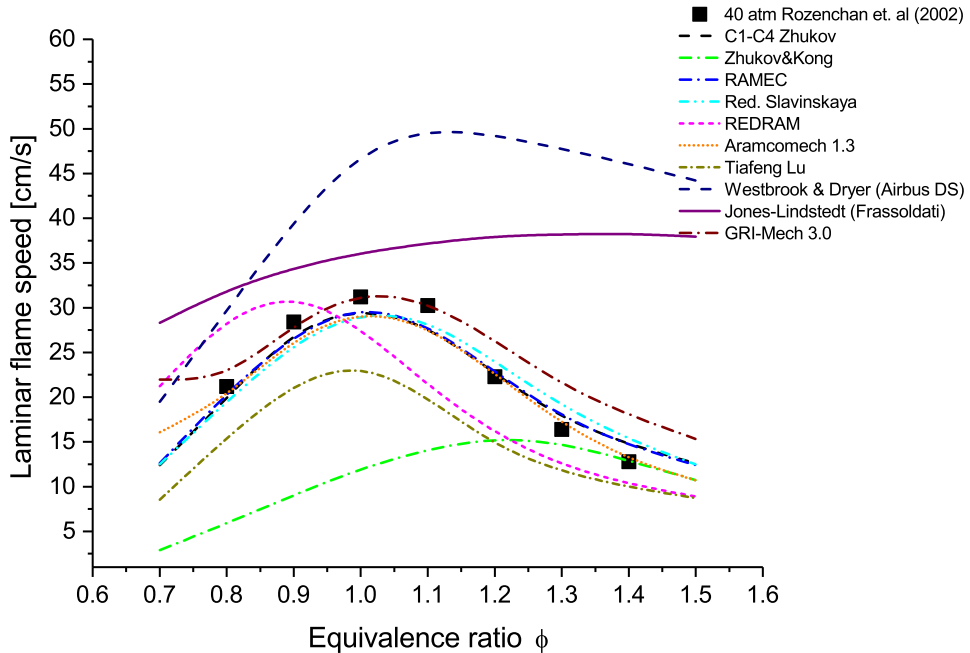
Test 3: $p = 40 \text{ atm}$, $T_u = 298 \text{ K}$, mixture = $\text{CH}_4/(\text{O}_2+\text{He})$


Figure 5.9.: Predicted premixed laminar flame speed by different reaction mechanisms and its comparison with experimental value at 40 atm

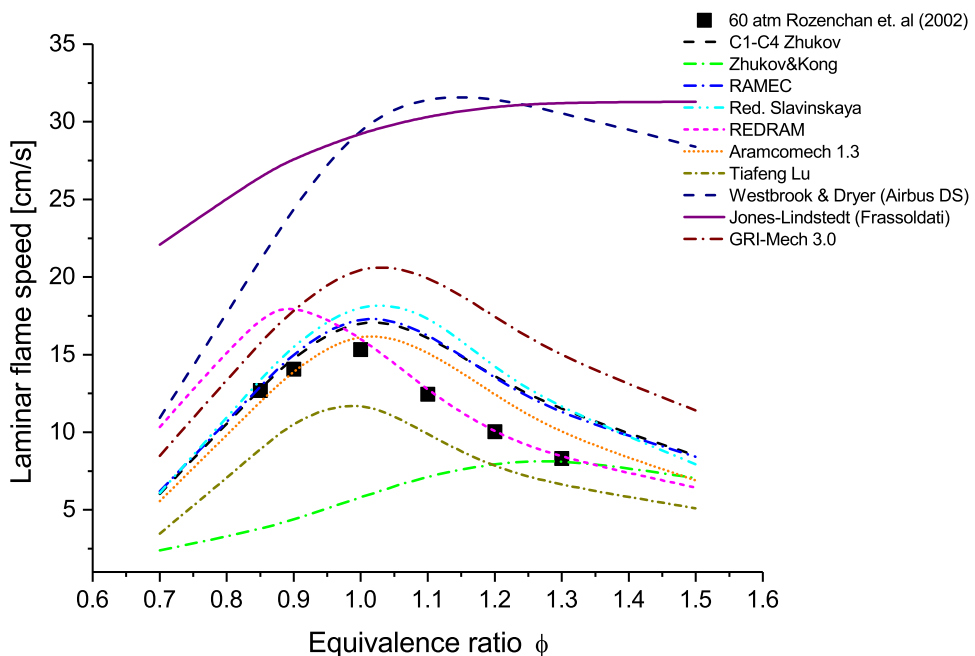
Test 4: $p = 60 \text{ atm}$, $T_u = 298 \text{ K}$, mixture = $\text{CH}_4/(\text{O}_2+\text{He})$


Figure 5.10.: Predicted premixed laminar flame speed by different reaction mechanisms and its comparison with experimental value at 60 atm

Table 5.2.: Absolute mean percentage error from experimental values of each reaction mechanism.

Reaction mechanism	MAPE (test 1)	MAPE (test 2)	MAPE (test 3)	MAPE (test 4)
C1-C4 Zhukov	11%	5%	5%	21%
Zhukov & Kong	42%	40%	43%	48%
RAMEC	11%	4%	6%	21%
Red.Slavinskaya	14%	10%	9%	27%
REDRAM	64%	26%	23%	13%
Aramcomech 1.3	10%	2%	4%	13%
Tiafeng Lu	27%	25%	28%	23%
Westbrook & Dryer (Airbus DS)	60%	92%	110%	145%
Jones–Lindstedt (Frassoldalti)	161%	41%	75%	154%
GRI-Mech 3.0	12%	8%	14%	51%

6. Development of a new CH₄/O₂ reaction mechanism

6.1. Analysis of development process of Zhukov & Kong

Zhukov & Kong is driven from C1-C4 Zhukov by applying the reduction methods reaction path analysis and sensitivity analysis. C1-C4 Zhukov is a detailed reaction mechanism, which is optimized for alkane oxidation from methane to n-heptane at elevated pressures. As shown in Table 1.1 C1-C4 Zhukov consists of 2329 reactions and 207 species, where its parent reaction mechanism RAMEC has 190 reactions and 38 species. The higher number of reactions and species in case of C1-C4 Zhukov results from higher reactivity of higher hydrocarbons, which increases with the number of carbon atoms as shown in Figure 6.1. Methane (CH₄) has only one carbon atom, therefore it has lower reactivity than the higher hydrocarbons for instance butane (C₄H₁₀) with its four carbon atoms.

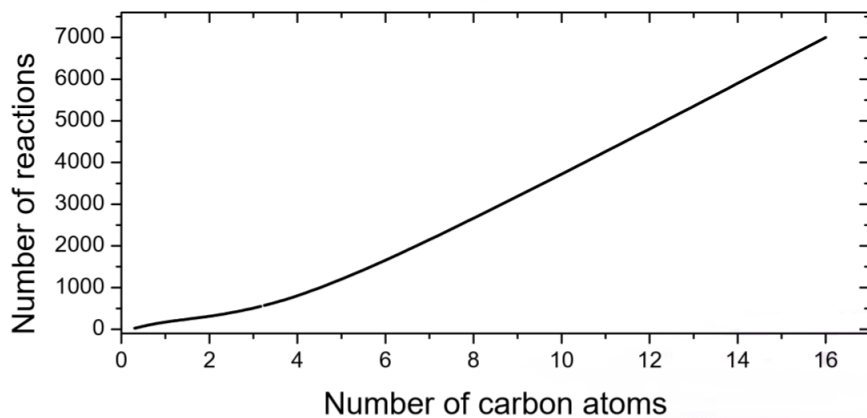


Figure 6.1.: Reactivity of carbon atoms [11].

The origin of these three reaction mechanisms RAMEC, C1-C4 Zhukov and Zhukov & Kong is shown in Figure 6.2, since RAMEC is a detailed CH₄/O₂ reaction mechanism optimized for elevated pressures, one important question occurs. Why was the reduction process started with C1-C4 Zhukov and not with RAMEC? Considering that Zhukov & Kong was developed for CH₄/O₂ combustion numerical simulations at elevated pressures, and RAMEC is an optimized CH₄/O₂ reaction mechanism for combustion modeling at high pressures, where C1-C4 Zhukov is an extension of RAMEC for higher hydrocarbons (methane to n-heptane).

The reason for choosing C1-C4 Zhukov as a parent reaction mechanism to develop a new reduced CH₄/O₂ reaction mechanism (Zhukov & Kong) was, to examine, whether the species with higher number of carbon atoms could improve the accuracy of the new reduced reaction mechanism, which is even better than that of its parent reaction mechanism (RAMEC). Since C1-C4 Zhukov contains species with higher number of carbon atoms, where RAMEC only has species with maximum 2 carbon atoms for instance C₂H₄, C₂H₅O₂ or C₂H₅.

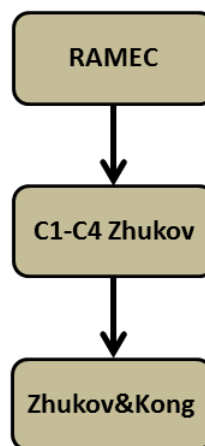


Figure 6.2.: Origin of Zhukov & Kong.

A brief description of the development process of Zhukov & Kong is given in this thesis. Detailed information regarding the development process can be found in [30], as aforementioned reaction path analysis and sensitivity analysis were performed to reduce C1-C4 Zhukov to Zhukov & Kong. After the reaction path analysis (at 60 bar and 100 bar) of C1-C4 Zhukov and removing reactions, which were considered to be unimportant. Sensitivity analysis was conducted for 60 bar to identify the non-rate limiting reactions for a further simplification. Ignition delay times and counterflow diffusion flame temperature were selected as parameters. Further reactions were removed after the validation against two ignition delay time experiments at 50 atm from Petersen et al. [100] and Zhukov et al. [8] in the Sensitivity analysis of ignition delay time. In a further Sensitivity analysis a verification against maximum reachable temperature at 60 bar was done assuming adiabatic conditions using counterflow diffusion flame simulation. In this verification a comparison of detailed (C1-C4 Zhukov) and reduced reaction mechanism (Zhukov & Kong) was made to examine, whether Zhukov & Kong is able to produce the same maximum temperature in the counterflow diffusion flame simulation as C1-C4 Zhukov. If a reaction showed a lower impact on the maximum reachable temperature in the sensitivity analysis of counterflow diffusion flame simulation, this reaction was considered to be unimportant, and therefore it was removed from the reaction mechanism.

It is assumed that removing reactions after a sensitivity analysis using maximum temperature as a reduction parameter in a counterflow diffusion flame simulation could be a reason, why Zhukov & Kong shows very good accuracy for predicting ignition delay time, but it does not deliver accurate results for predicting premixed laminar flame speed. Some important reactions could have been removed in the last development process of Zhukov & Kong, where several reactions were removed in the sensitivity analysis of a counterflow diffusion flame simulation. Because these reactions seemed to be non-rate limiting, since they did not show any impact on the maximum temperature. A counterflow diffusion flame simulation is conducted at 80 bar with several reaction mechanisms to investigate, whether any difference regarding the maximum temperature between the reaction mechanisms can be seen at higher pressure. Since some of them are optimized for low pressures for instance Red.Slavinskaya or Tiafeng Lu, while others have been developed for higher pressure for example Zhukov & Kong, RAMEC or REDRAM, as a result the reaction mechanism, which are not optimized for high pressures for instance Red.Slavinskaya or Tiafeng Lu should not be able to reach the same temperature as Zhukov & Kong, RAMEC or REDRAM. Salvinskaya et al. [29] reported, that their reaction mechanism is optimized for lean mixtures and low pressures. Petersen et al. [28], [31] claimed, that RAMEC and REDRAM haven been optimized for high pressure. The suitablitiy of these reactions mechanisms for high or low pressures as claimed by the developer is confirmed in Chapter 5.

As illustrated in Figure 6.3, all reaction mechanisms except REDRAM reach the same maximum temperature in the counterflow diffusion flame simulation. Even if some of them (Red.Slainvskaya, Tiafeng Lu) do not contain reactions, which become important for high pressure. Since these reaction mechanisms have been developed for application at lower pressures. But in the counterflow diffusion flame simulation even these reaction mechanisms reach the same maximum temperature as RAMEC, GRI-Mech 3.0 or Zhukov & Kong.

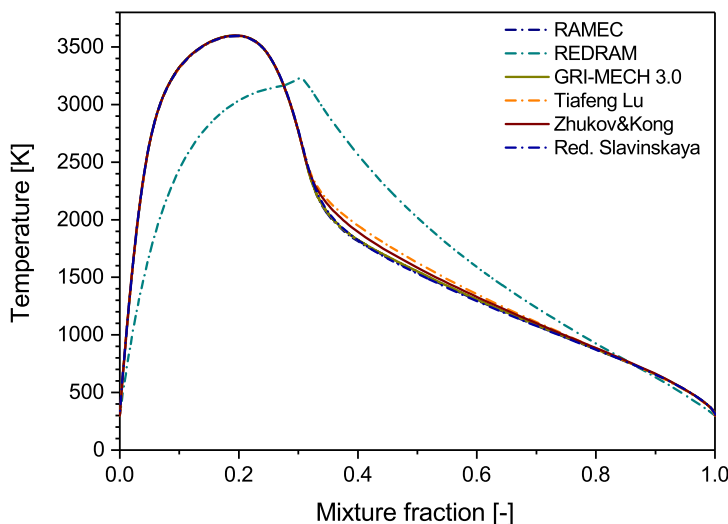


Figure 6.3.: Maximum temperature profile of several CH₄/O₂ reactions mechanism over mixture fraction at 80 bar.

The reason, why Zhukov & Kong is able to predict the ignition delay time very accurately, but it does not deliver accurate results in case premixed laminar flame speed, could be the last reduction step. In the last reduction step several reactions were removed after the sensitivity analysis of maximum reachable temperature in the counterflow diffusion flame simulation. As previously mentioned, in the counterflow diffusion flame simulation even the reaction mechanisms, which do not contain important reactions for high pressures, deliver the same maximum temperature as the reaction mechanisms, which are optimized for high pressures.

6.2. Development of NewMechanism

A different strategy is applied in this thesis to develop a new CH₄/O₂ reaction mechanism named NewMechanism, which is optimized for elevated pressures. But it should be also able to deliver acceptable results for a wide range of conditions from low pressures to high pressures and lean mixtures to rich mixtures. The development process of this new CH₄/O₂ reaction mechanism, named NewMechanism is shown in Figure 6.4.

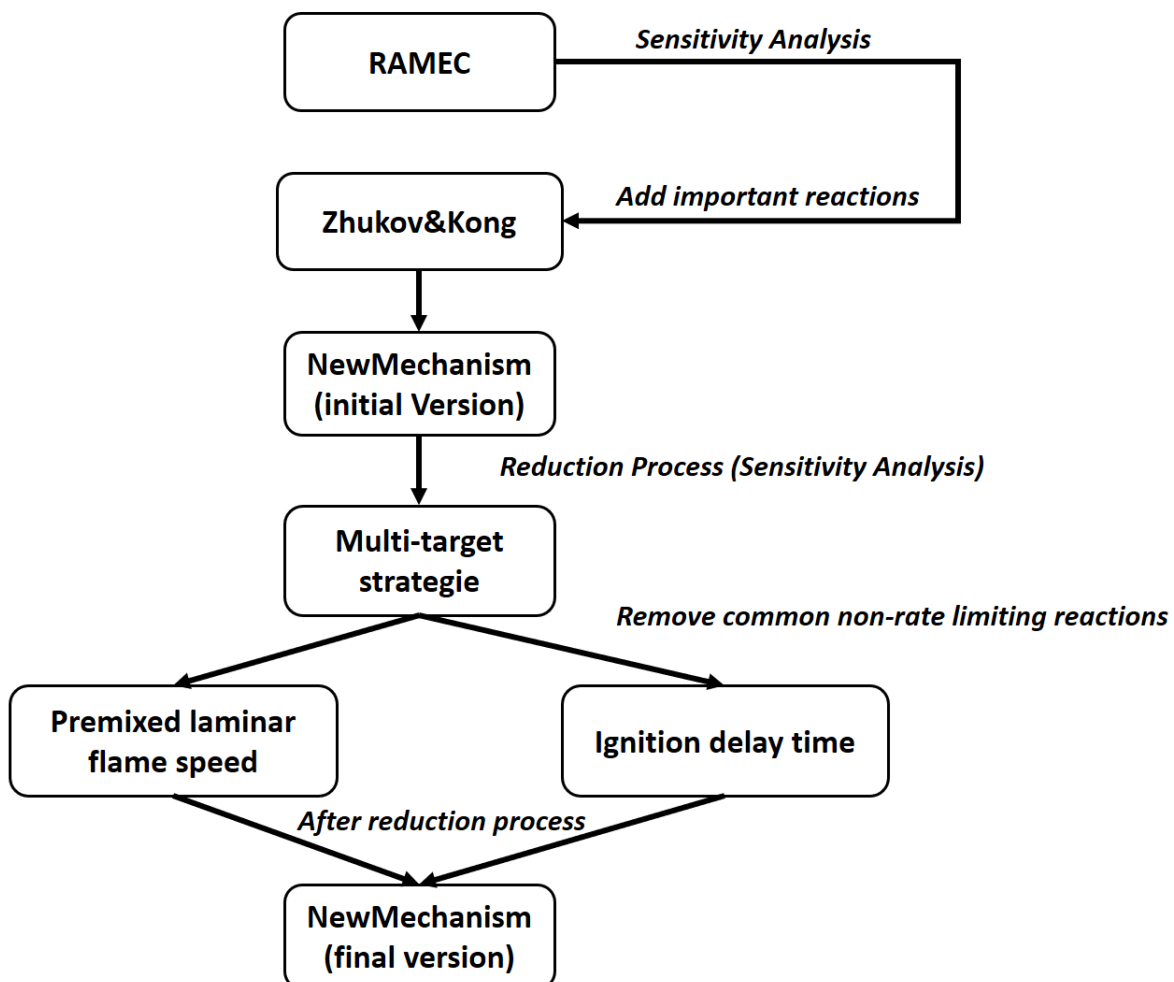


Figure 6.4.: Development strategy of NewMechanism.

First step of the development process of NewMechanism

In the first step of the development process a sensitivity analysis of premixed laminar flame speed is conducted using RAMEC, which is the parent reaction mechanism of C1-C4 Zhukov and Zhukov & Kong. Since C1-C4 Zhukov is optimized for higher hydrocarbons and therefore it contains 2329 reactions and 207 species, while RAMEC is an optimized CH₄/O₂ reaction mechanism for elevated pressures. As compared to C1-C4 Zhukov RAMEC only contains 190 reactions and 38 species. Therefore the better strategy would be to use RAMEC as a parent reaction mechanism instead of C1-C4 Zhukov in the sensitivity analysis to determine important reactions for premixed laminar flame speed, and include these reactions to Zhukov & Kong. A sensitivity analysis of premixed laminar flame speed is conducted for a wide range of conditions ranging from 15 atm to 100 atm and equivalence ratio of 0.5 to 2. The reactions, which are commonly important for these conditions are determined and added to Zhukov & Kong.

Identifying these important reactions is a very complex process. Because a reaction could be rate limiting for a specific condition, and as a result it could have a greater impact on the premixed laminar flame speed at this specific condition. But at other conditions the same reaction would become non-rate limiting and therefore it would be negligible. In Figure 6.5 the sensitivity of premixed laminar flame speed to two reactions from RAMEC is shown to illustrate the complexity of identifying common rate limiting reactions.

The reaction (Figure 6.5 (b)) of H₂O dissociation into OH and H radical shows a higher impact on the premixed laminar flame speed at 60 atm for fuel rich mixtures ($\phi = 1.0 - 1.5$), while for fuel lean condition ($\phi = 0.5$) it becomes negligible. Considering the influence of this reaction at 20 atm on premixed laminar flame speed a similar behaviour is shown, only for the specific condition of a stoichiometric mixture ($\phi = 1$) it has a greater influence on the premixed laminar flame speed. But for other conditions its impact is almost negligible ($\phi = 0.7$ or 1.4). The other reaction (Figure 6.5 (a)) is rate limiting at 20 atm for a equivalence ratio of 0.7 to 1. But it becomes non-rate limiting for the same pressure (20 atm) for fuel rich mixture ($\phi = 1.4$). At higher pressure (60 atm) it influences the premixed laminar flame speed for mixtures with an equivalence ratio of 0.5 - 1. But for rich mixture its influence is negligible. This behaviour of reactions makes the identification process of rate limiting very complex and time consuming. After the sensitivity analysis of premixed laminar flame speed with RAMEC 44 missing reactions in Zhukov & Kong are considered to be rate limiting for one of the load points within a range of pressures from 15 - 100 atm and equivalence ratio of 0.5 - 2. These reactions can be found in Appendix E. An initial version of a new CH₄/O₂ reaction mechanism named NewMechanism is developed by adding these 44 rate limiting reactions for premixed laminar flame speed to Zhukov & Kong. After the first step of the development process NewMechanism contains 94 reactions and 32 species. The initial version of NewMechanism and Zhukov & Kong are validated against premixed laminar flame speeds and ignition delay times. A significant improvement regarding the accuracy of predicting the laminar flame speed has been

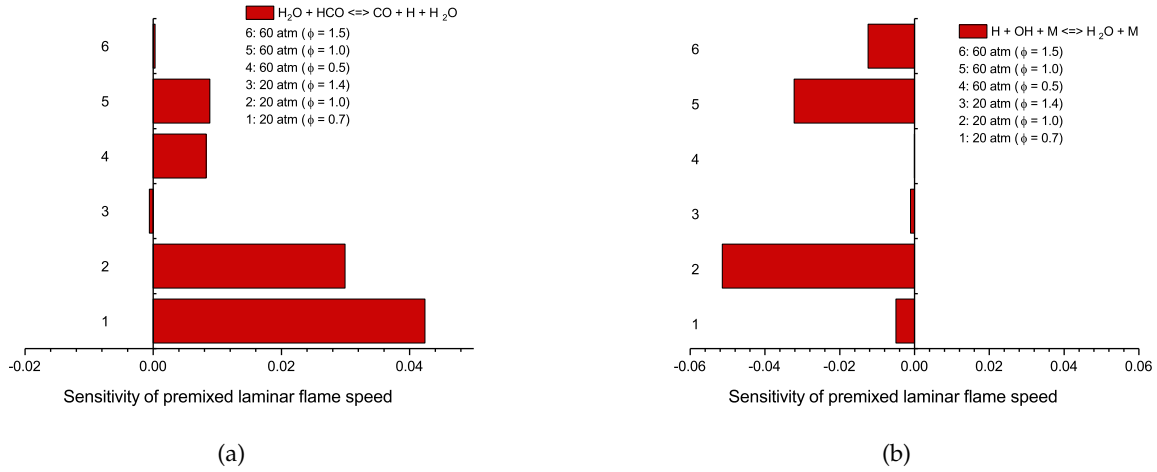


Figure 6.5.: Sensitivity analysis of premixed laminar flame speed at different conditions.

achieved by the initial version of NewMechanism as compared to Zhukov & Kong as shown in Figure 6.6. Zhukov & Kong does not predict the typical profile of laminar speed , which increases until the stoichiometric equivalence ratio ($\phi = 1$) and then starts decreasing. As compared to Zhukov & Kong NewMechanism achieves a far better accuracy of predicting laminar flame speed and also its typical profile (Figure 6.6).

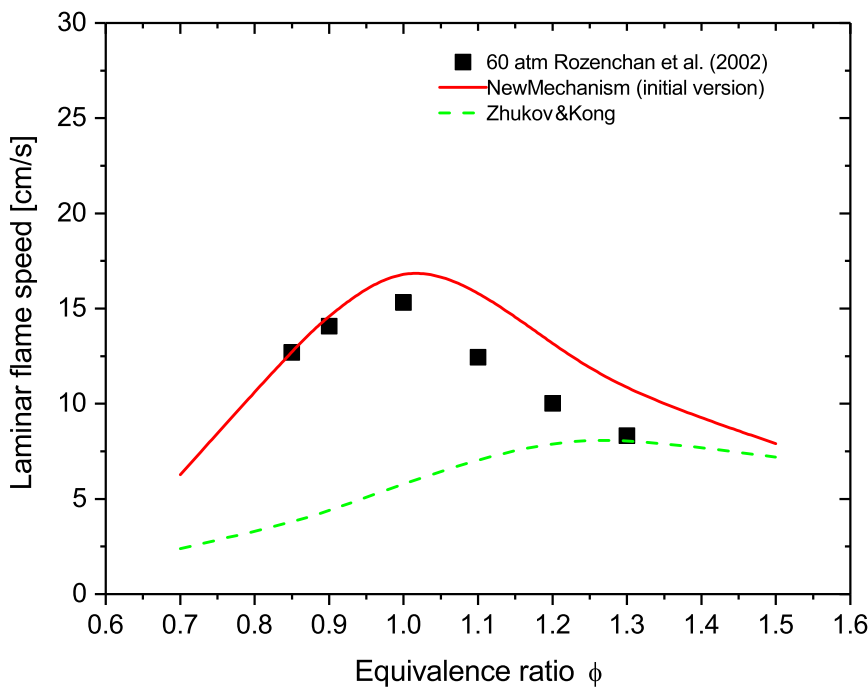


Figure 6.6.: Comparison of predicted premixed laminar flame speed by NewMechanism and Zhukov & Kong with experimental values.

When comparing the validation results of ignition delay time (Figure 6.7) NewMechanism predicts a lower ignition delay time than the measured value in the experiment. But Zhukov & Kong shows a much better accuracy of predicting the ignition delay time. One of the reason, why the accuracy of predicted ignition delay time by initial version of NewMechanism has declined by adding these 44 reactions and 8 species to Zhukov & Kong, could be the higher amount of chain-branching reactions in NewMechanism. Because it predicts an accelerated ignition (lower ignition delay time) as compared to the experimental value or Zhukov & Kong (Figure 6.7). This is a typical behaviour of a reaction mechanism, which contains higher amount of chain-branching reactions. Since these reactions lead to rapid formation of radicals, which initiate an accelerated ignition [28]. The same behaviour is shown by NewMechanism. It predicts an accelerated ignition after adding the 44 reactions and 8 species from RAMEC to Zhukov & Kong in the first development process of NewMechanism.

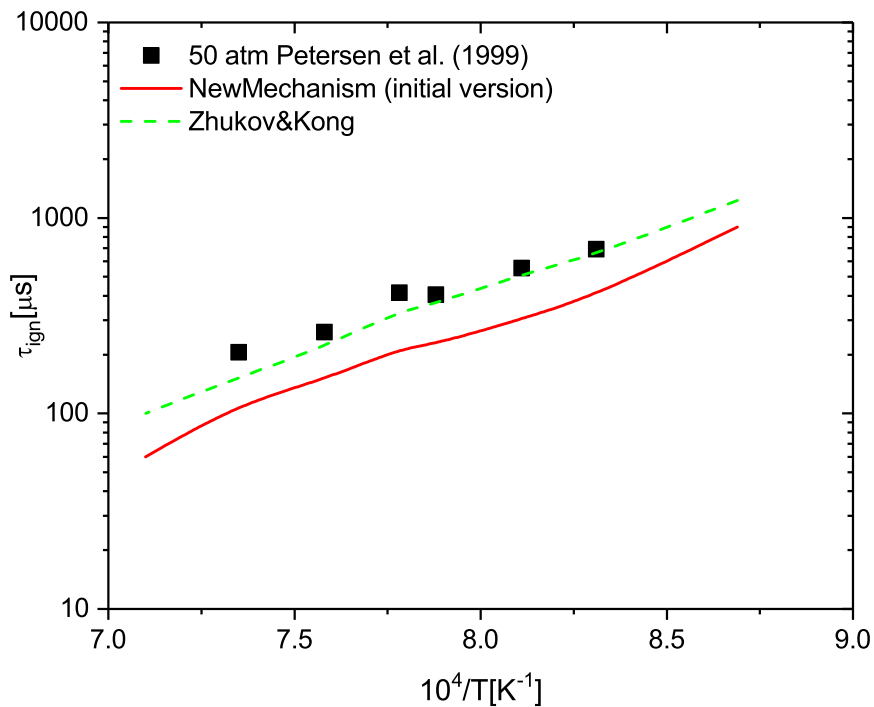


Figure 6.7.: Predicted ignition delay time by the reaction mechanisms NewMechanism and Zhukov & Kong and its comparison with experimental values.

Second step of the development process of NewMechanism

In the next step of the development process a multi-target strategy is applied. The aim is to determine common non rate limiting reactions for premixed laminar flame speed and ignition delay time, so that the initial version of NewMechanism can be reduced. Furthermore the accuracy of predicting ignition delay should also be improved by identifying the chain branching reactions, which lead to an accelerated ignition.

A further study of sensitivity analysis is conducted using the initial version of NewMechanism at a wide range of pressures from 15 to 100 atm and equivalence ratio of 0.5 - 2. After identifying a common non rate limiting reaction for several load points of premixed laminar flame speeds, this reaction is removed and the accuracy of predicted ignition delay time by NewMechanism is checked.

If it can be confirmed, that the removed reaction has negligible impact on the premixed laminar flame speeds and on ignition delay times as well, this leads to a permanent removal of this reaction, otherwise it is added back to NewMechanism, and the iteration is started again. As previously mentioned identifying a non rate limiting reaction for a wide range of load points is a very complex and time consuming procedure, which can take hundreds of iterations. Since a reaction can be non rate limiting for a specific load point, but for others it can have a great impact on the selected parameter in the sensitivity analysis as shown in Figure 6.5.

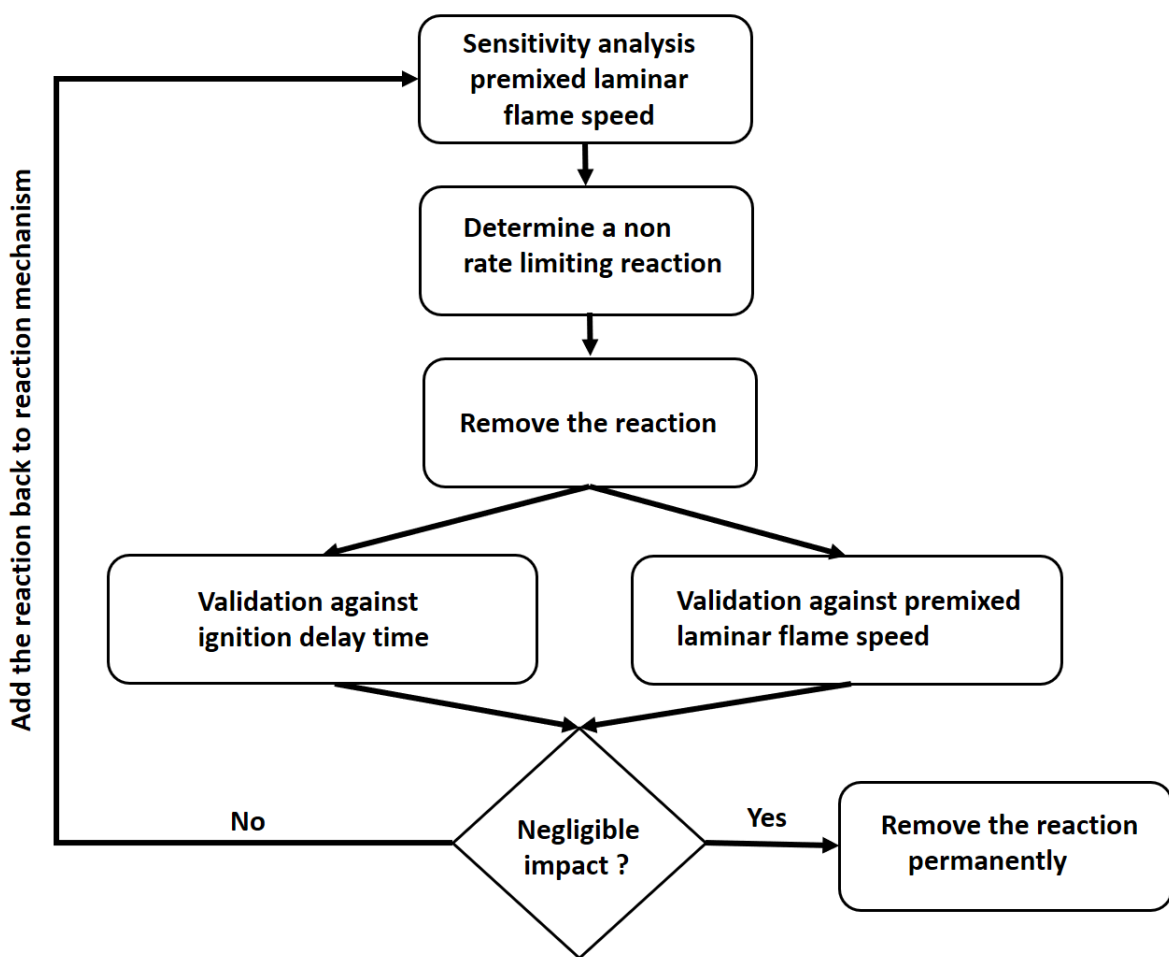


Figure 6.8.: Multi-target reduction strategy applied in the reduction process of NewMechanism

In the reduction process removing the reaction shown in Equation 6.1 led to a significant improvement of accuracy of NewMechanism predicting ignition delay time and premixed laminar flame speed as well as shown in Figure 6.9 and Figure 6.10. The version of NewMechanism with the reaction (Equation 6.1) predicts an accelerated ignition (lower ignition delay time), which would mean, as assumed previously, that this version of NewMechanism contains higher amount of chain branching reactions. Since these reactions produce radicals, which initiate the ignition process. If a reaction mechanism contains higher amount of chain branching reaction, it would predict an accelerated ignition. But the reaction shown in Equation 6.1 is not a chain branching reaction. Because this reaction leads to major sink of CH₃ radical, and it does not produce any ignition promoting radicals for instance OH or H radical.



A reason could not be found in this thesis, why the removal of the reaction (Equation 6.1) led to a significant improvement of accuracy of NewMechanism predicting both widely used validation parameters ignition delay time and premixed laminar flame speed. Therefore further investigations are needed to find out reason behind it. In the end of the reduction process the initial version of NewMechanism (94 reactions and 32 species) could reduced to the final version with 53 reactions and 26 species. For CH₄/O₂ combustion CFD simulation the species N₂, He and Ar, and the two reacions with N₂ and Ar can be removed from NewMechanism. This leads to 51 reactions and 23 species.

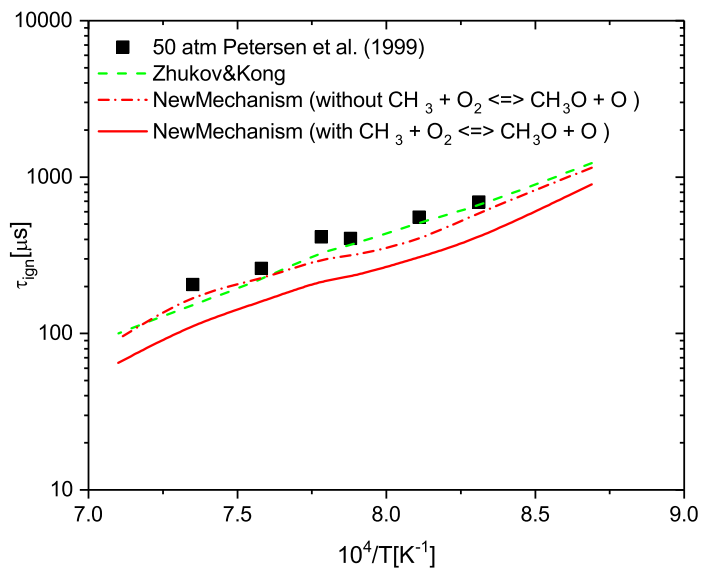


Figure 6.9.: Predicted ignition delay time by the reaction mechanism and its comparison with experimental values.

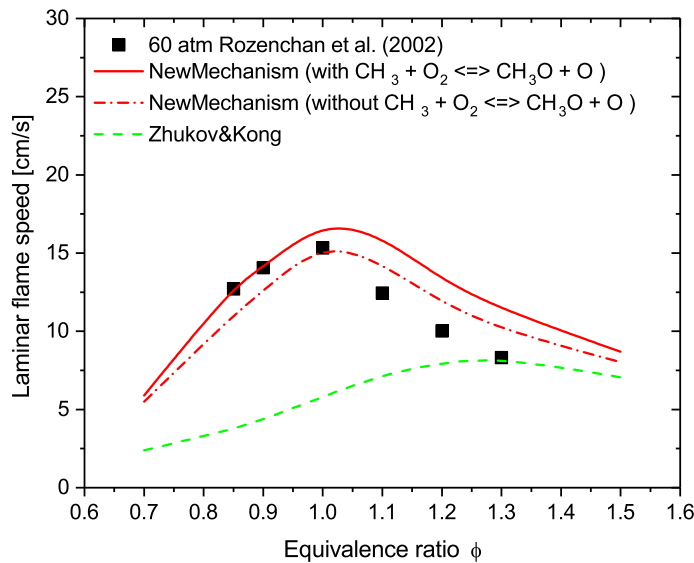


Figure 6.10.: Predicted premixed laminar flame speed and its comparison with experimental values.

An important evidence could be achieved in this thesis, that a higher number of reactions and species does not necessarily result in higher accuracy of a reaction mechanism predicting ignition delay time or premixed laminar flame speed. The accuracy of the initial version and final version of NewMechanism are taken into account to illustrate this phenomenon. The initial version of NewMechanism contains after the sensitivity analysis with RAMEC 94 reactions and 32 species. But its accuracy is lower than the final version of NewMechanism, which only contains 53 reactions and 26 species.

The comparison of accuracy of both versions of NewMechanism can be found in Appendix B. Before a reason behind this phenomenon can be delivered, further fundamental investigations are required. One could assume, that the final version is better optimized, because it contains the right combination of chain-branching and chain- termination reaction. But these are only assumptions without a proof. Therefore further research is recommended for a better understanding of this phenomenon.

6.3. Validation

Ignition delay time

The newly developed CH₄/O₂ reaction mechanism named NewMechanism is validated against a wide range of experiments (13 experiments) of ignition delay time from low pressure of 15 atm to very high pressure of 450 atm, and equivalence ratio of 0.4 - 6. Furthermore the accuracy of NewMechanism is compared with other reaction mechanisms from Table 1.1. Two validation results of ignition delay time experiments at different conditions are illustrated in Figure 6.11 and Figure 6.12, other validation results of all 13 tests can be found in Appendix E.

The accuracy of predicting ignition delay time is determined using the absolute mean percentage error (MAPE), the results are shown in Table 6.2.

As one can see in Figure 6.11 NewMechanism is able to predict the ignition delay time at 100 atm very accurately. NewMechanism produces an absolute mean percentage error of about 17% from the experimental values, which is comparable with its parent reaction mechanisms Zhukov & Kong, C1-C4 Zhukov and RAMEC. As discussed in Chapter 5 Red.Slavinskaya is not optimized for high pressure conditions, therefore it produces an error of 87% for predicting ignition delay time at 100 atm. But the error decreases at low pressure conditions of 25 atm, where Red.Slavinskaya predicts the igniton delay time with an error of 30%, which is a significant improvement considering the error of 87% at 100 atm. Tiafeng Lu accuracy also decreases at low pressures. It produces an error of 986% for predicting ignition delay time at 100 atm. But at low pressure conditions of 25 atm Tiafeng Lu shows a significant improvement of predicting ignition delay time, where it has an error 73%.

The global chemistry based reaction mechanism Jones–Lindstedt (Frassoldati) fails to predict igniton delay time for both tests (test 1, test2). For both test conditions it has a MAPE of greater than 1000%. As compared to Jones-Lindstedt (Frassoldati) Westbrook & Dryer (Airbus DS) delivers unexpectedly an error of about 80% for both tests. As discussed in Chapter 5 one of the reason, why a global chemistry based reaction mechanism (Westbrook & Dryer) has a competitive accuracy, which is comparable with other reaction mechanisms for instance Red.Slavinskaya at high pressures could be the modification by Riedmann et al. [34]. The authors added an important reaction (Equation 5.1) to the original version of Westbrook & Dryer. This reaction captures water dissociation and recombination effects occurring due to the elevated temperatures. The importance of this reaction is shown in the sensitivity analysis of premixed laminar flame speeds in Figure 6.5(b). Zhukov & Kong and its parent reaction mechanisms C1-C4 Zhukov and RAMEC achieve a similiar accuracy, since these reaction mechanisms have been optimized for high pressure conditions, they deliver an error of about 16 - 17 % for test 1 with 100 atm. But considering the error of 22 - 29% for test 2 at 25 atm their accuracy decreases slightly with decreasing pressure as expected. REDRAM shows a similar accuracy as Zhukov & Kong. The reason behind the similar accuracy of REDRAM, Zhukov & Kong, C1-C4 Zhukov is, that all of these reaction mechanisms are derived from RAMEC. As a result all four of them shows a similar behaviour. GRI-MECH 3.0 delivers an error of 183 % for test 2 with 25 atm, but for high pressure condition for instance test 1 with 100 atm, the error decreases to 12%. The validation results of ignition delay time of all reaction mechanism except NewMechansim have been already discussed in Chapter 5, therefore only a brief discussion of the results with focus on NewMechanism is given in this chapter.

As previously mentioned the reaction mechanims have been validated in this thesis against a wide range of pressures (15 - 450 atm) and equivalence ratio of 0.4 - 0.6. The validation results are given in Appendix E. Furthermore an absolute mean percentage error produced by each reaction mechanism for all 13 tests is given in Table 6.2. Considering the validation of

all reaction mechanisms for all 13 ignition delay time tests, a statement can be made for the suitability of the reaction mechanism to predict ignition delay time. C1-C4 Zhukov, Zhukov & Kong, RAMEC and REDRAM are able to predict ignition delay time for a wide range of conditions, they are better optimized for elevated pressures of up to 50 atm. But at lower pressures (15 - 25 atm) their accuracy of predicting ignition delay time is still in an acceptable range and comparable with other reaction mechanism, which are optimized for low pressure conditions for instance Red.Slavinskaya.

Red.Slavinskaya is optimized for lean mixtures and low pressures, therefore it delivers good validation results under an equivalence ratio of 1 and pressure of 25 atm. But this reaction mechanism is not able to predict ignition delay time for rich mixtures or elevated pressures. Tiafeng Lu is the other reaction mechanism, which is optimized for low pressures. As compared to Red.Slavinskaya Tiafeng Lu delivers a high error of greater than 1000% for test up to 20 atm. This reaction mechanism is only able to predict ignition delay time with an acceptable error of under 100% for low pressures. Under 20 atm pressure conditions Tiafeng Lu can deliver accurate results for ignition delay time for lean mixtures and rich mixtures as well (Appendix E).

The global chemistry based reaction mechanisms Jones-Lindstedt (Frassoldati) and Westbrook & Dryer (Airbus DS) show very different accuracy of predicting ignition delay time. Jones-Lindstedt (Frassoldati) fails to predict ignition delay time for any pressure condition up to 15 atm and equivalence ratio of up to 0.4. It has to be mentioned, that only relevant experiments up to 15 atm of ignition delay time are considered in this thesis. The reason behind the great MAPE, as produced by Jones-Lindstedt (Frassoldati) could be, that it has been developed according to global modeling methods. Therefore it does not contain any elementary reactions. The missing elementary reactions could lead to this unacceptable error of greater than 1000%. On the contrary the other global chemistry based reaction mechanism Westbrook & Dryer delivers acceptable error for all evaluated pressures and equivalence ratios ranges, which is under 100%. GRI-Mech 3.0 is suitable for intermediate pressure conditions. It is able to predict ignition delay time for pressures up to 5 - 450 atm and lean mixtures with a similar accuracy as compared to NewMechanism, Zhukov & Kong, C1-C4 Zhukov and RAMEC. In case of rich mixtures ($\phi > 1$) its accuracy decreases, but it remains still in acceptable range of an error of about 100%. The newly developed reaction mechanism in this thesis NewMechanism can be applied for a wide range of conditions. It is optimized for elevated pressures of 50 - 450 atm, but is also able to predict ignition delay for low pressure conditions of under 25 atm. Considering the equivalence ratio NewMechanism is not limited to a specific application for lean or rich mixtures as shown in Appendix E. When comparing the validation results of NewMechanism with other reaction mechanism, it can be said, that NewMechanism delivers an accuracy, which is comparable with the detailed reaction mechanisms C1-C4 Zhukov and RAMEC. The other two reduced reaction mechanisms Zhukov & Kong and REDRAM achieve a similar accuracy of predicting ignition delay time.

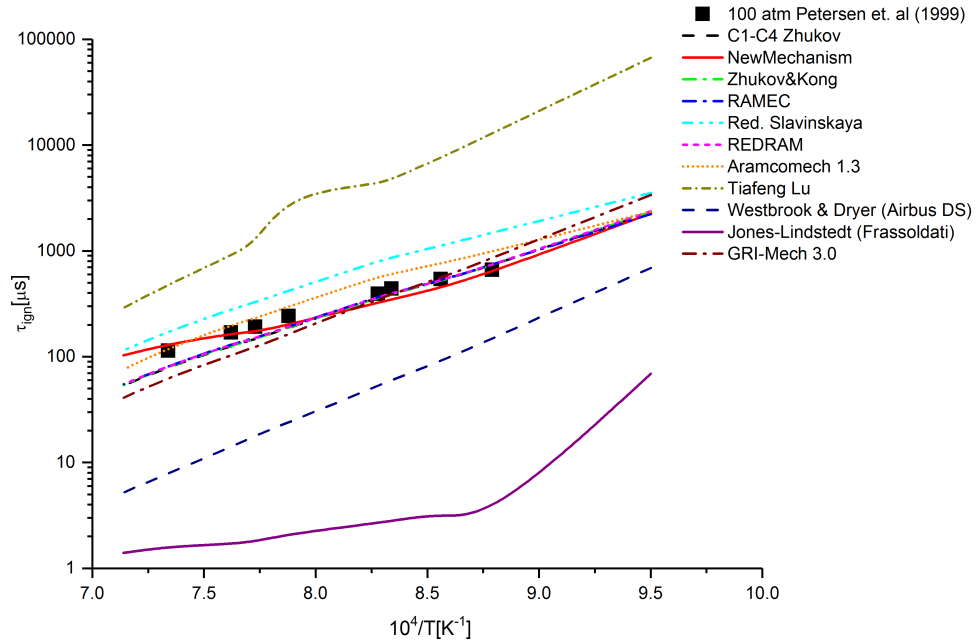
Test 1: $\phi = 0.4$, $p = 100$ atm, mixture = CH₄/(O₂+Ar)

Figure 6.11.: Comparison of simulation results using different reaction mechanisms with experimental values at 100 atm.

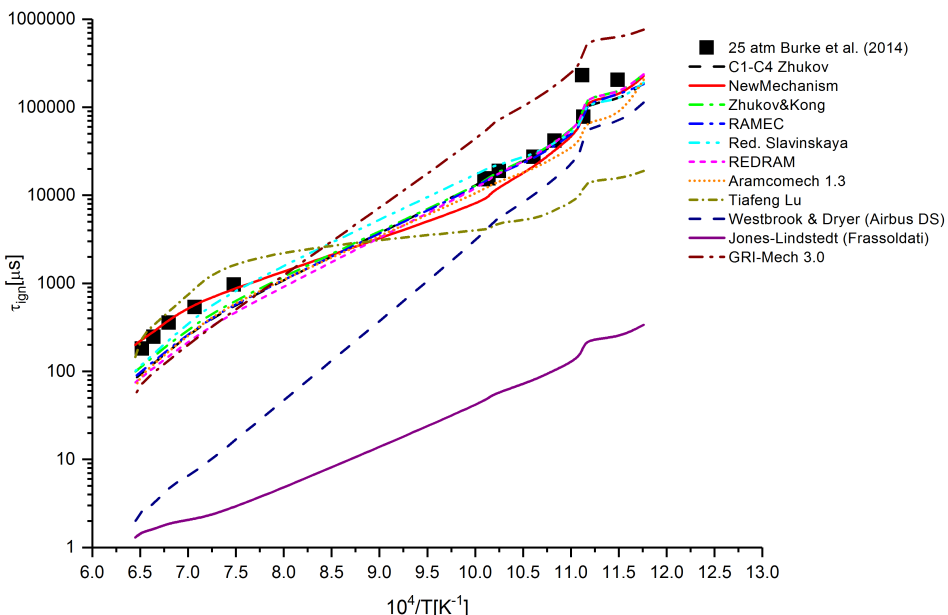
Test 2: $\phi = 2$, $p = 25$ atm, mixture = CH₄/(O₂+N₂)

Figure 6.12.: Comparison of simulation results using different reaction mechanisms with experimental values at 25 atm from [12].

Table 6.1.: Absolute mean percentage error from experimental values of each reaction mechanism.

Reaction mechanism	MAPE (test 1)	MAPE (test 2)	MAPE (all 13 tests)
C1-C4 Zhukov	18%	29%	22%
NewMechanism	22%	25%	22%
Zhukov & Kong	36%	22%	23%
RAMEC	19%	29%	22%
Red.Slavinskaya	14%	30%	85%
REDRAM	79%	22%	24%
Aramcomech 1.3	15%	36%	40%
Tiafeng Lu	986%	73%	>1000%
Westbrook & Dryer (Airbus DS)	88%	80%	92%
Jones–Lindstedt (Frassoldalti)	>1000%	>1000%	>1000%
GRI-Mech 3.0	12%	183%	93%

Premixed laminar flame speed

The validation results of premixed laminar flame speed have been already discussed in Chapter 5. The low accuracy of Zhukov & Kong of predicting premixed laminar flame speed as illustrated in Section 5.2 led to the development of NewMechanism. Therefore the focus of this brief discussion is the comparison of accuracy of Zhukov & Kong and NewMechanism with other reaction mechanisms. As previously described NewMechanism is developed in two basic development steps. In both development steps sensitivity analysis of premixed laminar flame speed was conducted to identify important reactions, which could have been removed in the last development step of Zhukov & Kong. So that these important reactions for predicting premixed laminar flame speed can be added to NewMechanism to increase the accuracy of predicting premixed laminar flame speed.

For the validation against premixed laminar flame speed 9 experiments with different mixtures, pressures and initial temperatures also referred as unburnt temperature are selected. No experiment with a pressure higher than 60 atm could be found in literature. Therefore 60 atm is the highest pressure and 5 atm the lowest pressure in the selected experiments. The validation results of all 9 experiments can be found in Appendix E. Two experiments conducted at 60 atm and 10 atm are selected for this brief discussion. The error (MAPE) produced by each reaction mechanism for test 1 (Figure 6.13), test 2 (Figure 6.14), and all 9 tests is given in Table 6.2.

NewMechanism delivers one of the best results for predicting premixed laminar flame as compared to other reaction mechanisms. A significant improvement could be achieved with NewMechanism as compared to its parent reaction mechanism Zhukov & Kong. In both tests

(test 1, test 2) Zhukov & Kong is not able to deliver accurate results. It produces the highest error of 43 - 48% as compared to other reaction mechanisms. In other tests, which can be found in Appendix E Zhukov & Kong accuracy still remains low for predicting premixed laminar flame speed. It produces an error of about 40% for all evaluated tests (Table 6.2). Furthermore it is also unable to predict the typical premixed velocity profile, which increases until the stoichiometric ratio ($\phi = 1$) and then starts decreasing. On the contrary NewMechanism describes the typical premixed laminar flame velocity profile very accurately. Other detailed reaction mechanism for instance C1-C4 Zhukov, RAMEC, Aramocmech 1.3 achieve a similar accuracy like NewMechanism.

The global chemistry based reaction mechanism Jones–Lindstedt (Frassoldati) and Westbrook & Dryer (Airbus DS) show a very good accuracy for the 10 atm test (Figure 6.13), where Jones–Lindstedt and Westbrook & Dryer have an error of 15% and 28% respectively. This higher accuracy is only for this specific test. One can see in Figure 6.13 Jones–Lindstedt produces a constant flame velocity of around 35 cm/s for all equivalence ratio. The actual velocity varies from 32 - 50 cm/s. This would mean, that this low error by Jones–Lindsted and Westbrook & Dryer results from the calculation method of absolute mean percentage error. For other tests both reaction mechanisms deliver an error of above 100% (Table 6.2). More detail other the validation against premixed laminar flame speed can be found in Section 5.2

Test 1: p = 10 atm, T_u = 298 K, mixture = CH₄/(O₂+He)

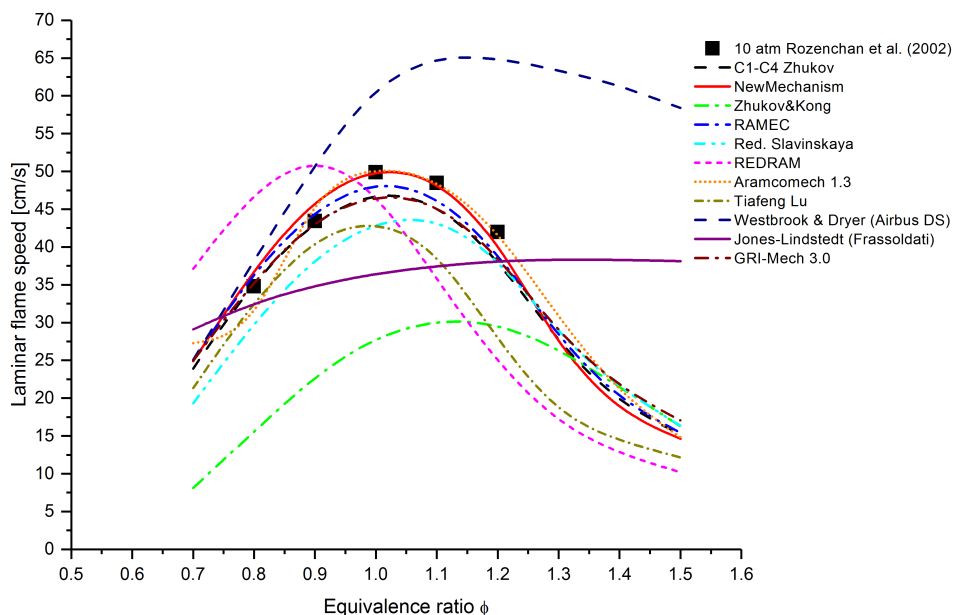


Figure 6.13.: Predicted premixed laminar flame speed by different reaction mechanisms and its comparison with experimental value at 10 atm

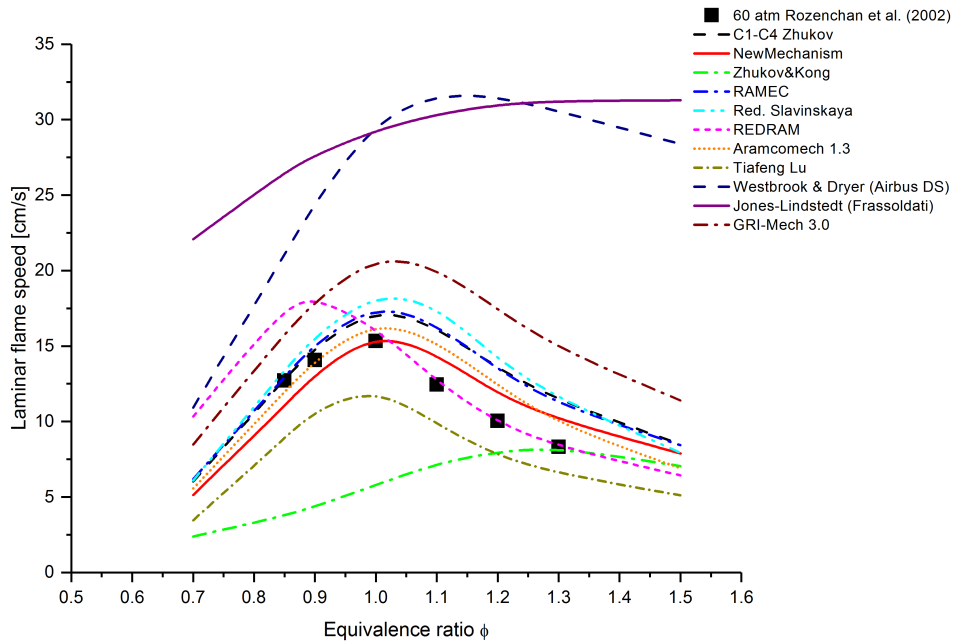
Test 2: p = 60 atm, T_u = 298 K, mixture = CH₄/(O₂+He)

Figure 6.14.: Comparison of simulation results using different reaction mechanisms with experimental values at 60 atm.

Table 6.2.: Absolute mean percentage error from experimental values of each reaction mechanism.

Reaction mechanism	MAPE (test 1)	MAPE (test 2)	MAPE (all 9 tests)
C1-C4 Zhukov	4%	20%	11%
NewMechanism	4%	13%	11%
Zhukov & Kong	43%	48%	40%
RAMEC	4%	21%	11%
Red.Slavinskaya	11%	27%	15%
REDRAM	26%	13%	42%
Aramcomech 1.3	7%	13%	8%
Tiafeng Lu	15%	23%	22%
Westbrook & Dryer (Airbus DS)	28%	145%	106%
Jones–Lindstedt (Frassoldati)	15%	154%	110%
GRI-Mech 3.0	9%	51%	18%

6.4. Verification

NewMechanism is further examined in a counterflow diffusion flame simulation. The aim is to conduct several counterflow diffusion flame simulations at different pressures with a very low scalar dissipation (χ), and compare the maximum temperature produced by each reaction mechanism with the theoretical flame temperature at equilibrium. This study cannot be used as a validation of the reaction mechanisms, because of lack of available suitable experimental data. Furthermore as discussed previously counterflow diffusion flame simulations are not suitable to make a statement about the accuracy of a reaction mechanism. Since NewMechanism delivers very accurate validation results for predicting igniton delay time and premixed laminar flame speed as well. But an important question has to be answered. Is NewMechanism also able to produce the same maximum temperature as its parent reaction mechanisms?

One of the main reasons to conduct this study are the validation and counterflow diffusion flame results (Figure 6.3) of the reduced reaction mechanism REDRAM. This reaction mechanism delivers very accurate results for predicting ignition delay time, but it is unable to predict premixed laminar flame speed or its typical profile. Moreover in the counterflow diffusion flame simulation REDRAM produces much lower temperature than the other reaction mechanism. It produces a maximum temperature of 3200 K at a stoichiometric mixture fraction of 0.2. As compared to other reaction mechanisms this temperature is about 280 K lower the temperature, predicted by the other reaction mechanisms (about 3480 K).

As previously described in Section 2.3 the scalar dissipation (χ) describes the degree of departure from the chemical equilibrium. A value of scalar dissipation of 0 refers to equilibrium. The higher the value of scalar dissipation is, the higher is the departure from the equilibrium. A higher value of scalar dissipation leads to higher diffusion, which results in rapid transport of cool material towards the flame. The chemical reactions cannot occur fast enough to maintain a sufficient pool of reactive species against the flow of incoming reactants in the counterflow diffusion flame simulation. This leads to extinction of the flame as shown in Figure 2.5. In a combustion process a higher value of scalar dissipation would mean, that the heat diffuses faster away from the reaction zone, which results in lower temperature. This temperature decrease associated with higher scalar dissipation is illustrated in Figure 6.15.

The widely known tool Chemical Equilibrium with Application (CEA) is utilized to calculate the theoretical equilibrium temperature values according to the mixture fraction. The maximum temperature predicted by CEA is a good indicator of the highest occurring temperature in a combustion process. Therefore conducting a counterflow diffusion flame simulation at a scalar dissipation of 0 would be ideal for the comparison, since a value of 0 refers to equilibrium, and a higher value indicates the departure from the equilibrium. Unfortunately the Cantera code shows major convergence problems at very small scalar dissipation values.

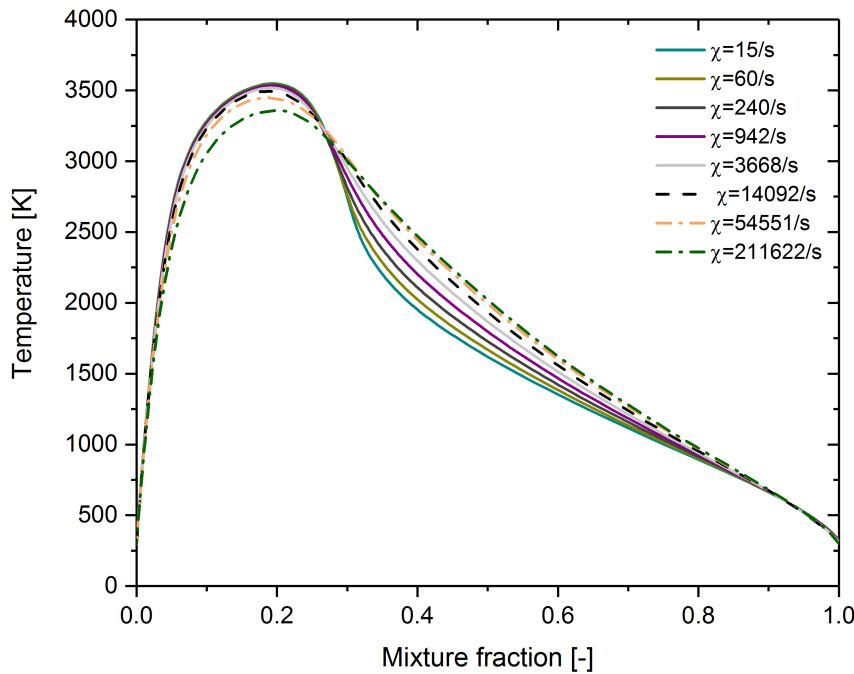


Figure 6.15.: Maximum temperature profile over mixture fraction at different scalar dissipation.

A specific minimum value of scalar dissipation, at which convergence problems occur, can not be determined. Because this value depends on pressure and the used reaction mechanism in the counterflow diffusion flame simulation. A reason for this, could be the sensitivity of reaction mechanisms to the applied pressure. Since some of the reaction mechanisms are optimized for low pressures (Red.Slavinskaya, Tiafeng Lu) as discussed before. Therefore the counterflow diffusion flame simulations conducted at high pressure (up to 60 bar) and low scalar dissipation ($\chi < 0.5$) with Red.Slavinskaya and Tiafeng Lu showed major convergence problems. Furthermore a converged solution using global chemistry based reaction mechanism Jones-Lindstedt (Frassoldati) and Westbrook & Dryer could not be found at high pressure and low scalar dissipation. Therefore the global chemistry reactions mechanisms and the detailed higher hydrocarbons reaction mechanims C1-C4 Zhukov and Aramcomech 1.3 are not included in this study. The reason for excluding the higher hydrocarbons reaction mechanisms is the prohibitive computational time needed for a counterflow diffusion flame simulation, which normally takes about several minutes (2-3 minutes) depending on the used reaction mechanism. In case of using higher hydrocarbons the computational time would increase to some days.

Four different verification tests at high pressure and low scalar dissipation are counducted in this study. The results of all four tests can be found in Appendix F. One of the test at 60 bar and χ of 0.5 is illustrated in Figure 6.16 . As expected all reaction mechanisms except REDRAM predict an identical maximum temperature at the stoichiometric mixture fraction. Only

REDRAM predicts a much lower temperature than the theoretical maximum temperature.

Test: $\chi = 1.5$, $p = 60$ bar, mixture = CH₄/O₂

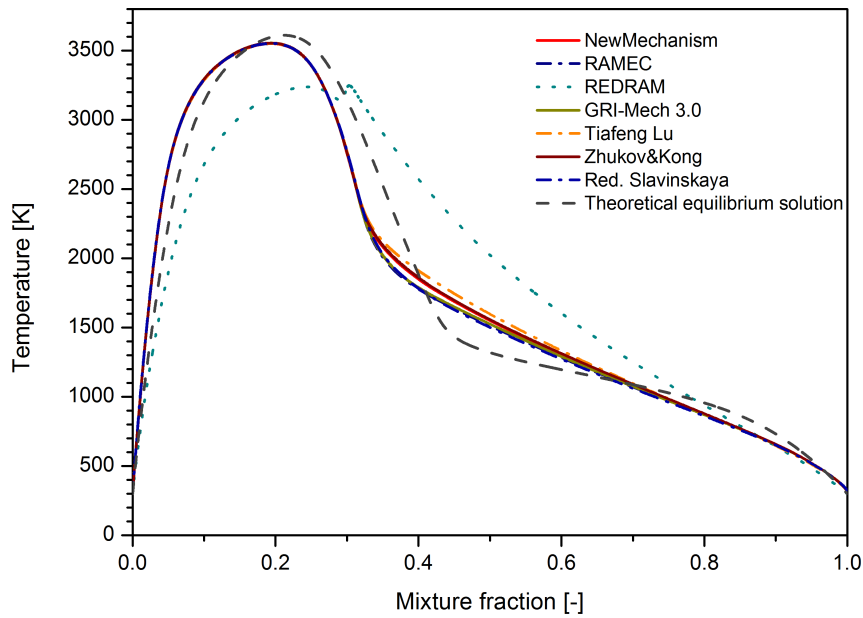


Figure 6.16: Comparison between theoretical equilibrium temperature with temperature profile of different reaction mechanisms at 60 bar over mixture fraction.

Three different reasons for a lower temperature than the theoretical maximum value can be identified. First as previously mentioned a scalar dissipation of 0 refers to equilibrium, a higher value than 0 indicates the departure from equilibrium. A value of 0 cannot be reached due to convergence problems by the Cantera code. Furthermore studying the Cantera code of counterflow diffusion flame in detail leads to the evidence, that the code does not produce an adiabatic flame, which results from its fluctuating enthalpy profile. This is the second reason for a lower temperature predicted by the reaction mechanisms. The third reason is, that a higher scalar dissipation ($\chi > 0$) results in higher diffusivity. This effect is investigated by Perakis in [6]. The author conducted several counterflow diffusion flame simulations using CH₄/O₂ at 1 bar and different scalar dissipation. At higher scalar dissipation CH₄ molecules enter the oxidizer-rich domains, which refers to a mixture fraction of greater than 0.2 as illustrated in Figure 6.17. As a result less methane is available for the formation of products and intermediate species. One can see in figure Figure 6.19, that the deperation from equilibrium leads to a decrease in mass fraction of H₂O and CO₂. As explained in Section 3 the formation of product and intermediate species influences the temperature. In the end a decrease in the formation of products due to methane diffusion into oxidizer rich domain results in lower temperature as well.

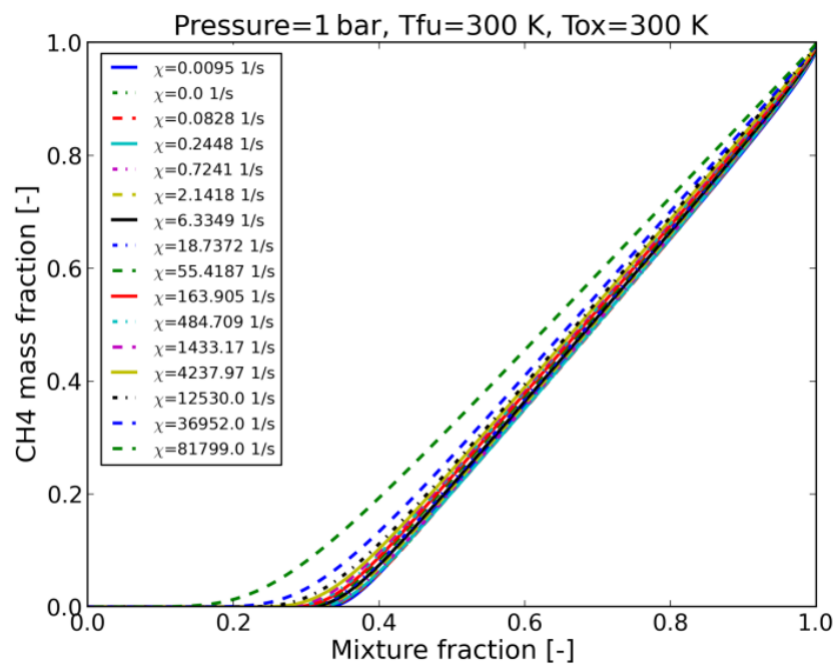


Figure 6.17.: CH₄ mass fraction over mixture fraction at different scalar dissipation [6].

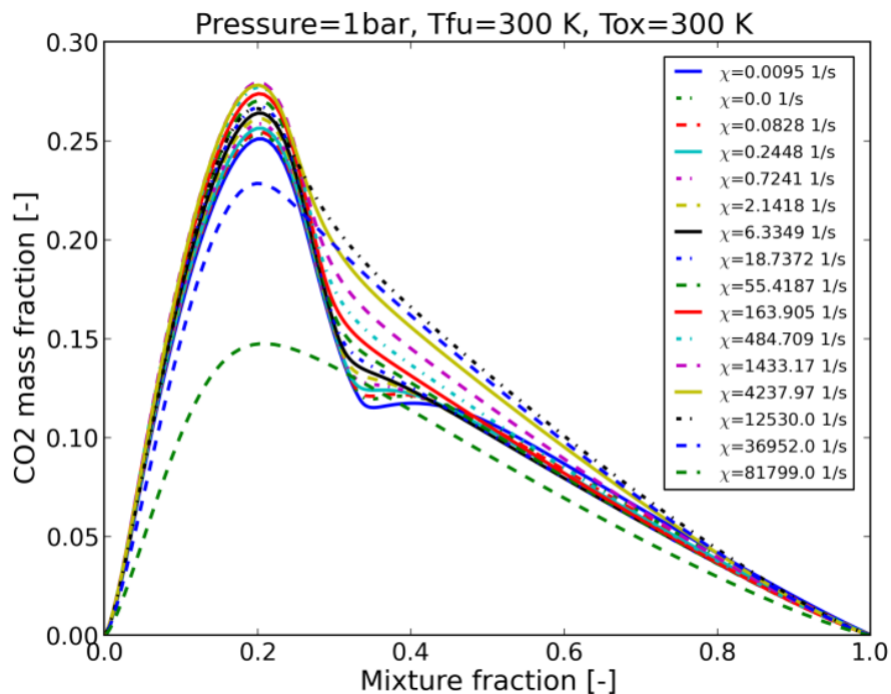


Figure 6.18.: CO₂ mass fraction over mixture fraction at different scalar dissipation [6].

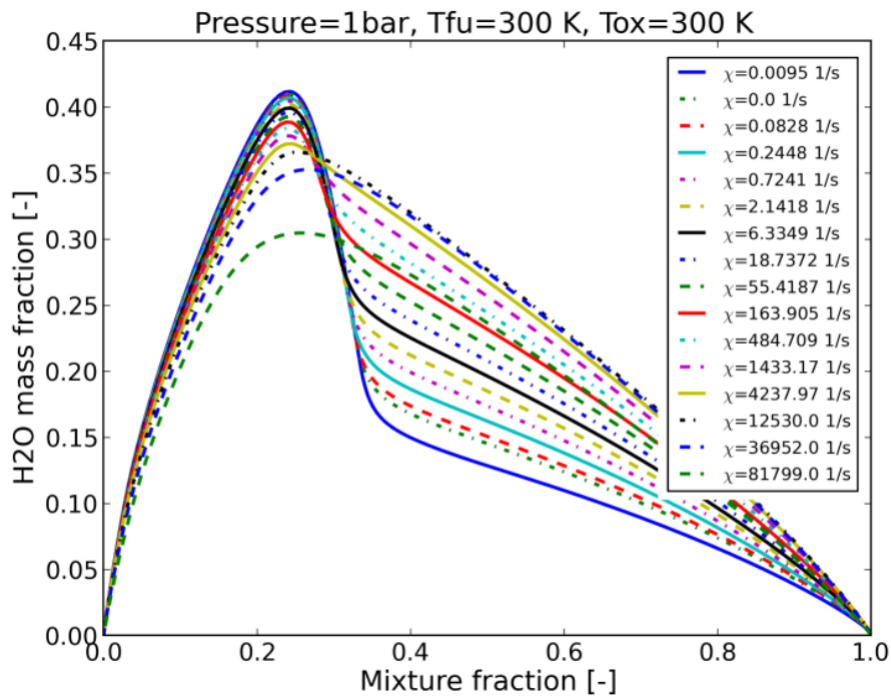


Figure 6.19.: H₂O mass fraction over mixture fraction at different scalar dissipation [6].

In this study it could be confirmed, that besides the good validation results of igniton delay time and premixed laminar flame speed NewMechanism is also able to produce the similar maximum temperature in counterflow diffusion flame simulation as its parent detailed reaction mechanism RAMEC.

7. 2D numerical simulation of the LUMEN nozzle

A 2D numerical simulation of LUMEN nozzle is conducted to investigate the impact of different chemistry models (frozen, finite rate and equilibrium chemistry) on the reactive centerline flow. The real nozzle flow is between the two extremes of equilibrium and frozen state, where it is closer to the frozen state considering the very low residence time of the flow in the nozzle, which cannot be enough sometimes under typical nozzle conditions (extremely high velocity) for a chemical reaction to occur [102]. The dimensionless Damkoehler number is used to describe the ratio of flow time scale (τ_f) to the chemical time scale (τ_c) as shown in Equation 2.47. A nozzle flow corresponds to very small Damkoehler number due to very high velocity, and resulting very small flow time scale.

The chemically frozen flow has a reaction rate of zero, and its gas composition is considered to remain constant from the combustion chamber outlet to the nozzle outlet. As a result no reactions and heat release occur inside the nozzle. On the contrary in the chemical equilibrium flow the reaction rate is considered to be infinite, and the gas adjusts its composition depending on the local temperature and pressure. The chemically frozen and chemical equilibrium are the two extreme descriptions of the actual condition of the real nozzle flow, which corresponds to a non equilibrium flow . For the description of non equilibrium flow a slow and complicated finite rate chemistry calculation is used in this thesis, which leads to a significant increase in computational times as compared to other chemistry models (frozen and equilibrium). Whereas the frozen flow chemistry model needs the lowest computational time, since the chemistry is assumed to be frozen.

The computational time in the finite rate chemistry model depends on the implemented reactions mechanism, where global chemistry based reaction mechanisms require the lowest computational time, and the detailed reaction mechanisms the highest. The computational time of reduced reaction mechanisms is significantly higher than the global chemistry based reaction mechanisms, but much lower than the detailed reaction mechanisms. The major reason for higher computational time of finite rate chemistry model in the CFD code, used in this thesis (ANSYS Fluent) is the number of species equations, which have to be solved, whereas the higher number of reactions have a minor effect on the computational time. A quantitative value for the required computational time for each reaction mechanism cannot be given, because the simulation cases were conducted using different computers with different computing power.

The main sources for the chemical reactions in the nozzle are, as follows

1. In case of an incomplete combustion in the combustion chamber unburnt fuel will lead to further combustion reactions in the nozzle. Moreover the dissociated species of combustion products for instance radicals will recombine as a result of rapid temperature drop due to flow expansion.
2. In case of a complete combustion only radical recombination will occur and effect the gas temperature in the nozzle.

Both scenarios combustion reactions and radical recombination are described by finite rate chemistry. A complete combustion of 100% is only a theoretical value, because even the most efficient combustion chambers achieve a combustion efficiency of about 90 - 97% [2]. Nevertheless a complete combustion is assumed in this numerical simulation, which is conducted using the newly developed CH₄/O₂ reaction mechanism named NewMechanism. Furthermore a comparison of different chemistry models impact on CH₄/O₂ and H₂/O₂ nozzle flow is also undertaken. A comprehensive H₂/O₂ reaction mechanism for high pressure combustion from Burke et al. [103] is utilized for H₂/O₂ LUMEN nozzle simulation. It has to be mentioned at this stage, that CH₄/O₂ will be used as propellants in LUMEN, therefore the conducted simulation with H₂/O₂ is only for a comparison from research point of view.

As mentioned before the commercial CFD solver ANSYS Fluent is used in this thesis, which uses the Finite Volume Method (FVM) for the numerical discretization of the partial differential equations (PDEs) into algebraic equations. Other methods for the numerical discretization of PDEs in space and time are Finite Difference Method (FDM) and Finite Element Method (FEM). All these three methods transform the PDEs into a system of nonlinear algebraic equations. Detailed information about the numerical discretization methods can be found in [72]. The detail description of numerical procedure, as applied in ANSYS Fluent is given in [65].

Considering the high velocity in the nozzle the flow is treated as inviscous in this simulation, as a result the turbulence and boundary layer effects are neglected. This simplification can be only made, if one is interested in the centerline flow. The aim of this study is to conduct a preliminary numerical simulation of the LUMEN nozzle, which is currently under development at DLR Lampoldshausen [35]. The LUMEN nozzle cannot be shown in this thesis, since no technical drawings are currently available. As a result the LUMEN nozzle for this numerical simulation is constructed with the help of available contour data.

The flow is assumed to be 2D axisymmetric. As a result only half of the nozzle is simulated. A structured mesh as shown in Figure 7.1 with around 52000 cells is used. The inlet gas composition and temperature at the nozzle entrance is determined with CEA assuming complete combustion at 60 bar for both cases (CH_4/O_2 and H_2/O_2). An oxidizer mass flow to fuel mass ratio (ROF) of 3.4 is used for CH_4/O_2 , which is one of the load point of LUMEN. A ROF of 6 is chosen for H_2/O_2 case, which corresponds to a real H_2/O_2 rocket engine for instance the first stage engine of Ariane 5 Vulcain [104].

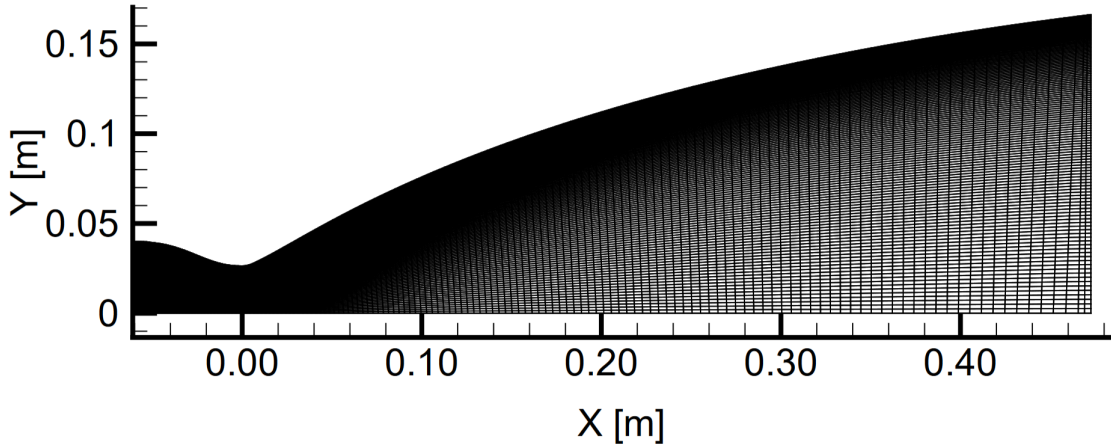


Figure 7.1.: Mesh of LUMEN nozzle.

7.1. Simulation results

For the frozen flow chemistry it is assumed, that the flow time scale is much smaller than the chemical time scale, corresponding to a very small Damkoehler number. This means, that the residence time of species is very small, therefore no chemical reactions or heat realease due to recombination of radicals occur inside the nozzle. As a result the gas composition remains constant. As shown in Figure 7.2 the centerline temperature of frozen flow (CH_4/O_2 and H_2/O_2) is much lower than the finite rate (non-equilibrium) and equilibrium chemistry flow. The temperature of frozen flow decreases due to expansion of the gas in the nozzle to around 1000 K for H_2/O_2 and CH_4/O_2 .

In case of equilibrium flow the recombination of major radicals for instance H and OH to H_2O as a result of flow expansion and temperature drop, leads to enormous release of chemical energy. A major portion of the chemical energy is converted to thermal energy, which increases the gas temperature as shown in Figure 7.2. As expected due to fast chemistry of $\text{H}_2\text{O}/\text{O}_2$ both chemistry models equilibrium and finite rate deliver the similar results for the temperature. On the contrary a significant difference is visible between equilibrium and finite rate flow for CH_4/O_2 as shown in Figure 7.2(b).

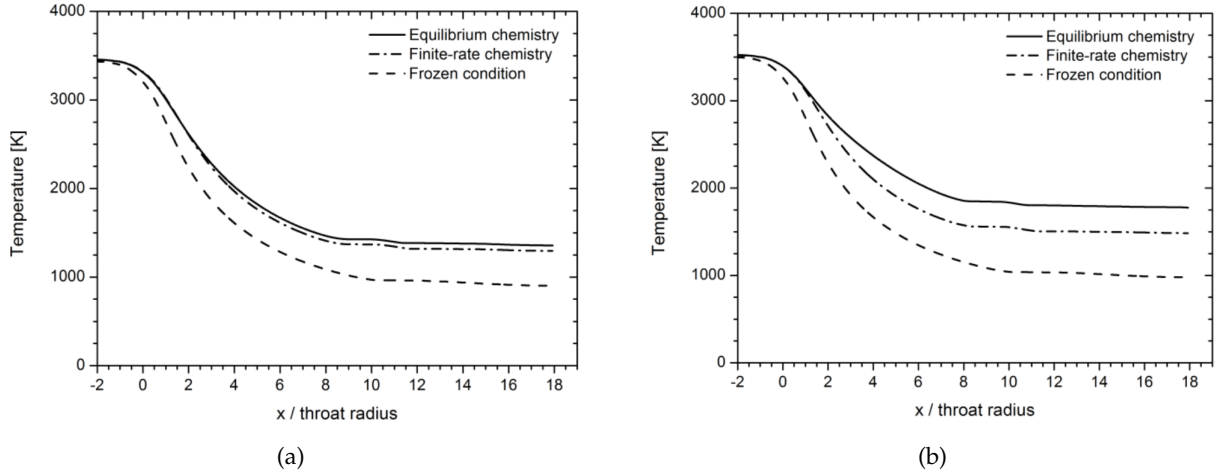


Figure 7.2.: Comparison of impact of different chemistry models on the centerline flow temperature of H₂/O₂ (a) and CH₄/O₂ (b).

In Figure 7.3 the impact of equilibrium and finite rate chemistry model on the CH₄/O₂ temperature distribution in the nozzle is illustrated. The upper part of the Figure 7.3 represents the equilibrium case and the bottom part the finite rate case. As one can see using the equilibrium chemistry model would lead to a overprediction of temperature and resulting heat flux in nozzle as compared to finite rate chemistry model. On the contrary both chemistry model equilibrium and finite rate would deliver a similar temperature distribution and resulting heat flux in case of H₂/O₂ as illustrate in Figure 7.4. Using a frozen chemistry model would underpredicts the temperature distribution and resulting heat flux distribution in both cases (CH₄/O₂ and H₂/O₂). This simulation is oversimplified, as discussed before, because it neglects the turbulence-chemistry interaction and boundary layer effects. Therefore a proper numerical simulation is required, so that a significant statement about the impact of chemistry model on heat flux distribution in the LUMEN nozzle can be delivered.

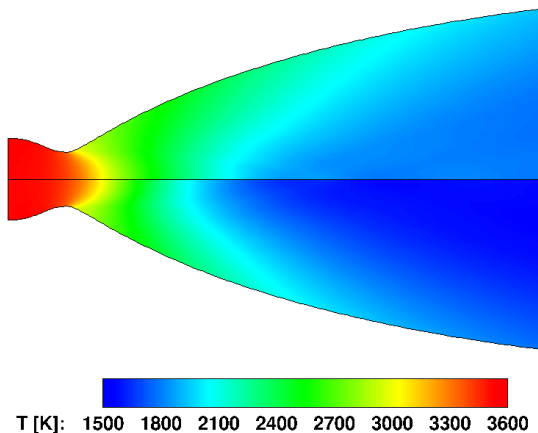


Figure 7.3.: CH₄/O₂ flow temperature distribution in the LUMEN nozzle (upper equilibrium and bottom finite rate chemistry).

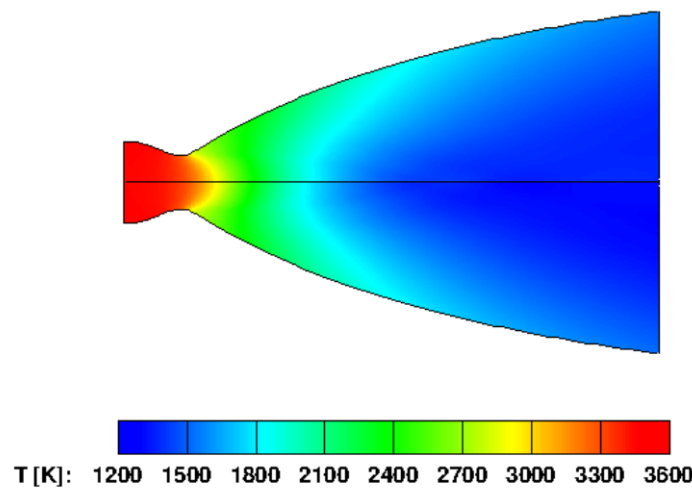


Figure 7.4.: H_2/O_2 flow temperature distribution in the LUMEN nozzle (upper equilibrium and bottom finite rate chemistry).

As discussed previously a major part of chemical energy release during the radical recombination process at equilibrium condition is converted to thermal energy, which increases the gas temperature. Only a minor portion of the chemical energy release is converted into mechanical energy to increase the pressure and velocity as shown in Figure 7.5 Figure 7.6, which contribute to the thrust, hence both chemistry models equilibrium and finite rate chemistry would predict similar thrust, whereas the frozen flow model would underpredict the thrust slightly. But considering very small Damkoheler number in the nozzle frozen flow is a sufficient chemistry model to predict the thrust of the nozzle in the design process. One of the advantages of applying this chemistry model is the low computational time as compared to equilibrium or finite rate model, since no chemistry has to be implemented.

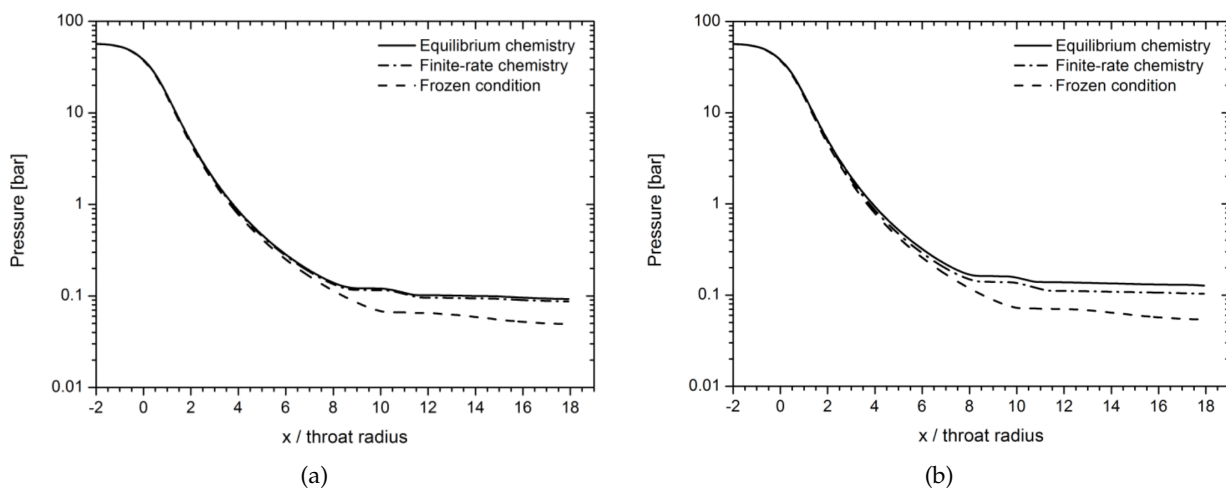


Figure 7.5.: Impact of the chemistry model on the centerline pressure, H_2/O_2 (a) and CH_4/O_2 (b).

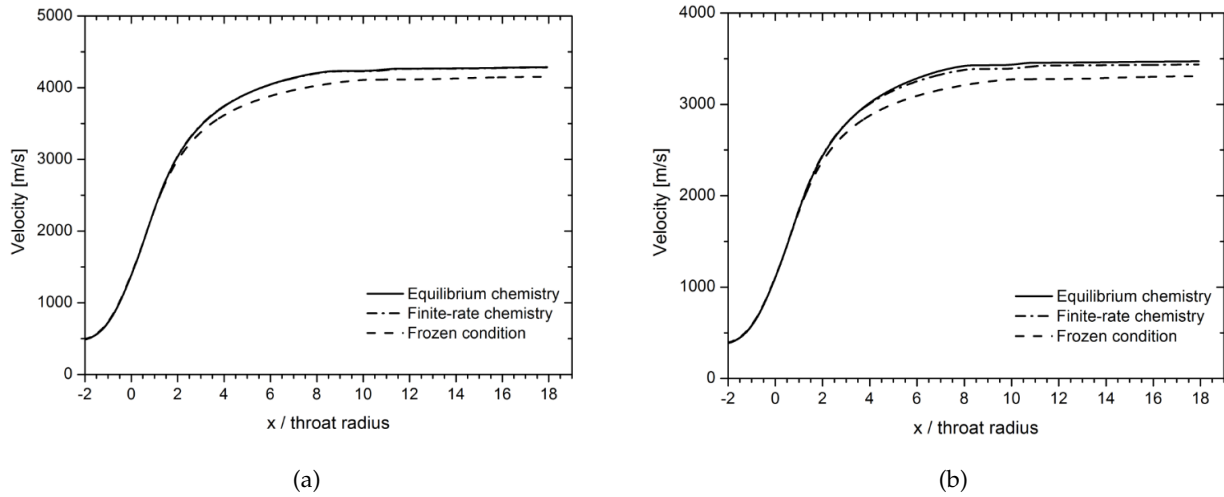


Figure 7.6.: Impact of the chemistry model on the centerline velocity, H_2/O_2 (a) and CH_4/O_2 (b).

In Figure 7.7 the impact of the chemistry model on the centerline Mach number is shown. It is evident, that the chemistry model, which leads to higher temperature, would underpredict the Mach number. Since Mach number is a function of temperature, and a higher temperature results in lower Mach number. Therefore the frozen chemistry model delivers the highest Mach number at the nozzle exit, and the equilibrium the lowest. Whereas the difference between the predicted Mach number by finite rate and equilibrium model is neglegible in case of H₂/O₂. Because both models deliver the same temperature as shown in Figure 7.2 (a).

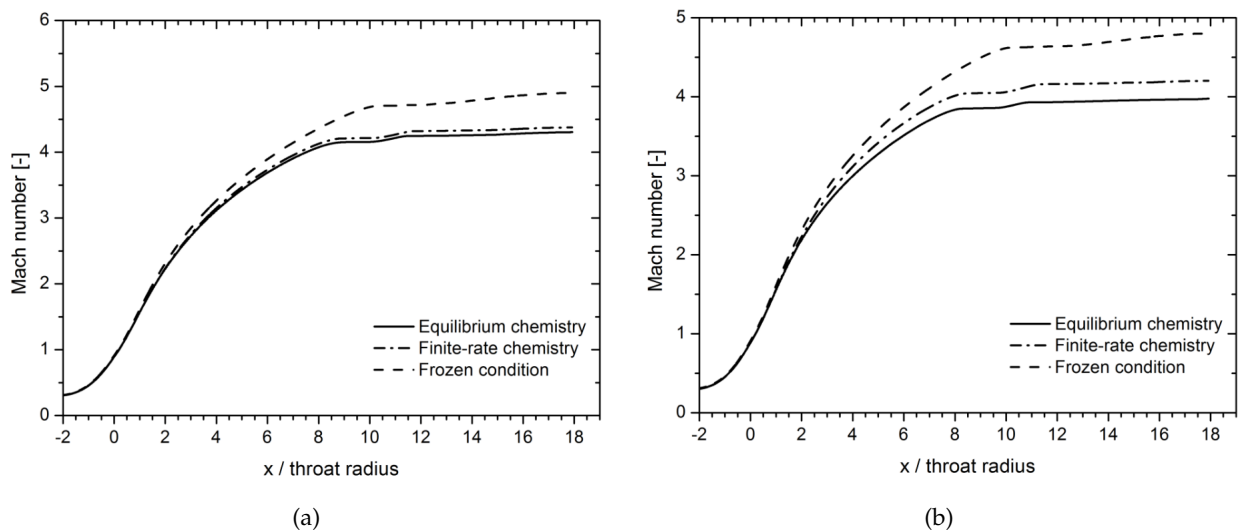


Figure 7.7.: Impact of the chemistry model on the centerline Mach number, H_2/O_2 (a) and CH_4/O_2 (b).

Comparison of NewMechanism with other CH₄/O₂ reaction mechanisms

For a further comparison of NewMechanism with other CH₄/O₂ reaction mechanisms the predicted centerline temperature until the nozzle throat is examined. Due to the larger flow time scale (higher Damkoehler number) in this area the impact of the chemistry is greater than the after nozzle throat area. Therefore this area is suitable for a simplified comparison of the reaction mechanisms. But this comparison cannot be used as a verification of the reaction mechanisms, since this simulation is oversimplified, because the flow is treated as inviscous. Moreover the turbulence chemistry interaction, boundary layer effects and the flame propagation are neglected. Furthermore the simulation is conducted with a complete burnt mixture.

Finite rate and equilibrium chemistry models are simulated, and the results are shown in Figure 7.8. As expected in case of equilibrium chemistry all reaction mechanisms deliver almost the identical temperature profile Figure 7.8 (b), this results from the infinitely fast reaction rate at equilibrium. Only the global chemistry based reaction mechanism Westbrook & Dryer predicts a much higher temperature profile as compared to the other reaction mechanisms.

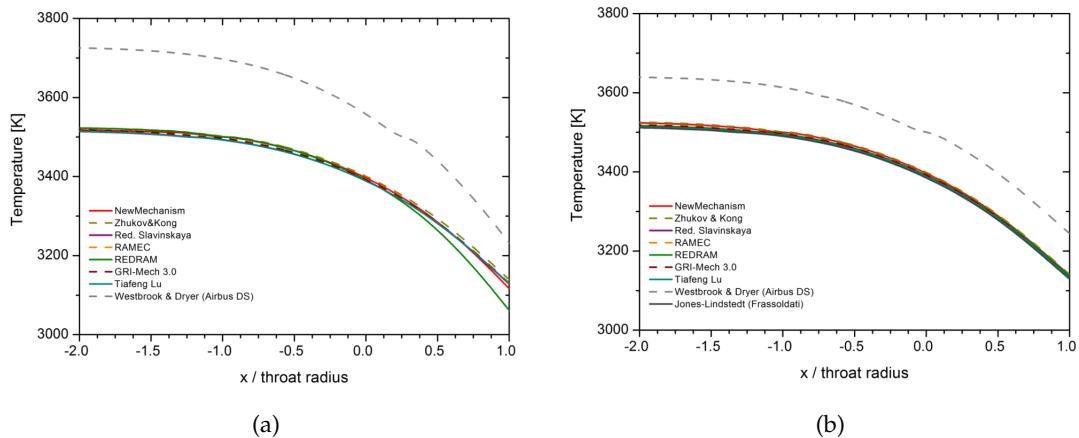


Figure 7.8.: Comparison of predicted centerline temperature by different CH₄/O₂ reaction mechanism, finite rate chemistry model (a), equilibrium chemistry model (b).

In case of finite rate chemistry (Figure 7.8 (a)) the simulation with Jones–Lindstedt could not reach a converged solution. As shown in Figure 7.9 Jones–Lindstedt produces extremely high temperatures, which lead to a divergence of the simulation. Considering the fact, that Jones–Lindstedt is a well known reaction mechanism, which is widely used in combustion simulation, the reason behind the extremely high temperature production could be the simulation boundary conditions of an initial temperature of around 3500 K and a pressure of 60 bar. Especially the initial temperature of about 3500 K could have impact on the reaction rate, which results in extremely high temperature. As a result the energy equation diverges. Westbrook & Dryer also predicts a much higher temperature, but not as much as Jones–Lindstedt. Other reaction mechanisms

except REDRAM predict a similar temperature profile. REDRAM predicted temperature shows a deviation from the others in the end of the nozzle throat.

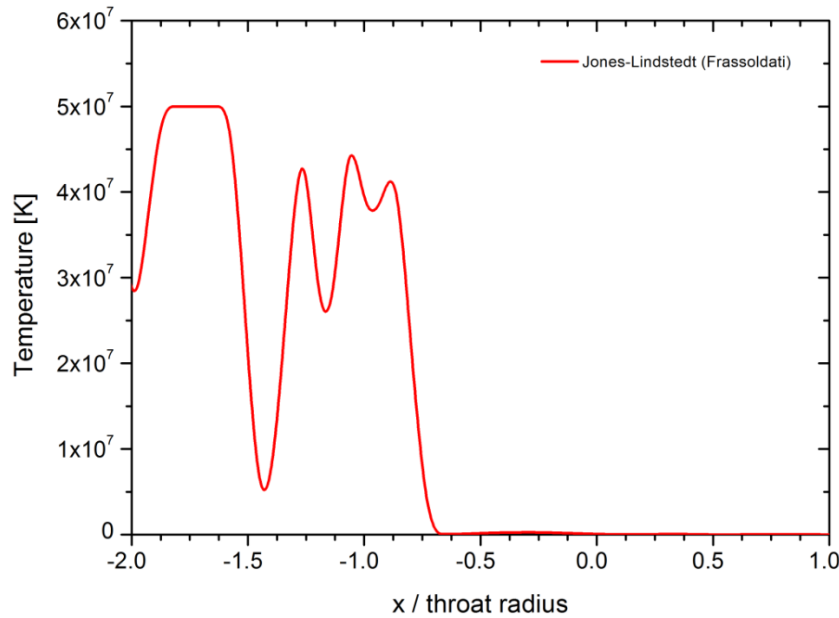


Figure 7.9.: Predicted centerline temperature by Jones–Lindestedt using finite rate chemistry model.

As previously mentioned Westbrook & Dryer predicts a much higher temperature profile at equilibrium, while other reaction mechanisms deliver almost the same temperature. Therefore the species mass fraction profile of Westbrook & Dryer and NewMechanism is compared for a further investigation. The centerline species mass fraction of the major species along the x axis is illustrated in Figure 7.10, The dashed line represents equilibrium condition and the full line is the species mass fraction profil at finite rate chemistry condition. As one can see in Figure 7.10 (b) Westbrook & Dryer predicts a decrease of the major intermediate species CO along the x axis at equilibrium condition, while at finite rate condition it predicts an increase of the species CO. NewMechanism predicts an increase of CO mass fraction at both conditions (equilibrium and finite rate chemistry).

A similar behaviour is seen for the other species. Considering the product species CO₂, a decreasing mass fraction at finite rate condition and increasing mass fraction at equilibrium condition is predicted by Westbrook & Dryer. The other product species H₂O increases a little near the nozzle throat area at finite rate condition, afterwards its mass fraction remains almost constant, whereas at equilibrium condition an increasing mass fraction is predicted, only in the area near after the nozzle throat a slightly decrease is seen, but it starts increasing after this position. On the contrary NewMechanism predicts an increasing CO₂ mass fraction, and a decreasing H₂O species mass fraction for both chemistry models (equilibrium and finite rate). The reason behind this species mass fraction and the overpredicted temperature profile by Westbrook & Dryer as shown in Figure 7.8 (b), which is even higher than the theoretical equilibrium temperature (3530 K, at 60 bar), could be the reaction

$\text{CO} + 0.5\text{O}_2 \rightarrow \text{CO}_2$ and $\text{CO}_2 \rightarrow \text{CO} + 0.5\text{O}_2$ (see Appendix H). Since this reaction is reversible, as a result it should have a value of 1 for the equilibrium constant K . But the equilibrium konstant for this reversable reaction does not have a value of 1. The equilibrium constant can be calculated using Figure 2.4, the required values for the reaction rate caculation are given in Appendix H. The forward reaction rate k_f ($\text{CO} + 0.5\text{O}_2 \rightarrow \text{CO}_2$) is higher than the backward reaction rate k_r ($\text{CO}_2 \rightarrow \text{CO} + 0.5\text{O}_2$). Therefore a higher production of CO_2 and a decrease of CO is seen. This could also explain the overpredicted temperature at equilibrium condition, since a higher production of product species CO_2 could lead to higher temperature.

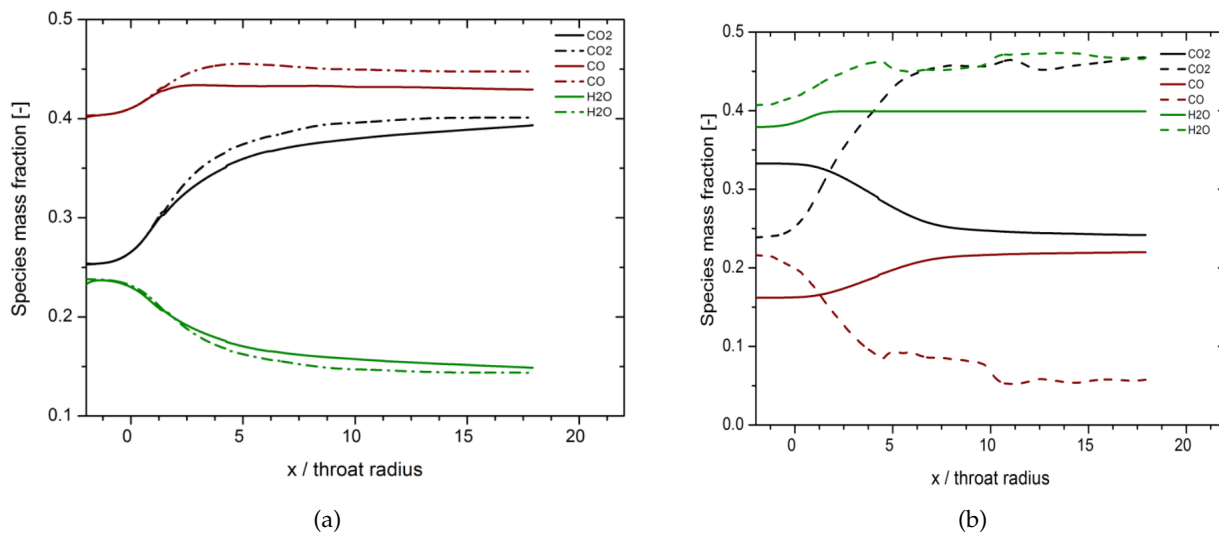


Figure 7.10.: Predicted mass fraction of major species along the centerline by NewMechanism (a) and Westbrook & Dryer(b).

8. Conclusion and Outlook

A validation study of different CH₄/O₂ reaction mechanisms is conducted in this thesis. Ignition delay times and premixed laminar flame speeds experiments are chosen as validation parameters. The validation results of the reaction mechanisms are compared. Detailed reaction mechanisms (Aramcomech 1.3, C1-C4 Zhukov, RAMEC and GRI-Mech 3.0), skeletal reaction mechanisms (Zhukov & Kong, Red.Slavinskaya,Tiafeng Lu and REDRAM) and global chemistry reaction mechanisms (Westbrook & Dryer and Jones–Lindstedt) are taken into account for this study. The emphasis of this thesis was to validate the newly developed skeletal reaction mechanism Zhukov & Kong against wide range of ignition delay times and premixed laminar flame speeds experiments at elevated pressures, and compare its validation results with other reaction mechanism's results. Zhukov & Kong delivers good validation results for ignition delay times, but it produces a mean absolute error of around 50 % for predicting premixed laminar flame speeds, which is much higher than its parent reaction mechanisms C1-C4 Zhukov (11%) and RAMEC (11%). Therefore a new CH₄/O₂ reaction mechanism is developed using Sensitivity analysis. Zhukov & Kong and RAMEC are used as its parent reaction mechanisms.

The development process of NewMechanism consists of 2 steps. In the first development step a Sensitivity analysis of premixed laminar flame speeds is conducted using RAMEC. The rate-limiting reactions are determined, and missing reactions are added back to Zhukov & Kong. In the second development step a Sensitivity analysis of premixed laminar flame speeds is conducted using the updated version of Zhukov & Kong. In this step non rate-limiting reactions are determined, and removed using a multi-target strategy, this means, a reaction is only removed, if it has neglegible impact on validation results of ignition delay times and premixed laminar flame speeds. The final version is named NewMechanism, it consists of 53 reactions and 26 species. But for pure CH₄/O₂ combustion it can reduced to 51 reactions and 23 species.

C1-C4 Zhukov, RAMEC, NewMechanism, Zhukov & Kong and REDRAM can be used for elevated pressures, rich and lean mixtures, whereas Red.Slavinskaya is optimized for low pressures and lean mixtures. Tiafeng Lu is better suitable for low pressures and rich mixutres. GRI-Mech 3.0 and Aramcomech 1.3 deliver good validation results for intermediate conditions. Jones–Lindstedt produces the highest error for predicting ignition delay times and premixed laminar flame speed as well, whereas the accuracy of Westbrook & Dryer is much lower than detailed and skeletal reaction mechanisms, but as compared to Jones–Lindstedt Westbrook & Dryer validation results are far better for both validation parameters.

Due to many simplifications made in the 2D numerical simulation conducted in this thesis no statement can be made for the suitability of the reaction mechanisms in CFD simulations, especially in the combustion simulations. Therefore, the author recommends further three studies to make a proper statement, an adiabatic, non adiabatic flamelet and a finite rate chemistry combustion simulation using RAMEC, Red.Salvinskaya, Zhukov & Kong, NewMechanism and GRI-Mech 3.0.

A. Identified rate limiting reactions for premixed laminar flame speed

The following reactions are considered to be rate limiting after conducting a sensitivity analysis of premixed laminar flame speed with RAMEC for a wide range of condition from 15 to 100 atm and equivalence ratio of 0.5 - 2. These reaction are added to Zhukov & Kong in the first development step of NewMechanism.

1. $\text{HCO} + \text{H}_2\text{O} \rightleftharpoons \text{H} + \text{CO} + \text{H}_2\text{O}$
2. $\text{CH}_3 + \text{HCO} \rightleftharpoons \text{CH}_4 + \text{CO}$
3. $\text{OH} + \text{C}_2\text{H}_4 \rightleftharpoons \text{C}_2\text{H}_3 + \text{H}_2\text{O}$
4. $\text{OH} + \text{CH}_3\text{OH} \rightleftharpoons \text{CH}_3\text{O} + \text{H}_2\text{O}$
5. $\text{OH} + \text{CH}_3 \rightleftharpoons \text{CH}_2 + \text{H}_2\text{O}$
6. $\text{OH} + \text{CH}_3 (+ \text{M}) \rightleftharpoons \text{CH}_3\text{OH} (+ \text{M})$
7. $2 \text{OH} \rightleftharpoons \text{O} + \text{H}_2\text{O}$
8. $\text{H} + \text{CH}_3\text{OH} \rightleftharpoons \text{CH}_2\text{OH} + \text{H}_2$
9. $\text{H} + \text{CH}_2\text{OH} \rightleftharpoons \text{OH} + \text{CH}_3$
10. $\text{H} + \text{CH}_2\text{O} (+ \text{M}) \rightleftharpoons \text{CH}_2\text{OH} (+ \text{M})$
11. $\text{H} + \text{HCO} \rightleftharpoons \text{H}_2 + \text{CO}$
12. $\text{O} + \text{C}_2\text{H}_6 \rightleftharpoons \text{OH} + \text{C}_2\text{H}_5$
13. $\text{O} + \text{C}_2\text{H}_5 \rightleftharpoons \text{CH}_3 + \text{CH}_2\text{O}$
14. $\text{O} + \text{HO}_2 \rightleftharpoons \text{OH} + \text{O}_2$
15. $\text{O} + \text{CH}_2\text{O} \rightleftharpoons \text{OH} + \text{HCO}$
16. $\text{O} + \text{C}_2\text{H}_4 \rightleftharpoons \text{CH}_3 + \text{HCO}$
17. $\text{H} + \text{HO}_2 \rightleftharpoons \text{O}_2 + \text{H}_2$
18. $\text{H} + \text{HO}_2 \rightleftharpoons 2 \text{OH}$
19. $\text{C}_2\text{H}_5 + \text{O}_2 \rightleftharpoons \text{HO}_2 + \text{C}_2\text{H}_4$

20. $\text{CH}_3\text{O}_2 + \text{H}_2\text{O}_2 \rightleftharpoons \text{CH}_3\text{O}_2\text{H} + \text{HO}_2$
21. $\text{OH} + \text{HCO} \rightleftharpoons \text{H}_2\text{O} + \text{CO}$
22. $\text{CH} + \text{O}_2 \rightleftharpoons \text{O} + \text{HCO}$
23. $\text{CH}_2 + \text{O}_2 \rightleftharpoons \text{OH} + \text{HCO}$
24. $\text{CH}_2(\text{S}) + \text{N}_2 \rightleftharpoons \text{CH}_2 + \text{N}_2$
25. $\text{CH}_2(\text{S}) + \text{O}_2 \rightleftharpoons \text{H} + \text{OH} + \text{CO}$
26. $\text{CH}_2(\text{S}) + \text{O}_2 \rightleftharpoons \text{CO} + \text{H}_2\text{O}$
27. $\text{CH}_2(\text{S}) + \text{H}_2\text{O} \rightleftharpoons \text{CH}_2 + \text{H}_2\text{O}$
28. $\text{CH}_2(\text{S}) + \text{CO}_2 \rightleftharpoons \text{CH}_2 + \text{CO}_2$
29. $\text{C}_2\text{H}_3 + \text{O}_2 \rightleftharpoons \text{HCO} + \text{CH}_2\text{O}$
30. $\text{H} + \text{H}_2\text{O}_2 \rightleftharpoons \text{HO}_2 + \text{H}_2$
31. $\text{H} + \text{C}_2\text{H}_2 (+ \text{M}) \rightleftharpoons \text{C}_2\text{H}_3 (+ \text{M})$
32. $\text{H} + \text{HCCO} \rightleftharpoons \text{CH}_2(\text{S}) + \text{CO}$
33. $\text{H} + \text{CH}_2\text{CO} \rightleftharpoons \text{CH}_3 + \text{CO}$
34. $\text{H} + \text{CH}_3\text{O} \rightleftharpoons \text{CH}_2(\text{S}) + \text{H}_2\text{O}$
35. $\text{OH} + \text{C}_2\text{H}_2 \rightleftharpoons \text{H} + \text{CH}_2\text{CO}$
36. $2 \text{CH}_3 \rightleftharpoons \text{H} + \text{C}_2\text{H}_5$
37. $\text{CH}_2\text{OH} + \text{O}_2 \rightleftharpoons \text{HO}_2 + \text{CH}_2\text{O}$
38. $\text{OH} + \text{CH}_3 \rightleftharpoons \text{CH}_2(\text{S}) + \text{H}_2\text{O}$
39. $2 \text{H} + \text{H}_2\text{O} \rightleftharpoons \text{H}_2 + \text{H}_2\text{O}$
40. $\text{CH}_2(\text{S}) + \text{H}_2\text{O} (+ \text{M}) \rightleftharpoons \text{CH}_3\text{OH} (+ \text{M})$
41. $\text{O} + \text{HCCO} \rightleftharpoons \text{H} + 2 \text{CO}$
42. $\text{O} + \text{CH}_2\text{CO} \rightleftharpoons \text{CH}_2 + \text{CO}_2$
43. $\text{CH}_2(\text{S}) + \text{CO}_2 \rightleftharpoons \text{CO} + \text{CH}_2\text{O}$
44. $\text{O} + \text{C}_2\text{H}_3 \rightleftharpoons \text{H} + \text{CH}_2\text{CO}$

B. Comparison of initial and final version of NewMechanism

Test: $\phi = 0.4$, $p = 50$ atm, mixture = $\text{CH}_4/(\text{O}_2+\text{AR})$

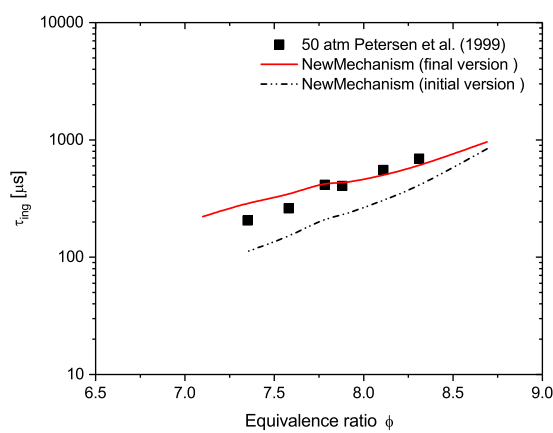


Figure B.1.: Comparison of simulation results using different versions of NewMechanism with experimental values at 50 atm.

Test: $p = 60$ atm, $T_u = 298$ K, mixture = $\text{CH}_4/(15\% \text{ O}_2 + 85\% \text{ HE})$

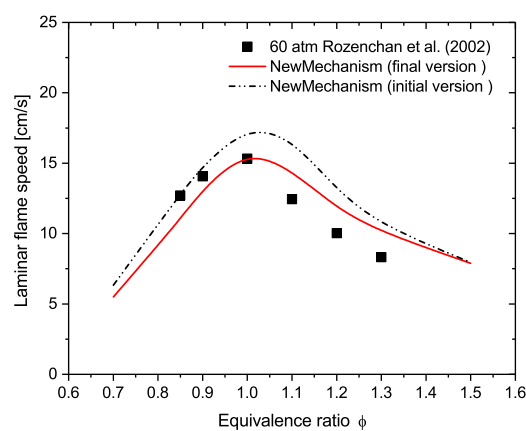


Figure B.2.: Comparison of simulation results using different versions of NewMechanism with experimental values at 60 atm.

C. Radical induced Ignition

As discussed in Chapter 4 a stoichiometric mixture of CH_4/O_2 does not auto ignite at 850 K and 1 bar. Another way to ignite this mixture at these conditions is to bombard it with H radicals, which will lead to ignition. H radical is used as an igniter in this study to initiate the chemistry.

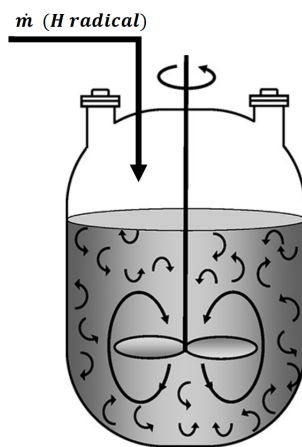


Figure C.1.: Massflow of H radical in PSR modified from [10].

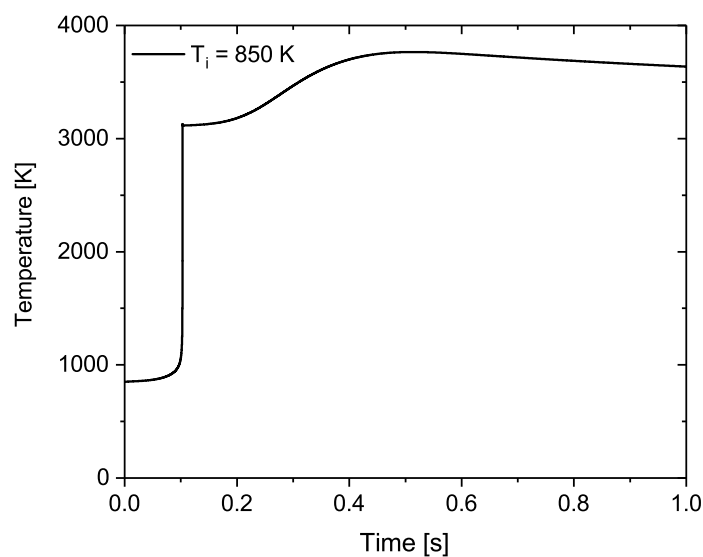
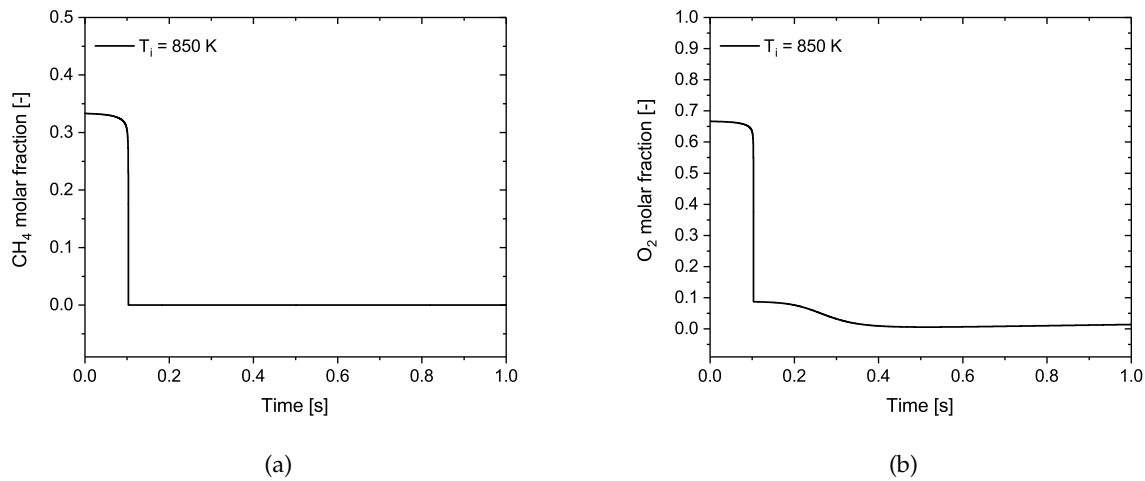
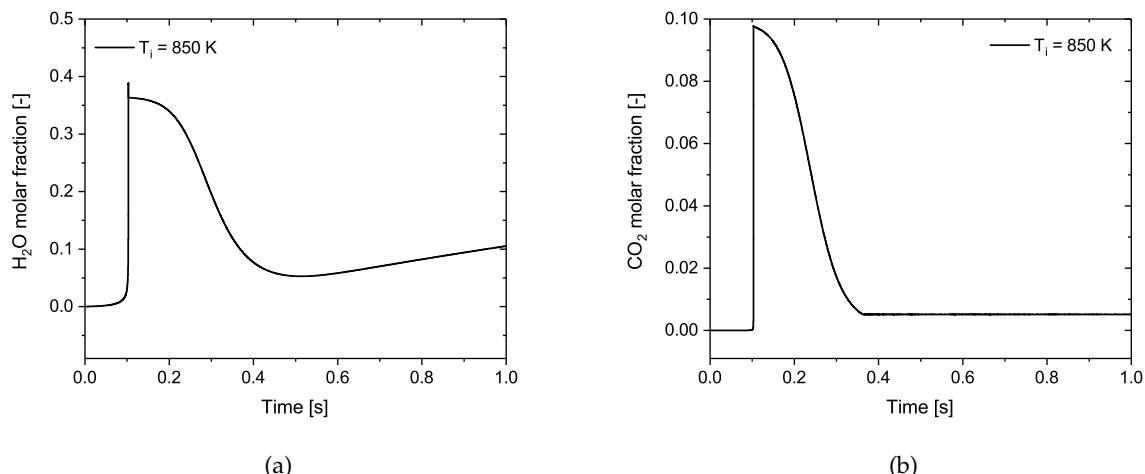


Figure C.2.: Temperature over time of a stoichiometric composition of CH_4/O_2 at 1 bar.

**Figure C.3.:** Molar fraction of fuel CH_4 and oxidizer O_2 .**Figure C.4.:** Molar fraction of fuel H_2O and oxidizer CO_2 .

D. Influence of thermochemistry data

In this study the influence of using different thermochemistry data is examined. To capture the influence of thermochemistry at different pressures two premixed laminar flame speed simulations are conducted at 20 atm and 60 atm. The reaction mechanism Zhukov & Kong is utilized by using two different thermochemistry data from C1-C4 Zhukov and Aramcomech 1.3. As one can see in Figure D.1 the influence of thermochemistry data is visible especially at higher pressure of 60 atm. As mentioned in Section 3.3 in case of diffusion flame for instance premixed laminar flame the transport of species becomes important. Therefore using different thermochemistry data especially transport data leads to different predicted flame speed by the same reaction mechanism as shown in Figure D.1, where the reaction mechanism Zhukov & Kong is used for both cases (20 atm, 60 atm).

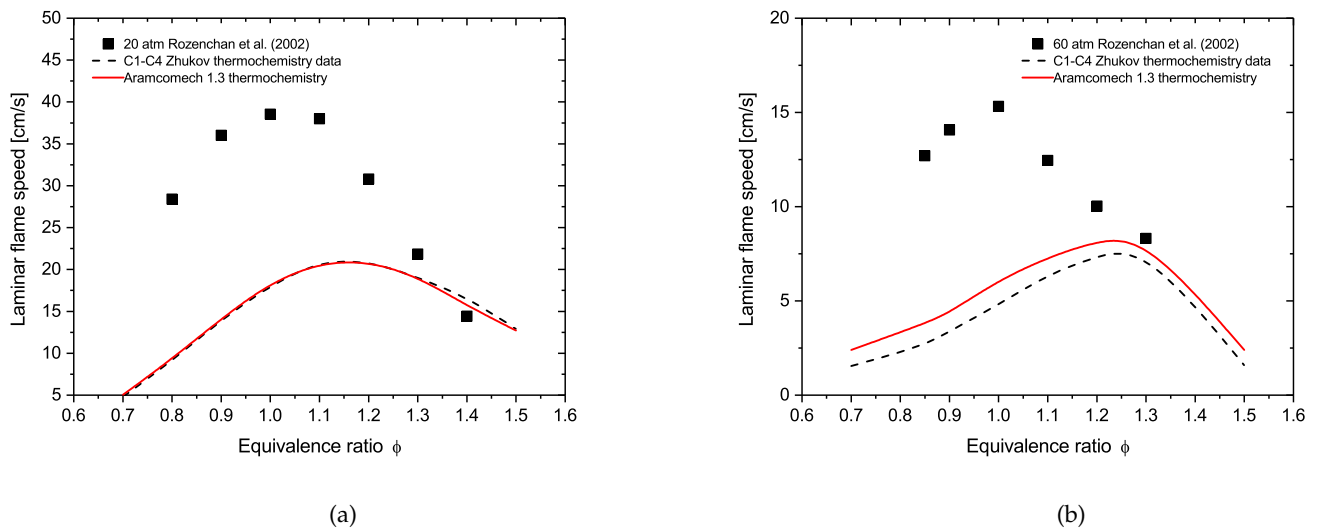


Figure D.1.: Premixed laminar flame speed simulation using different thermochemistry data and its comparison with experimental data.

E. Validation results

E.1. Validation against ignition delay time

Lean mixtures $\phi = 0.4 - 0.5$

Test 1: $\phi = 0.5$, $p = 20$ atm, mixture = $\text{CH}_4/(\text{O}_2+\text{N}_2)$

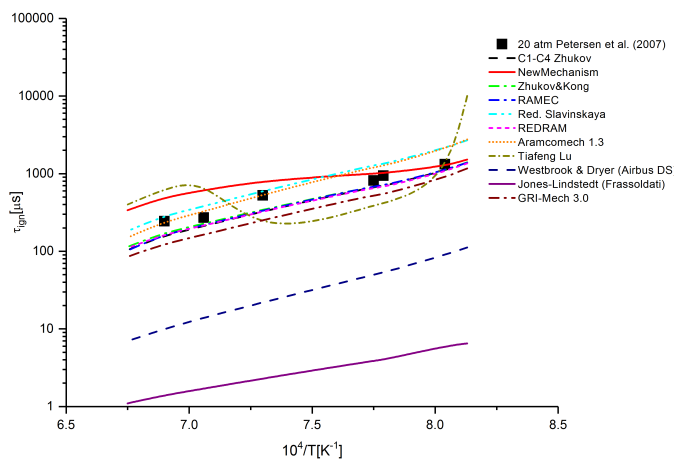


Figure E.1.: Comparison of simulation results using different reaction mechanisms with experimental values at 20 atm ($\phi = 0.5$).

Table E.1.: Absolute mean percentage error from experimental values of each reaction mechanism at 20 atm ($\phi = 0.5$).

Reaction mechanism	MAPE (test 1)
C1-C4 Zhukov	25%
NewMechanism	53%
Zhukov & Kong	23%
RAMEC	24%
Red.Slavinskaya	40%
REDRAM	26%
Aramcomech 1.3	28%
Tiafeng Lu	101%
Westbrook & Dryer (Airbus DS)	95%
Jones–Lindstedt (Frassoldati)	>1000%
GRI-Mech 3.0	42%

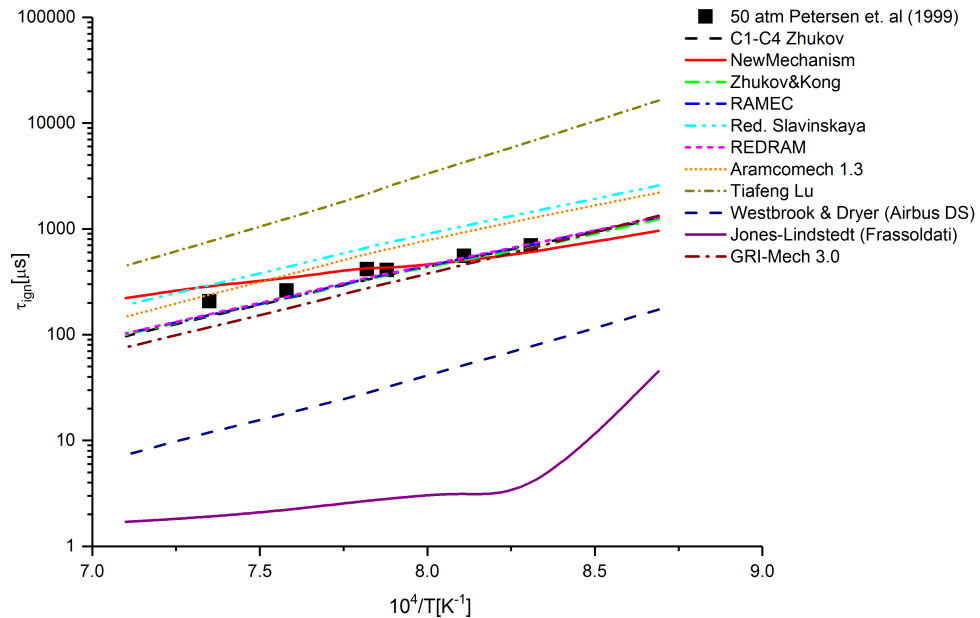
Test 2: $\phi = 0.4$, $p = 50$ atm, mixture = CH₄/(O₂+AR)

Figure E.2.: Comparison of simulation results using different reaction mechanisms with experimental values at 50 atm ($\phi = 0.4$).

Table E.2.: Absolute mean percentage error from experimental values of each reaction mechanism at 50 atm ($\phi = 0.4$).

Reaction mechanism	MAPE (test 2)
C1-C4 Zhukov	13%
NewMechanism	17%
Zhukov & Kong	13%
RAMEC	12%
Red.Slavinskaya	76%
REDRAM	11%
Aramcomech 1.3	50%
Tiafeng Lu	517%
Westbrook & Dryer (Airbus DS)	92%
Jones–Lindstedt (Frassoldati)	>1000%
GRI-Mech 3.0	26%

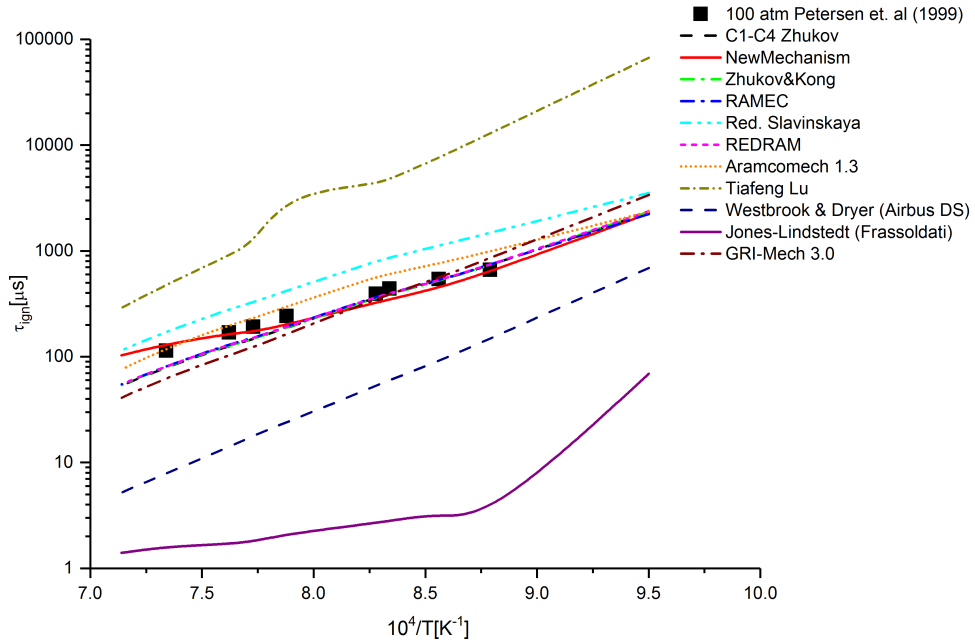
Test 3: $\phi = 0.4$, $p = 100$ atm, mixture = CH₄/(O₂+AR)


Figure E.3.: Comparison of simulation results using different reaction mechanisms with experimental values at 100 atm ($\phi = 0.4$).

Table E.3.: Absolute mean percentage error from experimental values of each reaction mechanism at 100 atm ($\phi = 0.4$).

Reaction mechanism	MAPE (test 3)
C1-C4 Zhukov	17%
NewMechanism	13%
Zhukov & Kong	16%
RAMEC	15%
Red.Slavinskaya	87%
REDRAM	16%
Aramcomech 1.3	30%
Tiafeng Lu	968%
Westbrook & Dryer (Airbus DS)	88%
Jones–Lindstedt (Frassoldati)	>1000%
GRI-Mech 3.0	12%

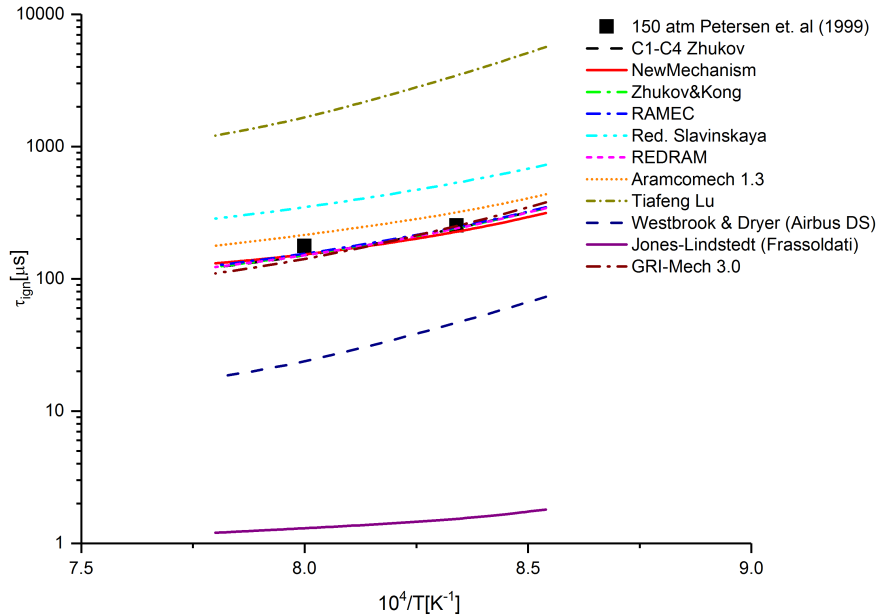
Test 4: $\phi = 0.4$, $p = 150$ atm, mixture = CH₄/(O₂+AR)

Figure E.4.: Comparison of simulation results using different reaction mechanisms with experimental values at 150 atm($\phi = 0.4$).

Table E.4.: Absolute mean percentage error from experimental values of each reaction mechanism at 150 atm ($\phi = 0.4$).

Reaction mechanism	MAPE (test 4)
C1-C4 Zhukov	12%
NewMechanism	14%
Zhukov & Kong	11%
RAMEC	10%
Red.Slavinskaya	100%
REDRAM	12%
Aramcomech 1.3	21%
Tiafeng Lu	>1000%
Westbrook & Dryer (Airbus DS)	84%
Jones–Lindstedt (Frassoldati)	>1000%
GRI-Mech 3.0	12%

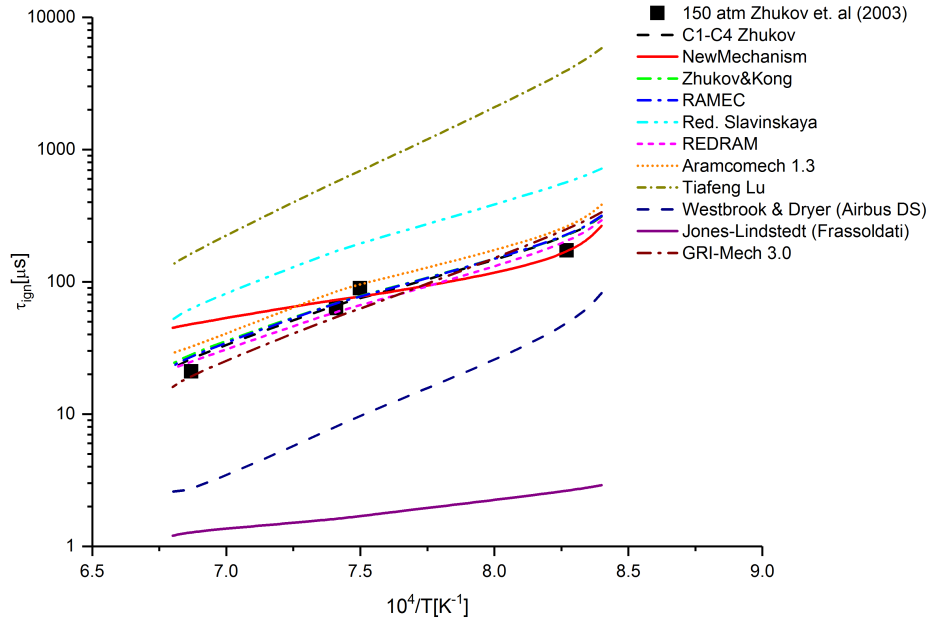
Test 5: $\phi = 0.5$, $p = 150$ atm, mixture = CH₄/(Air)


Figure E.5.: Comparison of simulation results using different reaction mechanisms with experimental values at 150 atm ($\phi = 0.5$).

Table E.5.: Absolute mean percentage error from experimental values of each reaction mechanism at 150 atm ($\phi = 0.5$).

Reaction mechanism	MAPE (test 5)
C1-C4 Zhukov	18%
NewMechanism	44%
Zhukov & Kong	21%
RAMEC	20%
Red.Slavinskaya	180%
REDRAM	14%
Aramcomech 1.3	33%
Tiafeng Lu	>1000%
Westbrook & Dryer (Airbus DS)	84%
Jones–Lindstedt (Frassoldati)	>1000%
GRI-Mech 3.0	20%

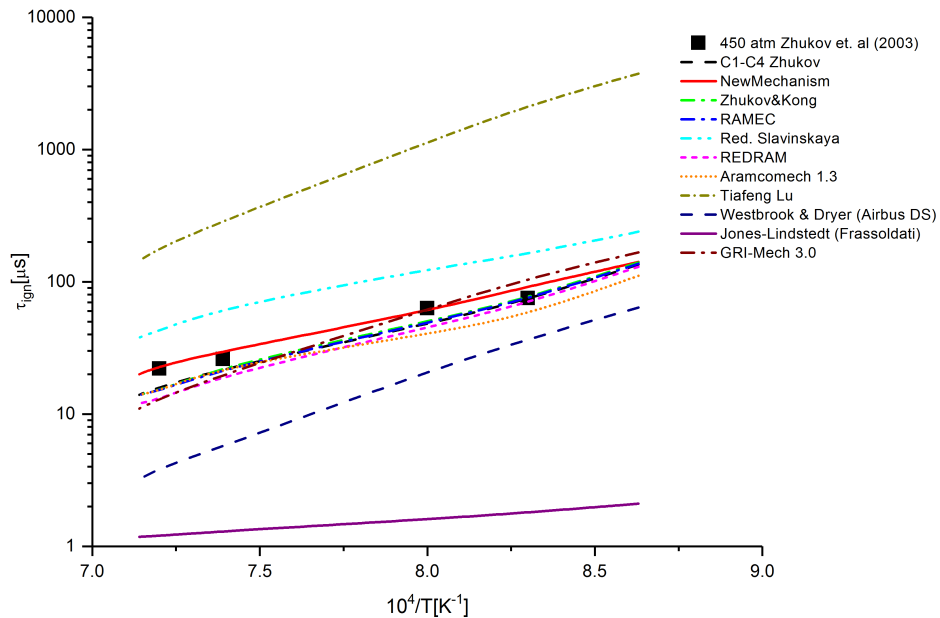
Test 6: $\phi = 0.5$, $p = 450$ atm, mixture = CH₄/(Air)

Figure E.6.: Comparison of simulation results using different reaction mechanisms with experimental values at 450 atm ($\phi = 0.5$).

Table E.6.: Absolute mean percentage error from experimental values of each reaction mechanism at 450 atm ($\phi = 0.5$).

Reaction mechanism	MAPE (test 6)
C1-C4 Zhukov	18%
NewMechanism	12%
Zhukov & Kong	16%
RAMEC	18%
Red.Slavinskaya	112%
REDRAM	25%
Aramcomech 1.3	26%
Tiafeng Lu	>1000%
Westbrook & Dryer (Airbus DS)	69%
Jones–Lindstedt (Frassoldatti)	>1000%
GRI-Mech 3.0	27%

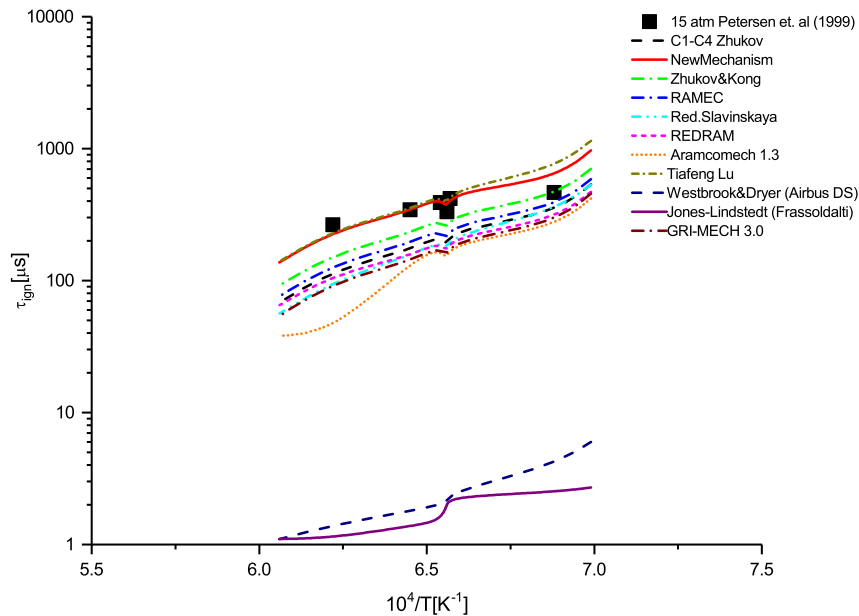
Rich mixtures $\phi = 1 - 6$ **Test 7: $\phi = 6$, $p = 15$ atm, mixture = $\text{CH}_4/(\text{O}_2+\text{HE})$** 

Figure E.7.: Comparison of simulation results using different reaction mechanisms with experimental values at 15 atm ($\phi = 6$).

Table E.7.: Absolute mean percentage error from experimental values of each reaction mechanism at 15 atm ($\phi = 6$).

Reaction mechanism	MAPE (test 7)
C1-C4 Zhukov	45%
NewMechanism	10%
Zhukov & Kong	45%
RAMEC	38%
Red.Slavinskaya	49%
REDRAM	50%
Aramcomech 1.3	60%
Tiafeng Lu	16%
Westbrook & Dryer (Airbus DS)	>1000%
Jones–Lindstedt (Frassoldatti)	>1000%
GRI-Mech 3.0	154%

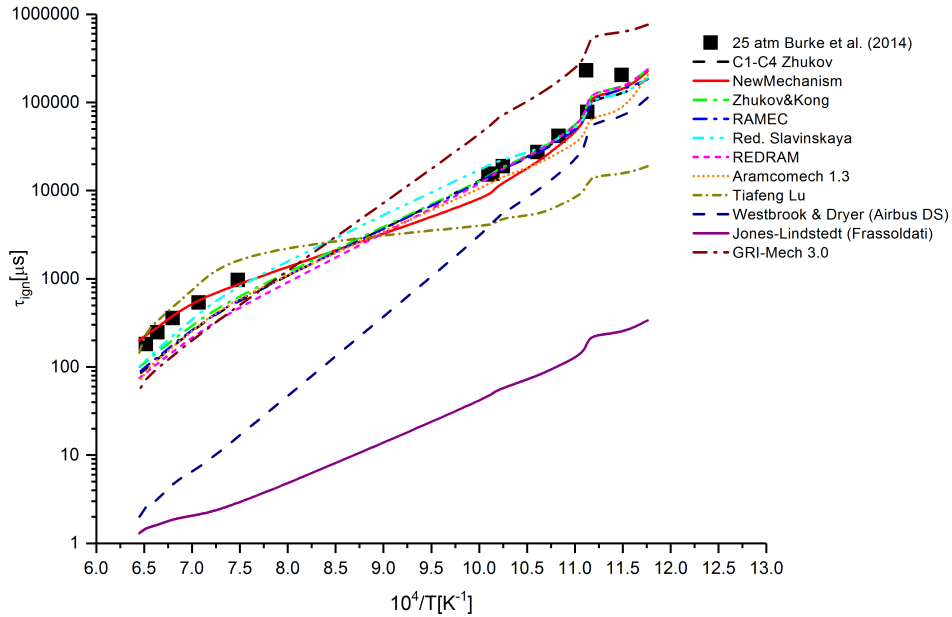
Test 8: $\phi = 2$, $p = 25$ atm, mixture = $\text{CH}_4/(\text{O}_2+\text{N}_2)$


Figure E.8.: Comparison of simulation results using different reaction mechanisms with experimental values at 25 atm ($\phi = 2$) from [12].

Table E.8.: Absolute mean percentage error from experimental values of each reaction mechanism at 25 atm ($\phi = 2$).

Reaction mechanism	MAPE (test 8)
C1-C4 Zhukov	29%
NewMechanism	25%
Zhukov & Kong	22%
RAMEC	29%
Red.Slavinskaya	30%
REDRAM	22%
Aramcomech 1.3	36%
Tiafeng Lu	73%
Westbrook & Dryer (Airbus DS)	80%
Jones–Lindstedt (Frassoldati)	>1000%
GRI-Mech 3.0	183%

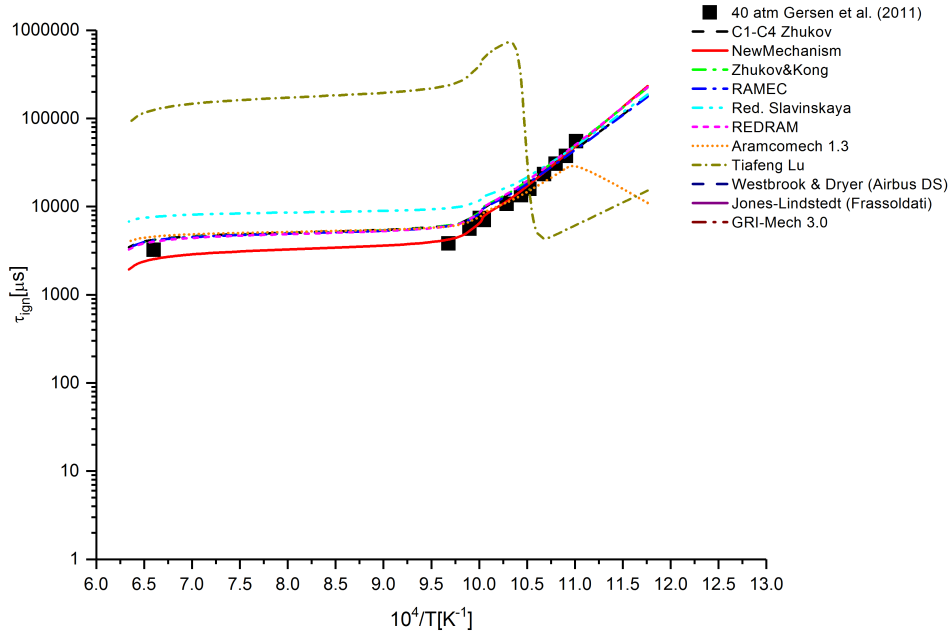
Test 9: $\phi = 1$, $p = 40$ atm, mixture = $\text{CH}_4/(\text{O}_2+\text{N}_2+\text{AR})$


Figure E.9.: Comparison of simulation results using different reaction mechanisms with experimental values at 40 atm ($\phi = 1$) from [13].

Table E.9.: Absolute mean percentage error from experimental values of each reaction mechanism at 40 atm ($\phi = 1$) from [13].

Reaction mechanism	MAPE (test 9)
C1-C4 Zhukov	22%
NewMechanism	6%
Zhukov & Kong	26%
RAMEC	21%
Red.Slavinskaya	60%
REDRAM	26%
Aramcomech 1.3	22%
Tiafeng Lu	>1000%
Westbrook & Dryer (Airbus DS)	61%
Jones–Lindstedt (Frassoldati)	>1000%
GRI-Mech 3.0	201%

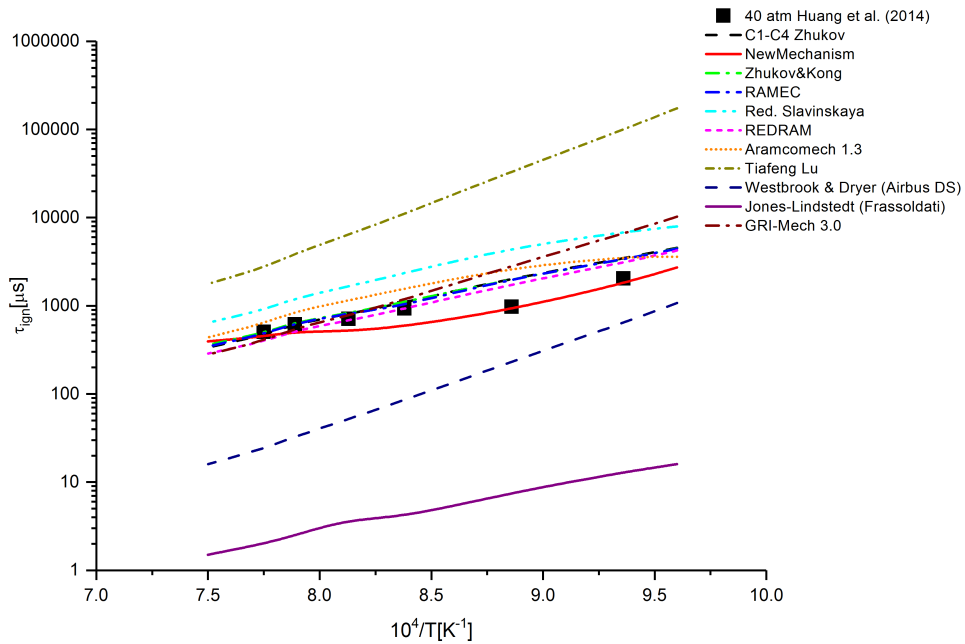
Test 10: $\phi = 1.3$, $p = 40$ atm, mixture = CH₄/(O₂+N₂)

Figure E.10.: Comparison of simulation results using different reaction mechanisms with experimental values at 40 atm ($\phi = 1.3$) from [14].

Table E.10.: Absolute mean percentage error from experimental values of each reaction mechanism atm 40 atm ($\phi = 1.3$).

Reaction mechanism	MAPE (test 10)
C1-C4 Zhukov	37%
NewMechanism	18%
Zhukov & Kong	36%
RAMEC	35%
Red.Slavinskaya	178%
REDRAM	28%
Aramcomech 1.3	75%
Tiafeng Lu	>1000%
Westbrook & Dryer (Airbus DS)	86%
Jones-Lindstedt (Frassoldati)	>1000%
GRI-Mech 3.0	80%

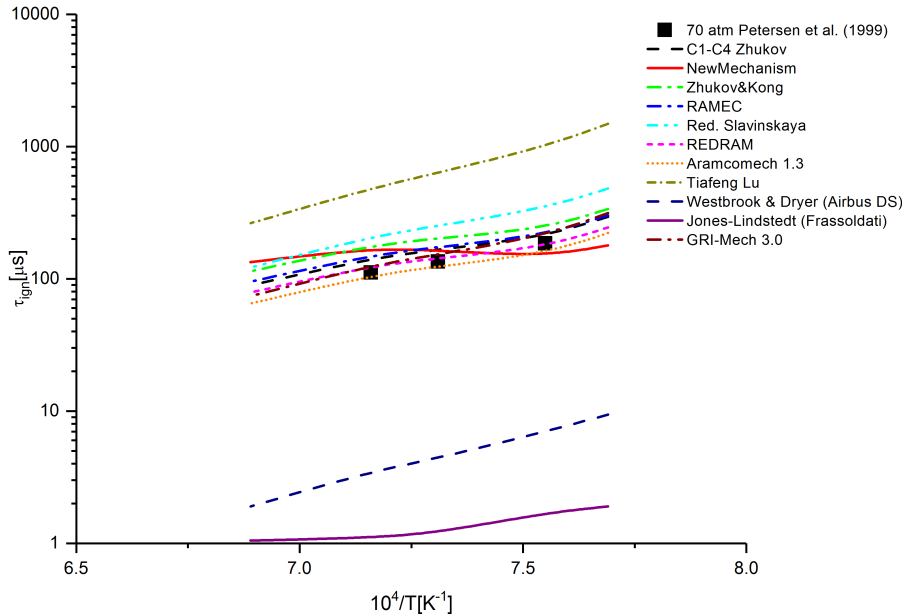
Test 11: $\phi = 6$, $p = 70$ atm, mixture = CH₄/(O₂+HE)

Figure E.11.: Comparison of simulation results using different reaction mechanisms with experimental values at 70 atm ($\phi = 6$).

Table E.11.: Absolute mean percentage error from experimental values of each reaction mechanism atm 70 atm ($\phi = 6$).

Reaction mechanism	MAPE (test 11)
C1-C4 Zhukov	21%
NewMechanism	32%
Zhukov & Kong	47%
RAMEC	27%
Red.Slavinskaya	86%
REDRAM	8%
Aramcomech 1.3	10%
Tiafeng Lu	381%
Westbrook & Dryer (Airbus DS)	96%
Jones-Lindstedt (Frassoldati)	>1000%
GRI-Mech 3.0	14%

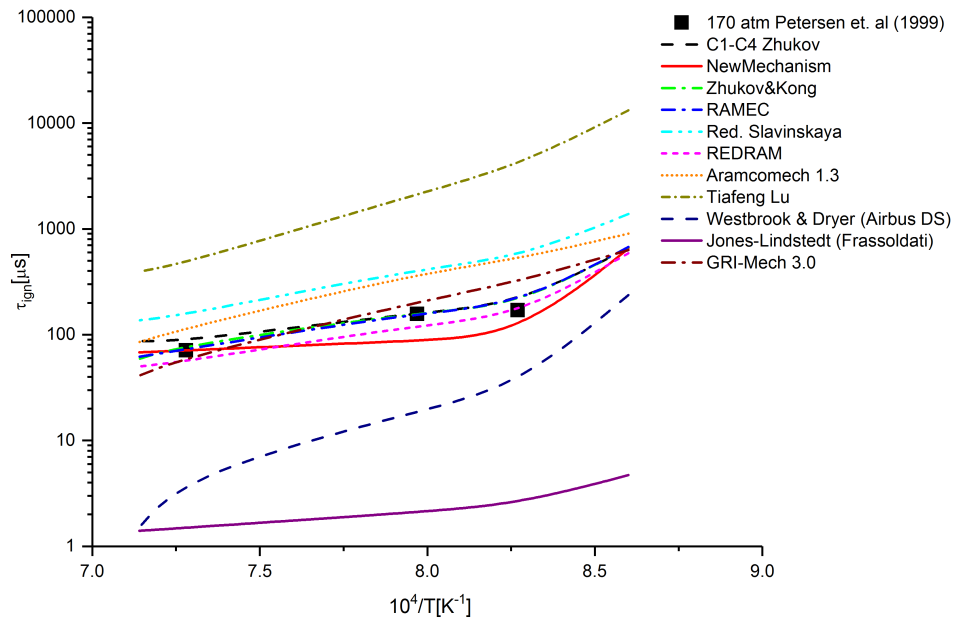
Test 12: $\phi = 3$, $p = 170$ atm, mixture = CH₄/(O₂+N₂)


Figure E.12.: Comparison of simulation results using different reaction mechanisms with experimental values at 170 atm ($\phi = 3$).

Table E.12.: Absolute mean percentage error from experimental values of each reaction mechanism at 170 atm ($\phi = 3$).

Reaction mechanism	MAPE (test 12)
C1-C4 Zhukov	12%
NewMechanism	29%
Zhukov & Kong	9%
RAMEC	5%
Red.Slavinskaya	165%
REDRAM	18%
Aramcomech 1.3	131%
Tiafeng Lu	>1000%
Westbrook & Dryer (Airbus DS)	87%
Jones–Lindstedt (Frassoldati)	>1000%
GRI-Mech 3.0	42%

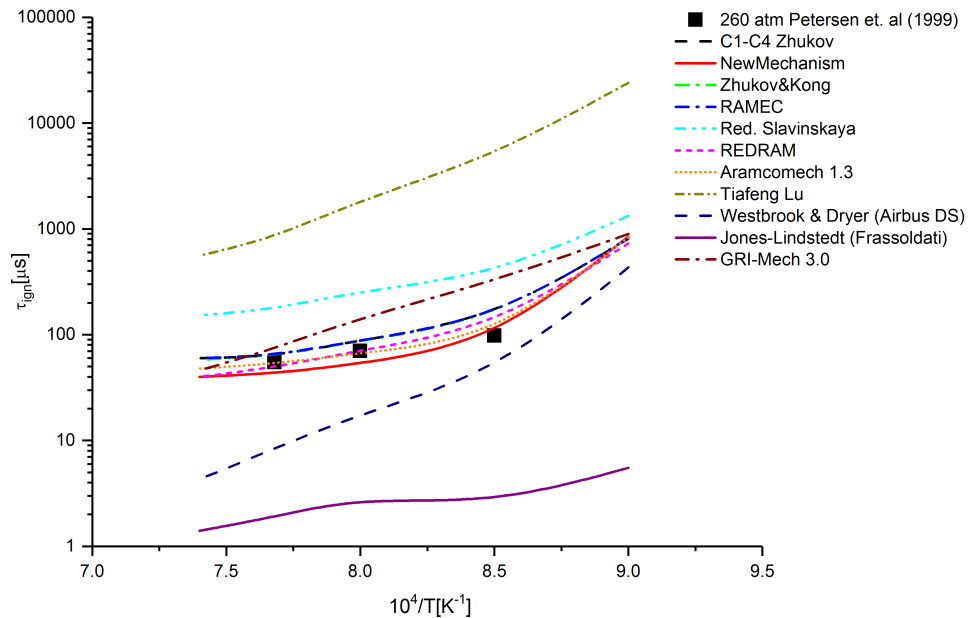
Test 13: $\phi = 3$, $p = 260$ atm, mixture = CH₄/(O₂+N₂)


Figure E.13.: Comparison of simulation results using different reaction mechanisms with experimental values at 260 atm ($\phi = 3$).

Table E.13.: Absolute mean percentage error from experimental values of each reaction mechanism at 260 atm ($\phi = 3$).

Reaction mechanism	MAPE (test 13)
C1-C4 Zhukov	27%
NewMechanism	19%
Zhukov & Kong	27%
RAMEC	28%
Red.Slavinskaya	253%
REDRAM	11%
Aramcomech 1.3	4%
Tiafeng Lu	>1000%
Westbrook & Dryer (Airbus DS)	72%
Jones-Lindstedt (Frassoldati)	>1000%
GRI-Mech 3.0	122%

E.2. Validation against premixed laminar flame speed

Test 1: $p = 5 \text{ atm}$, $T_u = 298 \text{ K}$, mixture = $\text{CH}_4/\text{(Air)}$

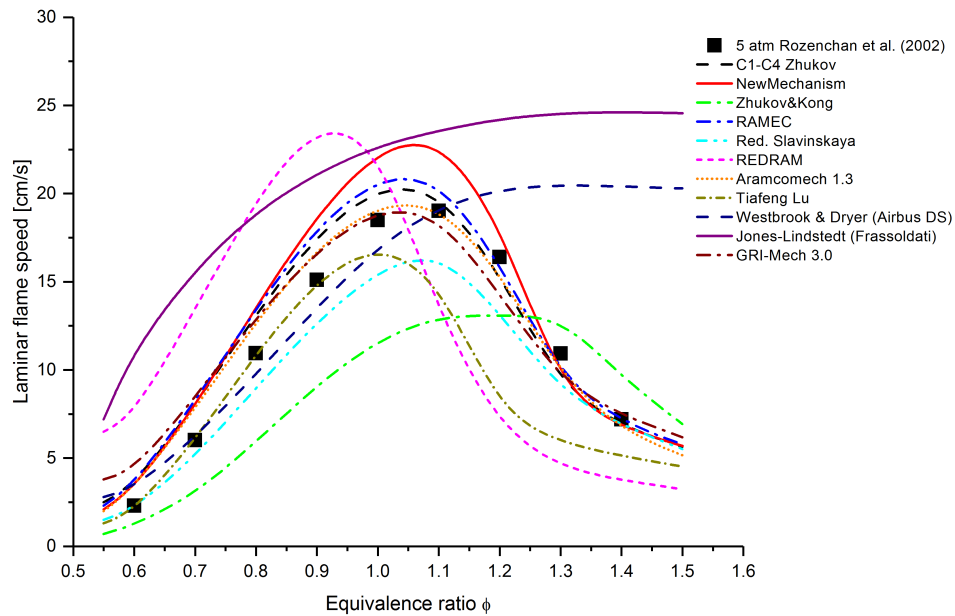


Figure E.14.: Predicted premixed laminar flame speed by different reaction mechanisms and its comparison with experimental value at 5 atm

Table E.14.: Absolute mean percentage error from experimental values of each reaction mechanism at 5 atm.

Reaction mechanism	MAPE (test 1)
C1-C4 Zhukov	18%
NewMechanism	22%
Zhukov & Kong	36%
RAMEC	19%
Red.Slavinskaya	14%
REDRAM	79%
Aramcomech 1.3	15%
Tiafeng Lu	19%
Westbrook & Dryer (Airbus DS)	41%
Jones–Lindstedt (Frassoldati)	125%
GRI-Mech 3.0	21%

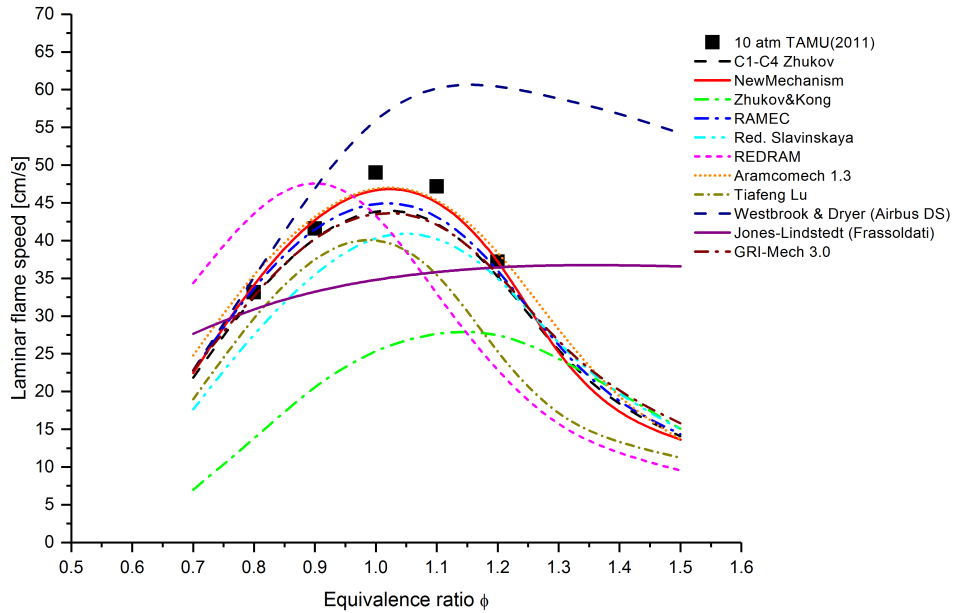
Test 2: $p = 10 \text{ atm}$, $T_u = 295 \text{ K}$, mixture = $\text{CH}_4/(\text{O}_2+\text{HE})$


Figure E.15.: Predicted premixed laminar flame speed by different reaction mechanisms and its comparison with experimental value at 10 atm from [15]

Table E.15.: Absolute mean percentage error from experimental values of each reaction mechanism at 10 atm.

Reaction mechanism	MAPE (test 2)
C1-C4 Zhukov	4%
NewMechanism	4%
Zhukov & Kong	26%
RAMEC	4%
Red.Slavinskaya	13%
REDRAM	26%
Aramcomech 1.3	5%
Tiafeng Lu	17%
Westbrook & Dryer (Airbus DS)	26%
Jones–Lindstedt (Frassoldati)	16%
GRI-Mech 3.0	5%

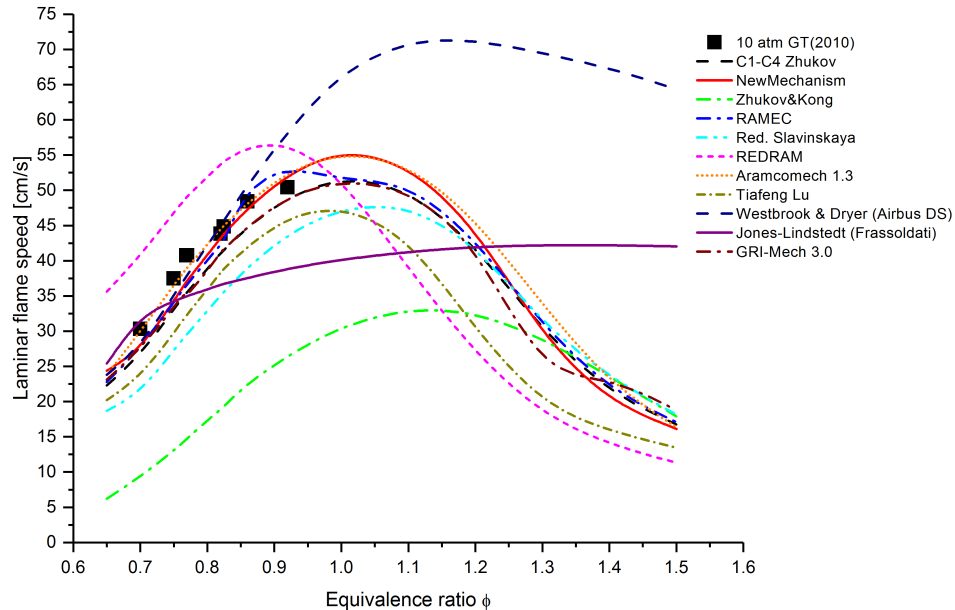
Test 3: $p = 10 \text{ atm}$, $T_u = 325 \text{ K}$, mixture = $\text{CH}_4/(\text{O}_2+\text{HE})$


Figure E.16.: Predicted premixed laminar flame speed by different reaction mechanisms and its comparison with experimental value at 10 atm from [16]

Table E.16.: Absolute mean percentage error from experimental values of each reaction mechanism at 10 atm.

Reaction mechanism	MAPE (test 3)
C1-C4 Zhukov	9%
NewMechanism	6%
Zhukov & Kong	60%
RAMEC	7%
Red.Slavinskaya	23%
REDRAM	7%
Aramcomech 1.3	2%
Tiafeng Lu	6%
Westbrook & Dryer (Airbus DS)	7%
Jones–Lindstedt (Frassoldatti)	15%
GRI-Mech 3.0	9%

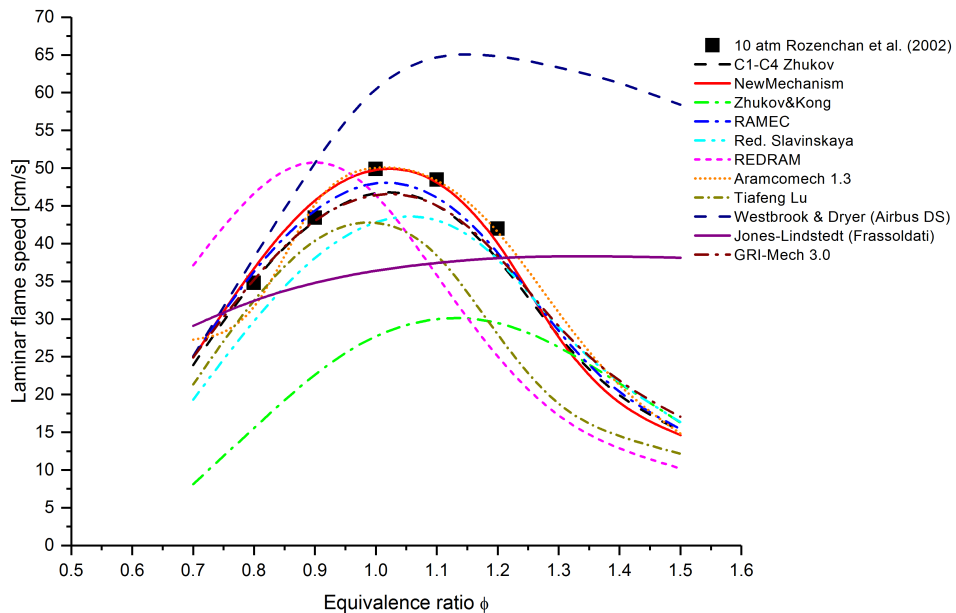
Test 4: $p = 10 \text{ atm}$, $T_u = 298 \text{ K}$, mixture = $\text{CH}_4/(\text{O}_2+\text{HE})$


Figure E.17.: Predicted premixed laminar flame speed by different reaction mechanisms and its comparison with experimental value at 10 atm

Table E.17.: Absolute mean percentage error from experimental values of each reaction mechanism at 10 atm.

Reaction mechanism	MAPE (test 4)
C1-C4 Zhukov	4%
NewMechanism	4%
Zhukov & Kong	43%
RAMEC	4%
Red.Slavinskaya	11%
REDRAM	26%
Aramcomech 1.3	7%
Tiafeng Lu	15%
Westbrook & Dryer (Airbus DS)	28%
Jones–Lindstedt (Frassoldatti)	15%
GRI-Mech 3.0	9%

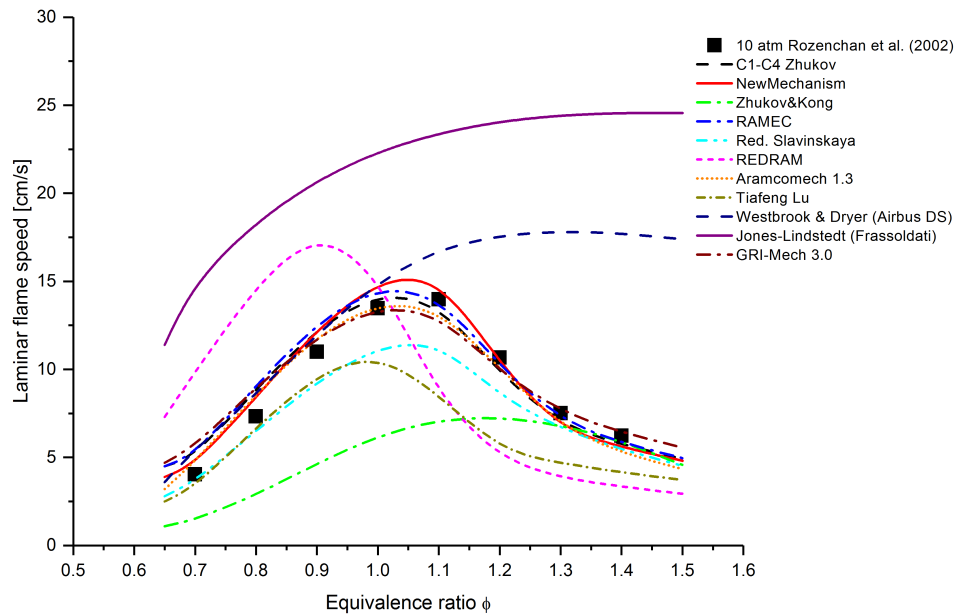
Test 5: $p = 10 \text{ atm}$, $T_u = 298 \text{ K}$, mixture = CH_4/Air


Figure E.18.: Predicted premixed laminar flame speed by different reaction mechanisms and its comparison with experimental value at 10 atm

Table E.18.: Absolute mean percentage error from experimental values of each reaction mechanism at 10 atm.

Reaction mechanism	MAPE (test 5)
C1-C4 Zhukov	11%
NewMechanism	12%
Zhukov & Kong	42%
RAMEC	11%
Red.Slavinskaya	14%
REDRAM	64%
Aramcomech 1.3	10%
Tiafeng Lu	27%
Westbrook & Dryer (Airbus DS)	60%
Jones–Lindstedt (Frassoldati)	161%
GRI-Mech 3.0	12%

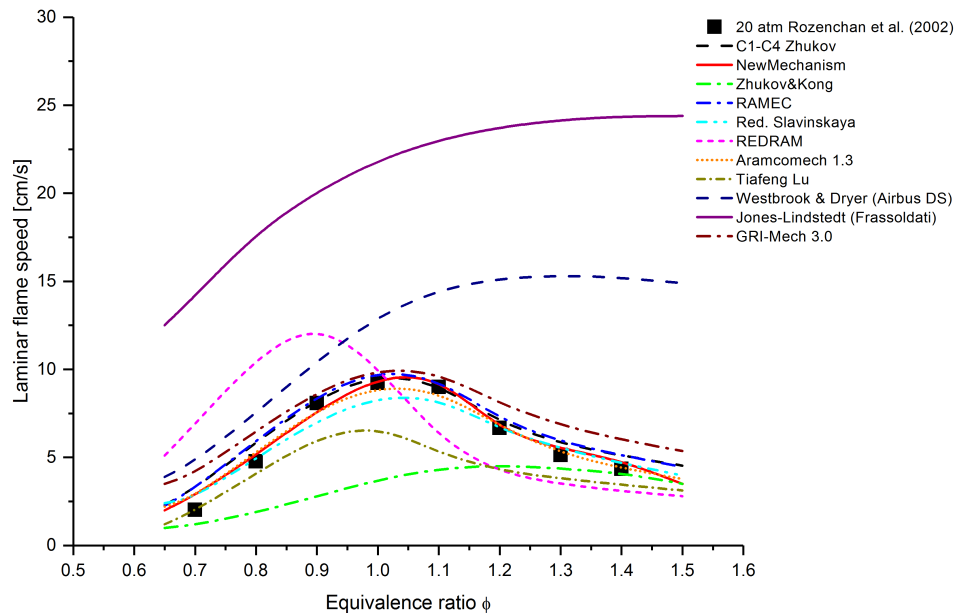
Test 6: $p = 20 \text{ atm}$, $T_u = 298 \text{ K}$, mixture = CH_4/Air


Figure E.19.: Predicted premixed laminar flame speed by different reaction mechanisms and its comparison with experimental value at 20 atm

Table E.19.: Absolute mean percentage error from experimental values of each reaction mechanism at 20 atm.

Reaction mechanism	MAPE (test 6)
C1-C4 Zhukov	18%
NewMechanism	11%
Zhukov & Kong	42%
RAMEC	18%
Red.Slavinskaya	10%
REDRAM	71%
Aramcomech 1.3	8%
Tiafeng Lu	24%
Westbrook & Dryer (Airbus DS)	113%
Jones–Lindstedt (Frassoldati)	300%
GRI-Mech 3.0	31%

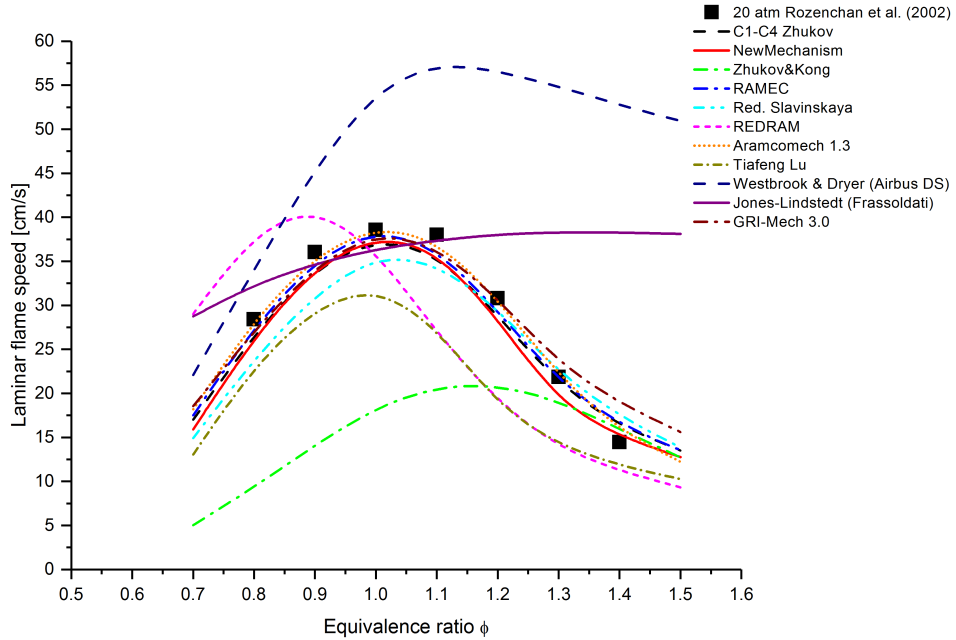
Test 7: $p = 20 \text{ atm}$, $T_u = 298 \text{ K}$, mixture = $\text{CH}_4/(\text{O}_2+\text{HE})$


Figure E.20.: Predicted premixed laminar flame speed by different reaction mechanisms and its comparison with experimental value at 20 atm

Table E.20.: Absolute mean percentage error from experimental values of each reaction mechanism at 20 atm.

Reaction mechanism	MAPE (test 7)
C1-C4 Zhukov	5%
NewMechanism	6%
Zhukov & Kong	40%
RAMEC	4%
Red.Slavinskaya	10%
REDRAM	26%
Aramcomech 1.3	2%
Tiafeng Lu	25%
Westbrook & Dryer (Airbus DS)	92%
Jones–Lindstedt (Frassoldati)	41%
GRI-Mech 3.0	8%

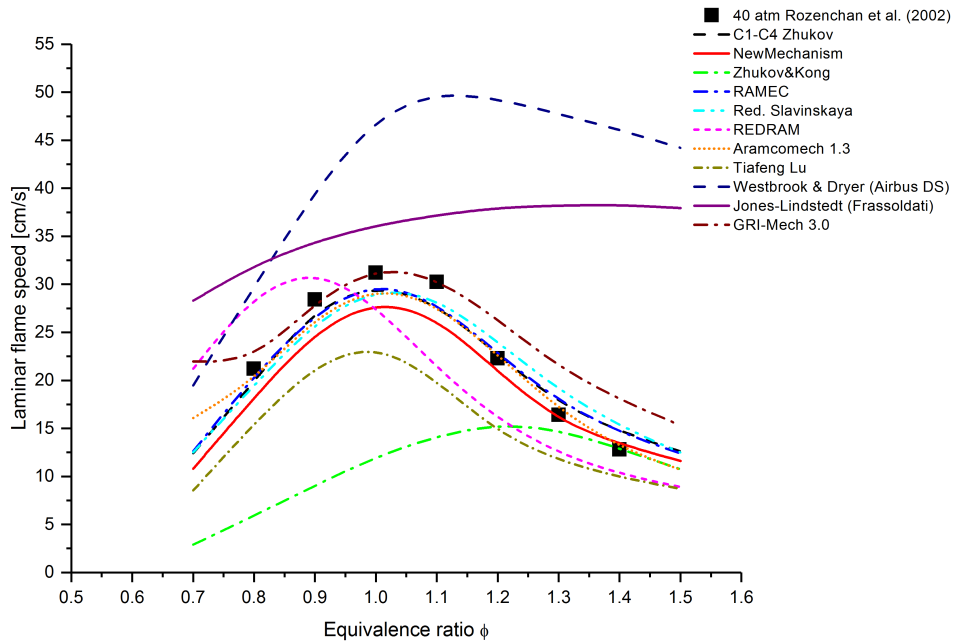
Test 8: $p = 40 \text{ atm}$, $T_u = 298 \text{ K}$, mixture = $\text{CH}_4/(\text{O}_2+\text{HE})$ 

Figure E.21.: Predicted premixed laminar flame speed by different reaction mechanisms and its comparison with experimental value at 40 atm

Table E.21.: Absolute mean percentage error from experimental values of each reaction mechanism at 40 atm.

Reaction mechanism	MAPE (test 8)
C1-C4 Zhukov	5%
NewMechanism	9%
Zhukov & Kong	43%
RAMEC	6%
Red.Slavinskaya	9%
REDRAM	23%
Aramcomech 1.3	4%
Tiafeng Lu	28%
Westbrook & Dryer (Airbus DS)	110%
Jones–Lindstedt (Frassoldati)	75%
GRI-Mech 3.0	14%

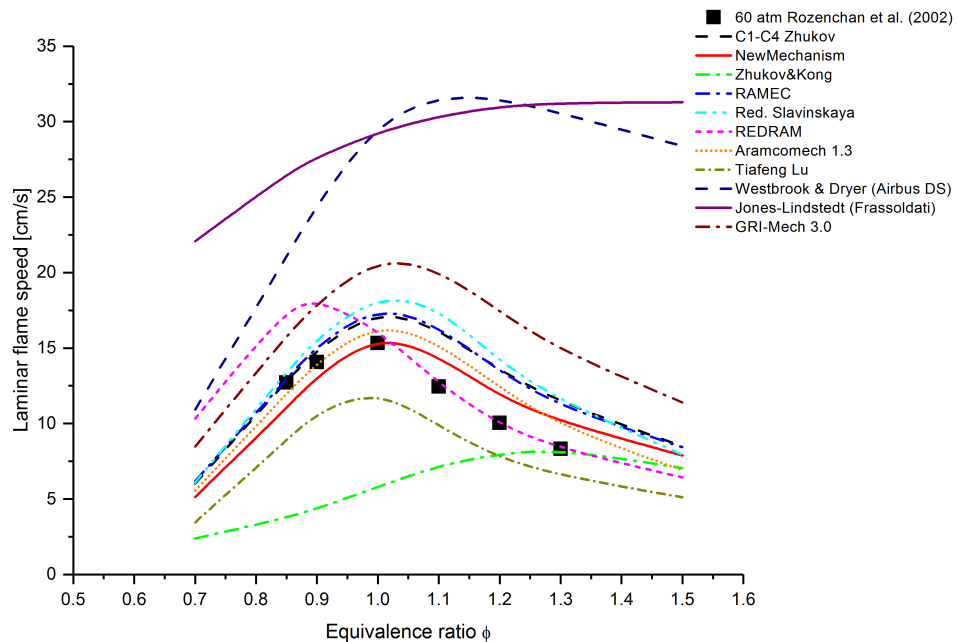
Test 9: $p = 60 \text{ atm}$, $T_u = 298 \text{ K}$, mixture = $\text{CH}_4/(\text{O}_2+\text{HE})$


Figure E.22.: Predicted premixed laminar flame speed by different reaction mechanisms and its comparison with experimental value at 60 atm

Table E.22.: Absolute mean percentage error from experimental values of each reaction mechanism at 60 atm.

Reaction mechanism	MAPE (test 8)
C1-C4 Zhukov	20%
NewMechanism	13%
Zhukov & Kong	48%
RAMEC	21%
Red.Slavinskaya	27%
REDRAM	13%
Aramcomech 1.3	13%
Tiafeng Lu	23%
Westbrook & Dryer (Airbus DS)	145%
Jones–Lindstedt (Frassoldati)	154%
GRI-Mech 3.0	51%

F. Verification results

Test 1: $\chi = 0.9$, $p = 20$ bar, mixture = CH₄/O₂

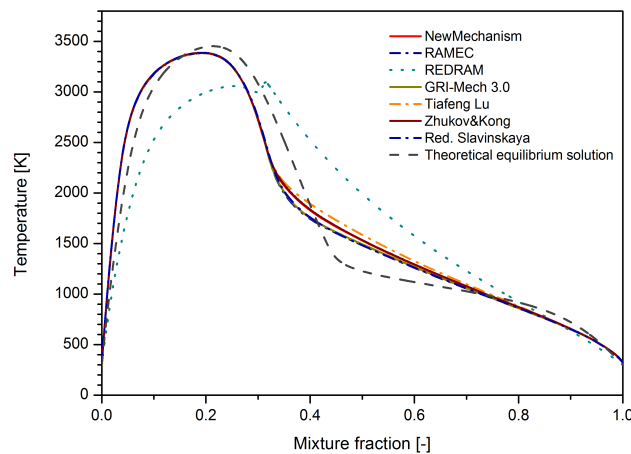


Figure F.1.: Comparison between theoretical equilibrium temperature with temperature profile of different reaction mechanisms at 20 bar over mixture fraction.

Test 2: $\chi = 0.5$, $p = 30$ bar, mixture = CH₄/O₂

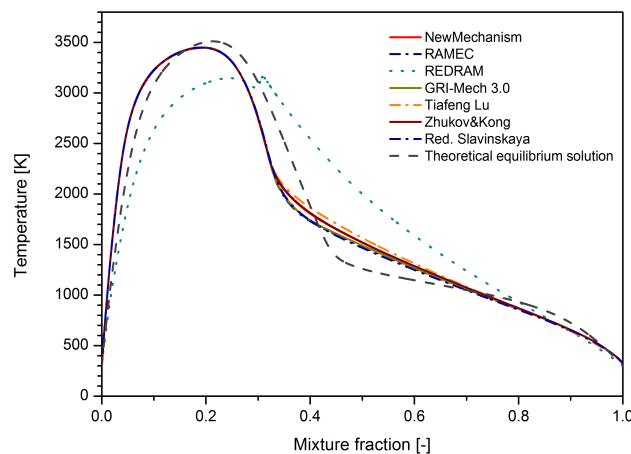


Figure F.2.: Comparison between theoretical equilibrium temperature with temperature profile of different reaction mechanisms at 30 bar over mixture fraction.

Test 3: $\chi = 1.5$, $p = 60$ bar, mixture = CH₄/O₂

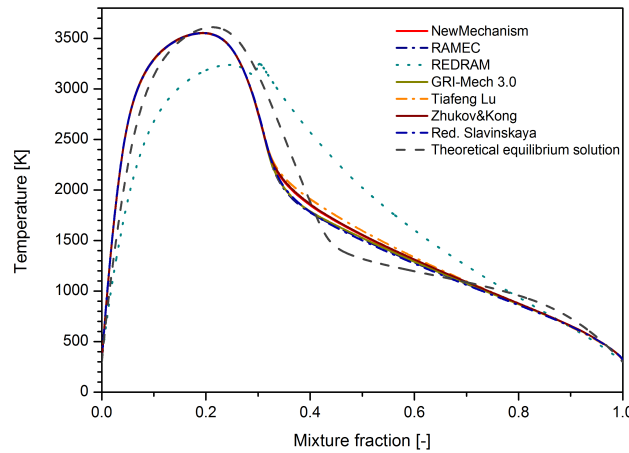


Figure F.3.: Comparison between theoretical equilibrium temperature with temperature profile of different reaction mechanisms at 60 bar over mixture fraction.

Test 4: $\chi = 3.8$, $p = 80$ bar, mixture = CH₄/O₂

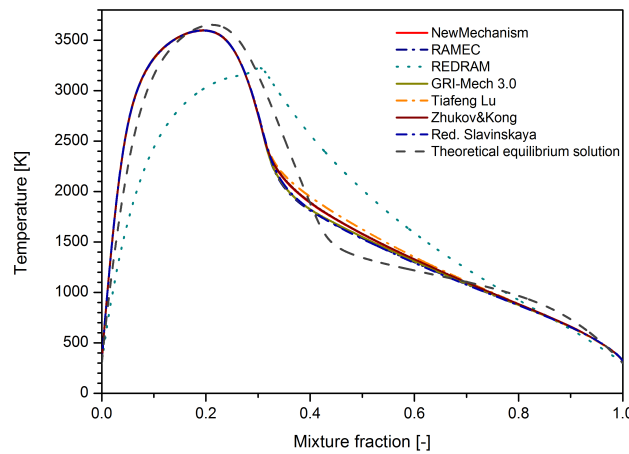


Figure F.4.: Comparison between theoretical equilibrium temperature with temperature profile of different reaction mechanisms at 80 bar over mixture fraction.

G. NewMechanism in CHEMKIN format

This CH₄/O₂ reaction mechanism named NewMechanism is developed within framework of this thesis. Detailed information about the development process can be found in Chapter 6. It is recommended by the author to use the thermodynamic and transport data from [25].

ELEMENTS

H C O N AR HE

END

SPECIES

H₂ H O O₂ OH H₂O HO₂ H₂O₂

CH₃ CH₄ CO CO₂ HCO CH₂ O CH₃O

C₂H₃ C₂H₄ C₂H₅ C₂ H₆ CH₃O₂ N₂ AR HE CH₃OH

CH₂OH CH₃O₂H

END

REACTIONS CAL/MOLE

H+O₂+M<=>HO₂+M 2.800E+18 -0.860 0.00

O₂/0.00 / H₂

O/0.00 / CO/0.75/CO₂/1.50/

C₂H₆/1.50/

N₂/0.00 / AR/0.00/

H+2O₂<=>HO₂+O₂ 3.000E+20 -1.720 0.00

H+CH₂O(+M)<=>CH₃O(+M) 5.400E+11 0.454 2600.00

LOW / 2.200E+30 -4.800 5560.00 /

TROE/ 0.7580 94.00 1555.00 4200.00 /

H₂/2.00 / H₂O/6.00 / CH₄/2.00/AR/0.00//

CO/1.50 / CO₂/2.00 / C₂H₆/3.00/AR/0.00/

$2\text{OH}(+\text{M}) \rightleftharpoons \text{H}_2\text{O}_2(+\text{M})$ 7.400E+13 -0.370 0.00
 LOW / 2.300E+18 -0.900 -1700.00 /
 TROE/ 0.7346 94.00 1756.00 5182.00 /
 $\text{H}_2/2.00/\text{H}_2\text{O}/6.00/\text{CH}_4/2.00/\text{AR}/0.7/$
 $\text{CO}/1.50/\text{CO}_2/2.00/\text{C}_2\text{H}_6/3.00\text{AR}/0.7/$
 $\text{OH}+\text{HO}_2 \rightleftharpoons \text{O}_2+\text{H}_2\text{O}$ 2.900E+13 0.000 -500.00
 $\text{OH}+\text{H}_2\text{O}_2 \rightleftharpoons \text{HO}_2+\text{H}_2\text{O}$ 1.750E+12 0.000 320.00
 DUPLICATE
 $\text{OH}+\text{H}_2\text{O}_2 \rightleftharpoons \text{HO}_2+\text{H}_2\text{O}$ 5.800E+14 0.000 9560.00
 DUPLICATE
 $\text{OH}+\text{CH}_4 \rightleftharpoons \text{CH}_3+\text{H}_2\text{O}$ 1.000E+08 1.600 3120.00
 $2\text{HO}_2 \rightleftharpoons \text{O}_2+\text{H}_2\text{O}_2$ 1.300E+11 0.000 -1630.00
 DUPLICATE
 $2\text{HO}_2 \rightleftharpoons \text{O}_2+\text{H}_2\text{O}_2$ 4.200E+14 0.000 12000.00
 DUPLICATE
 $\text{HO}_2+\text{CH}_3 \rightleftharpoons \text{O}_2+\text{CH}_4$ 1.000E+12 0.000 0.00
 $\text{HO}_2+\text{CH}_3 \rightleftharpoons \text{OH}+\text{CH}_3\text{O}$ 2.000E+13 0.000 0.00
 $\text{HO}_2+\text{CO} \rightleftharpoons \text{OH}+\text{CO}_2$ 1.500E+14 0.00 23600.00
 $\text{HO}_2+\text{CH}_2\text{O} \rightleftharpoons \text{HCO}+\text{H}_2\text{O}_2$ 1.000E+12 0.000 8000.00
 $\text{CH}_3+\text{O}_2 \rightleftharpoons \text{OH}+\text{CH}_2\text{O}$ 3.600E+10 0.000 8940.00
 $\text{CH}_3+\text{H}_2\text{O}_2 \rightleftharpoons \text{HO}_2+\text{CH}_4$ 2.450E+04 2.470 5180.00
 $\text{CH}_3+\text{CH}_2\text{O} \rightleftharpoons \text{HCO}+\text{CH}_4$ 3.320E+03 2.810 5860.00
 $\text{CH}_3\text{O}+\text{HO}_2 \rightleftharpoons \text{CH}_2\text{O}+\text{H}_2\text{O}_2$ 1.200E+13 0.000 0.00
 $\text{CH}_3\text{O}_2+\text{CH}_3 \rightleftharpoons \text{CH}_3\text{O}+\text{CH}_3\text{O}$ 3.000E+13 0.000 -1200.00
 $\text{CH}_3\text{O}+\text{O}_2 \rightleftharpoons \text{HO}_2+\text{CH}_2\text{O}$ 4.280E-13 7.600 -3530.00
 $\text{CH}_3+\text{O}_2 \rightleftharpoons \text{CH}_3\text{O}_2$ 1.700E+60 -15.100 18785.00
 $\text{CH}_3\text{O}+\text{CH}_3 \rightleftharpoons \text{CH}_2\text{O}+\text{CH}_4$ 2.410E+13 0.000 0.00
 $\text{O}+\text{CH}_4 \rightleftharpoons \text{OH}+\text{CH}_3$ 1.020E+09 1.500 8600.00
 $\text{H}+\text{O}_2 \rightleftharpoons \text{O}+\text{OH}$ 8.300E+13 0.000 14413.00
 $\text{H}+\text{C}_2\text{H}_4(+\text{M}) \rightleftharpoons \text{C}_2\text{H}_5(+\text{M})$ 1.080E+12 0.454 1820.00

$\text{H} + \text{C}_2\text{H}_4(+\text{M}) \rightleftharpoons \text{C}_2\text{H}_5(+\text{M})$ 1.080E+12 0.454 1820.00
 LOW / 1.200E+42 -7.620 6970.00 /
 TROE/ 0.9753 210.00 984.00 4374.00 /
 $\text{H}_2/2.00/\text{H}_2\text{O}/6.00/\text{CH}_4/2.00/$
 $\text{CO}/1.50/\text{CO}_2/2.00/\text{C}_2\text{H}_6/3.00/\text{AR}/0.70/$
 $\text{H} + \text{O}_2 + \text{H}_2\text{O} \rightleftharpoons \text{HO}_2 + \text{H}_2\text{O}$ 9.380E+18 -0.760 0.00
 $\text{O} + \text{H}_2 \rightleftharpoons \text{H} + \text{OH}$ 5.000E+04 2.670 6290.00
 $\text{O} + \text{CH}_3 \rightleftharpoons \text{H} + \text{CH}_2\text{O}$ 8.430E+13 0.000 0.00
 $\text{H} + \text{CH}_3(+\text{M}) \rightleftharpoons \text{CH}_4(+\text{M})$ 1.270E+16 -0.630 383.00
 LOW / 2.477E+33 -4.760 2440.00 /
 TROE/ 0.7830 74.00 2941.00 6964.00 /
 $\text{H}_2/2.00/\text{H}_2\text{O}/6.00/\text{CH}_4/2.00/$
 $\text{CO}/1.50/\text{CO}_2/2.00/\text{C}_2\text{H}_6/3.00/\text{AR}/0.70/$
 $\text{H} + \text{C}_2\text{H}_4 \rightleftharpoons \text{C}_2\text{H}_3 + \text{H}_2$ 1.325E+06 2.530 12240.00
 $\text{H} + \text{C}_2\text{H}_6 \rightleftharpoons \text{C}_2\text{H}_5 + \text{H}_2$ 1.150E+08 1.900 7530.00
 $\text{OH} + \text{H}_2 \rightleftharpoons \text{H} + \text{H}_2\text{O}$ 2.160E+08 1.510 3430.00
 $\text{OH} + \text{C}_2\text{H}_6 \rightleftharpoons \text{C}_2\text{H}_5 + \text{H}_2\text{O}$ 3.540E+06 2.120 870.00
 $\text{HCO} + \text{O}_2 \rightleftharpoons \text{HO}_2 + \text{CO}$ 7.600E+12 0.000 400.00
 $\text{HCO} + \text{M} \rightleftharpoons \text{H} + \text{CO} + \text{M}$ 1.870E+17 -1.000 17000.00
 $\text{H}_2/2.00/\text{H}_2\text{O}/12.0/\text{CH}_4/2.00/$
 $\text{CO}/1.50/\text{CO}_2/2.00/\text{C}_2\text{H}_6/3.00/$
 $\text{CH}_3 + \text{OH} \rightleftharpoons \text{CH}_2\text{O} + \text{H}_2$ 8.000E+12 0.000 0.00
 $\text{OH} + \text{CO} \rightleftharpoons \text{H} + \text{CO}_2$ 4.760E+07 1.228 70.00
 $\text{OH} + \text{CH}_2\text{O} \rightleftharpoons \text{HCO} + \text{H}_2\text{O}$ 3.430E+09 1.180 -447.00
 $\text{H} + \text{CH}_2\text{O} \rightleftharpoons \text{HCO} + \text{H}_2$ 2.300E+10 1.050 3275.00
 $\text{H} + \text{CH}_4 \rightleftharpoons \text{CH}_3 + \text{H}_2$ 6.600E+08 1.620 10840.00
 $\text{H} + \text{O}_2 + \text{N}_2 \rightleftharpoons \text{HO}_2 + \text{N}_2$ 2.600E+19 -1.240 0.00
 $\text{H} + \text{O}_2 + \text{AR} \rightleftharpoons \text{HO}_2 + \text{AR}$ 7.000E+17 -0.800 0.00
 $\text{HCO} + \text{H}_2\text{O} \rightleftharpoons \text{H} + \text{CO} + \text{H}_2\text{O}$ 2.244E+18 -1.000 17000.00
 $\text{CH}_3 + \text{HCO} \rightleftharpoons \text{CH}_4 + \text{CO}$ 2.648E+13 0.000 0.00

2CH₃(+M)<=>C₂H₆(+M) 2.120E+16 -0.970 620.00
LOW / 1.770E+50 -9.670 6220.00/
TROE/ 0.5325 151.00 1038.00 4970.00 /
H₂/2.00/ H₂O/6.00/ CH₄/2.00/
CO/1.50/ CO₂/2.00/ C₂H₆/3.00/ AR/0.70/
OH+C₂H₄<=>C₂H₃+H₂O 3.600E+06 2.000 2500.00
H+CH₃OH<=>CH₂OH+H₂ 1.700E+07 2.100 4870.00
H+HO₂<=>O₂+H₂ 2.800E+13 0.000 1068.00
H+HO₂<=>2OH 1.340E+14 0.000 635.00
C₂H₅+O₂<=>HO₂+C₂H₄ 8.400E+11 0.000 3875.00
CH₃O₂+H₂O₂<=>CH₃O₂H+HO₂ 2.40E+12.000 9942.00
C₂H₃+O₂<=>HCO+CH₂O 3.980E+12 0.000 -240.00
2CH₃<=>H+C₂H₅ 4.990E+12 0.100 10600.00
END

H. Westbrook & Dryer reaction mechanism in CHEMKIN format

ELEMENTS

H O C

END

SPECIES

CH₄ O₂ CO H₂O CO₂ H OH

END

REACTIONS CAL/MOLE

CH₄+1.5O₂ →CO+2H₂O 1.612E+13 0.000 47800.00

FORD / CH4 0.7 /

FORD / O2 0.8 /

CO+0.5O₂ →CO₂ 2.24E+15 0.000 40700.00

CO₂ → CO+0.5O₂ 5.104E+11 0.000 40700.00

H₂O = H+OH 2.300E+22 -3.000 120000.00

END

I. Nomenclature

Latin symbols

A	Pre-exponential factor	[1/s]
A	Area	[m ²]
c_e	Effective exit velocity	[m/s]
c_p	Specific heat capacity at constant pressure	[J/(kgK)]
c_v	Specific heat capacity at constant volume	[J/(kgK)]
D	Mass diffusivity	[m ² /s]
Da	Damkoehler number	[−]
E	Energy	[J]
E_s	Sensitivity coefficient	[−]
F	Thrust	[N]
g	Gravitational acceleration	[9.81m/s ²]
h	Specific static enthalpy	[J/kg]
l	length	[m]
I_{sp}	Specific impulse	[s]
J	Diffusion flux	[m ² /s]
K	Equilibrium constant	[−]
k	reaction rate	[1/s]
k_B	Boltzmann constant	[J/K]
Le	Lewis number	[−]
\dot{m}	Mass flow	[kg/s]
m	Mass	[kg]
M	Molar mass	[kg/mol]
Nu	Nusselt number	[−]
p	Pressure	[bar]

Pr	Prandtl number	[$-$]
Q	Source or sink	[$J/m^3 s$]
Re	Reynolds number	[$-$]
R	Universal gas constant	[$J/(molK)$]
s	Specific entropy	[$J/(kgK)$]
S_m	Mass source term	[kg/s]
S_h	Energy source term	[W]
S_i	Species source term	[$kg/m^3 s$]
T	Temperature	[K]
t	Time	[s]
u	Velocity	[m/s]
v	Velocity	[m/s]
V	Volume	[m^3]
x, y, z	Spatial coordinates	[m]
W	Density of conserved variable	[J/m^3]
X	Molar fraction	[$-$]
Y	Mass fraction	[$-$]
Z	Mixture fraction	[$-$]

Greek symbols

α	Strain rate	[$1/s$]
α	Thermal diffusivity	[m^2/s]
ε	Wall depth of Lennard–Jones	[J]
λ	Thermal conductivity	[W/mK]
μ	Dynamic viscosity	[$kg/m\ s$]
ν	Stoichiometric coefficient	[$-$]
ρ	Density	[kg/m^3]
ϕ	Equivalence ratio	[$-$]
τ	Time scale	[s]
τ_{ing}	Ignition delay time	[s]
τ_{ind}	Induction time	[s]

χ	Scalar dissipation rate	[1/s]
σ	Collision diameter	[m]
Ω	Reduced collision integral	[–]

Indices

0	Initial
a	Activation
a	Ambient
b	Burnt
b	Temperature exponent
c	Combustion chamber
$chem$	Chemical
e	Exit of the nozzle
f	Forward
f	Fuel
ox	Oxidizer
r	Backward
r	Reaction
rot	Rotation
s	Species
st	Stoichiometric
$trans$	Translation
t	Total
th	Nozzle throat
u	Unburnt
vib	Vibration

Abbreviations

0D	Zero Dimension
1D	One Dimension
2D	Two Dimension
3D	Three Dimension
Airbus DS	Airbus Defence and Space
B.Sc	Bachelor of Science
BE-3	Blue Engine 3
CEA	Chemical Equilibrium with Applications
CFD	Computational Fluid Dynamics
DLR	Deutsches Zentrum fuer Luft-und Raumfahrt
DNS	Direct Numerical Simulation
ESA	European Space Agency
GOX	Gaseous Oxygen
GCH ₄	Gaseous Methane
GN2	Gaseous Oxygen
HTPB	Hydroxyl-Terminated Polybutadiene
LOX	Liquid Oxygen
LH ₂	Liquid Hydrogen
LN2	Liquid Nitrogen
LNG	Liquefied Natural Gas
LES	Large Eddy Simulation
MMH	Monomethylhydrazine
M.Sc	Master of Science
MAPE	Mean Absolute Percentage Error
ODE	Ordinary Differential Equation
PDE	Partial Differential Equation
PhD	Doctor of Philosophy
RANS	Reynolds-Averged Navier-Stokes Equations
RP-1	Rocket Propellant 1 (Refined Petroleum 1)

SpaceX	Space Exploration Technologies Corporation
TUM	Technical University of Munich
UniBW	University of Bundeswehr
URANS	Unsteady Reynolds-Averaged Navier-Stokes Equations

Bibliography

- [1] O. J. Haidn. *Advanced Rocket Engines*. Advances on Propulsion Technology for High-Speed Aircraft, 2008.
- [2] O. J. Haidn. *Script of lecture Grundlagen Raumfahrtantriebe*. Chair of Turbomachinery and Flight Propulsion, TU Munich, 2016.
- [3] P. Atkins. *Atkins' physical chemistry*. Oxford University Press, 2006.
- [4] U. Mass J. Warnatz and R. W. Dibble. *Combustion 4th Edition*. Springer- Verlag Berlin Heidelberg, 2006.
- [5] D. Parker. [Online] [Available:<https://pixels.com/featured/propane-gas-flame-from-a-bunsen-burner-david-parker.html>], [Accessed:4.8.2017].
- [6] N. Perakis. *Flamelet modeling and simulation of CH₄/O₂ rocket thrust chambers*. Technical University of Munich, Master's thesis, 2016.
- [7] X. Wang H. Huo and V. Yang. *A general study of counterflow diffusion flames at subcritical and supercritical condition: Oxygen/hydrogen mixtures*. Combustion and Flame, vol. 161, pp. 3040 - 3050, 2014.
- [8] V. A. Sechenov V. P. Zhukov and A. Yu. Straikovskii. *Spontaneous Ignition of Methane Air Mixtures in a Wide Range of Pressure*. Combustion, Explosion, and Shock Waves, vol. 39, no. 5, pp. 487-495, 2003.
- [9] D. Goodwin. *Cantera workshop, Introduction*. California Institute of Technology, Division of Engineering and Applied Science, 2004.
- [10] H. Folger. *Elements of Chemical Reaction Engineering*. Prentice Hall, Part of the Prentice Hall International Series in the Physical and Chemical Engineering Sciences series, 2016.
- [11] V. P. Zhukov. *Kinetic Modelling of n-Decane Ignition at High Pressure*. 20th International Colloquium on the Dynamics of Explosion and Reactive Systems, Poitiers, France, 2007.
- [12] U. Burke and K. Somers. *An ignition delay and kinetic modeling study of methane, dimethyl ether and their mixtures at high pressures*. Combustion and Flame, 2014.
- [13] S. Gersen and A. Mokhov. *Ignition promoting effect of NO₂ on methane, ethane and methane/ethane mixtures in a rapid compression machine*. Proceedings of the Combustion Institute, 2014.

- [14] Z. Huang and Y. Zhang. *Experimental and modeling study on ignition delay of lean mixtures of methane, hydrogen, oxygen and argon at elevated pressures, Comubstion and Flame.* 2012.
- [15] C. Vagelopoulos and F. Egolfopoulos. *Direct Experimental Determinatin of Laminar Flame Speeds.* Proceedings of the Combustion Institue 27, pp. 513-519, 1998.
- [16] Y. Kocher and J. Seitzmann. *Laminar flame speed measured and modeling of alkane blends at elevated pressures with various diluents.* Proceedings of ASME Turbo Expo, Vancouver, British Columbia, Canada, 2011.
- [17] C. Zheng and G. Ruofei. *LM-3A Series Launch Vehicle User's Manuel.* China Aerospace Science and Technology Corporation, 2011.
- [18] H. Burkhardt and M. Stippel. *Comparative Study of Kersosene and Methane Propellant Engines for Reusable Liquied Booster Stages.* 4th International Conference on Launcher Technology, Space Launcher Liquid Propulsion, 2002.
- [19] H. Vernin and P. Pempe. *LOX/CH4 and LOX/LH2 Heavy Launch Vehicle comparison.* 45th AIAA/ASME/SAE/ASEE Joint Propulsion Conference & Exhibit, Denver, Colorado, 2009.
- [20] G. P. Sutton and O. Biblarz. *Rocket propulsion elements.* John Wiley & Sons, INC, New York, Brinsbane, 2001.
- [21] O. J. Haidn. *Script of Lecture Raumfahrtantriebe 1, TU Munich.* WS 16/17.
- [22] SFBTR40. [Online], [Available:<http://www.sfbtr40.de/index.php?id=home>], [Accessed:14.6.2017].
- [23] O. J. Haidn and O. Knab. *Test Case BKS-2, Single Element Combustin Chamber GCH4/GOX.* Technical University of Munich, 2013.
- [24] O. J. Haidn. *Test Case BKS-2, 7 Elements Combustin Chamber GCH4/GOX.* Technical University of Munich, 2014.
- [25] W. Metlcalfe and S. Burke. *A Hierarchical and Comarative Kinetic Modeling Study of C1-C2 Hydrocarbons and Oxygenated Fuels.* International Journal of Chemical Kinetics, vol. 45, pp. 638-675, 2013.
- [26] V. P. Zhukov. *Kinetic Model of Alkane Oxidation at high Pressure from Methane to N-Heptane.* Combustion and Theory Modelling, vol.13, no. 3, pp. 427-442, 2009.
- [27] G. P. Smith and D. Golden. *GRI-Mech 3.0 reaction mechanism,* Gas Research Institute. www.me.berkeley.edu/grimech/, 2016.
- [28] E. Petersen and D. Davidson. *Kinetics Modeling of Shock Induced Ignition in Low Diluation CH₄/O₂ at High Pressures and Intermediate Temperatures.* Combustion and Flame vol. 117, pp. 272-290, 1999.

- [29] N. Slavinskaya et al. *Methane Skeletal Mechanism for Space Propulsion Applications*. Propulsion and Energy Forum, 2016.
- [30] V. P. Zhukov and A. Kong. *A Compact Reaction Mechanism of Methane Oxidation at High Pressures*. Progress in Reaction Kinetics and Mechanism, forthcoming, 2018.
- [31] E. Petersen and R. Hanson. *Reduced Kinetics Mechanisms for Ram Accelerator Combustion*. Journal of Propulsion and Power, 1999.
- [32] T. Feng Lu and C. Law. *A criterion based on computational singular perturbation for the identification of quasi steady state species, A reduced mechanism for methane oxidation with NO chemistry*. Combustion and Flame, vol. 154, pp. 761-774, 2008.
- [33] A. Frassoldati. *Simplified kinetic schemes for oxy-fuel combustion*. Sonderforschungsbereich/Transregio 40- Summer Program Report, 2015.
- [34] H. Riedmann and O. Knab. *Two dimensional and three dimensional RANS Simulations of a GOX/GCH₄ Single Element Combustion Chamber*. 1st International Conference on Sustainable Fossil Fuel for Future Energy, 2009.
- [35] R. Hahn and G. Waxenegger. *Utilization of LOX/LCH₄ for Expander-Bleed Cycle at Upper Stage Engine Application*, 7th European Conference for Aeronautics and Space Sciences (EUCASS). 2015.
- [36] Y. Daimon and H. Terashima. *Combustion modeling study for GCH₄/GOx single element combustion chamber*. Project presentation in the SFBTRR40 Summer Program, Technical University of Munich, 2015.
- [37] P. Afonos V. Serrano and D. Bastos. *Numerical Evaluation of the Flow inside the transonic nozzle of a direct connect supersonic combustion research facility*. 18th International Congress of Mechanical Engineering, 2005.
- [38] U. Rana M. Luo and O.J. Haidn. *Modeling investigation of liquid oxygen flashing spray with CFD*. International Journal of Heat and Mass Transfer, forthcoming, 2018.
- [39] N. K. Truong R. J. Stalker and R. G. Morgan. *Effect of hydrogen-air non-equilibrium chemistry on the performance of a model scramjet thrust nozzle*. The Aeronautical Journal, 2004.
- [40] M. Marmurena. *A computational fluid dynamics investigation of rocket nozzle flow for frozen and shifting chemical equilibrium*. The Aeronautical Journal, 2004.
- [41] S. Gopalakrishnan. *Modeling of thermal non-equilibrium in superheated injector flows*. University of Massachusetts, Dissertation, 2010.
- [42] N. Georgiadis D. A. Yoder and M. Gara. *Frozen chemistry effects on nozzle performance simulations*. 38th Fluid Dynamics Conference and Exhibit, AIAA, Seattle Washington, 2008.

- [43] M. M. Sanchez. *Script of lecture Rocket propulsion*. Massachusetts Institute of Technology, 2005.
- [44] K. T. Aung M. Hassan and G. M. Faeth. *Measured and predicted properties of laminar premixed methane/air flames at various pressures*. Combustion and Flame, vol. 115, pp. 539 - 550, 1998.
- [45] N. Peters and B. Rogg. *Lecture notes in physics, Reduced kinetic mechanisms for application in combustion systems*. Springer-Verlag, Berlin Heidelberg, 1993.
- [46] T. Turanyi and A. S. Tomlin. *Analysis of kinetic reaction mechanisms*. Springer-Verlag, Berlin Heidelberg, 2014.
- [47] H. K. Moffat D. G. Goodwin and R. L. Speth. *Cantera: An object-oriented software toolkit for chemical kinetics, thermodynamics and transport processes* [Online] [Available:<http://www.cantera.org/docs/sphinx/html/index.html>], [Accessed:4.5.2017].
- [48] F. L. Dryer D. J. Hautman and K. P. Schlug. *A multiple-step overall kinetics mechanism for the oxidation of hydrocarbons*. Combustion Science and Technology, vol. 25, no. 5, pp. 219-235, 1981.
- [49] J. F. Griffiths. *Reduced kinetic models and their application to practical combustion systems*. Progress in Energy Combustion Science, vol. 21, pp. 25-107, 1995.
- [50] J. M. Simmie. *Detailed chemical kinetic models for the combustion of hydrocarbon fuels*. Progress in Energy Combustion Science, vol. 29, pp. 599-634, 2003.
- [51] P. M. Lefdal G. Paczko and N. Peters. *Reduced reaction schemes for methane, methanol and propane flames*. 21st Symposium (International) on combustion/The Combustion Institute, pp. 739-748, 1986.
- [52] S. Rolland and J. M. Simmie. *The comparison of detailed chemical kinetics mechanisms: Application to the combustion of methane*. Wiley InterScience online, 2004.
- [53] T. M. Slonae and P. D. Ronney. *A comparison of ignition phenomena modelled with detailed and simplified kinetics*. Combustion Science and Technology, vol. 88, pp. 1-13, 1992.
- [54] L. Vervisch P. Domingo and D. Veynante. *Autoignition and flame propagation effects in LES of burned gases diluted turbulent combustion*. Proceedings of the summer program, Center for Turbulence Research, France, 2006.
- [55] F. E. Fendell G. F. Carrier and F. E. Marble. *The effect of strain rate on diffusion flames*. SIAM J. Appl. Math, vol. 28, no. 2, 1975.
- [56] G. Lacaze and J. Oefelein. *A non-premixed combustion model based on flame structure analysis at supercritical pressures*. US Department of Energy Publications, University of Nebraska-Lincoln, 2012.

- [57] N. Zong G. Ribert and V. Yang. *Counterflow diffusion flames of general fluids: Oxygen/hydrogen mixtures*. Combustion and Flame, vol. 154, pp. 319-330, 2008.
- [58] B. A. Williams E. M. Fisher and J. W. Fleming. *Determination of the strain in counterflow diffusion flames from flow conditions*. Proceedings of the eastern states section of the combustion institute, pp. 191-194, 1997.
- [59] T. Fiala and T. Sattelmayer. *Nonpremixed counterflow flames: Scaling rules for batch simulations*. Journal of Combustion, vol., 2014.
- [60] P. G. Hill J. Haung and W. K. Bushe. *Shock-tube study of methane ignition under engine-relevant conditions: experiments and modeling*. Combustion and Flame, vol. 136, pp. 25-42, 2004.
- [61] A. Vandel E. Varea and V. Modica. *Measurement of laminar flame speed for high pressure and high temperature conditions validation of the facility and development of new tool for post-processing*. 15th International Symposium on application laser techniques to fluid mechanics, Lisbon, Portugal, July, 2010.
- [62] S. N. Vaden Y. N. Kochar and T. Lieuwen. *Laminar flame speed of hydrocarbons fuels with preheat and low oxygen content*. 48th AIAA Aerospace Sciences Meeting Including the New Horizons Forum and Aerospace Exposition, Orlando, Florida, January, 2010.
- [63] P. Gerlinger. *Numerische Verbrennungssimulation, effiziente numerische Simulation turbulenter Verbrennung*. Springer- Verlag Berlin Heidelberg, 2005.
- [64] Y. Zeldovich and D. Frank-Kamenetskii. *The theory of thermal propagation of flames*. Zh Fiz Khim 12:100, 1938.
- [65] ANSYS Inc. *ANSYS Fluent Theory Guide*. ANSYS, Inc, Release 14, 2011.
- [66] N. Peters. *Combustion Theory, CEFRC Summer School Princeton*. June - July, 2010.
- [67] R. Bilger. *The structure of turbulent nonpremixed flames*. in Twenty-second Symposium (International) on Combustion,Pittsburgh, PA,USA, 1988.
- [68] B. Williams and J. Fleming. *Determination of the strain in counterflow diffusion flames from flow conditions*. Proceedings of the Eastern States Section of the Combustion Institute, pp. 191-194, 2012.
- [69] G. Fendell and F. Marble. *The effect of strain rate on diffusion flames*. SIAM Journal on applied mathematics vol. 28 no. 2, pp. 463-500, 1975.
- [70] L. Guilhem and J. Oefelein. *A non-premixed combustion model based on flame structure analysis at supercritical pressures*. Combustion and Flame vol. 159.6, pp. 2987-2103, 1975.
- [71] E. Petersen and D. Davidson. *Kinetics Modeling of Shock-Induced Ignition in Low Dilution CH₄/O₂ Mixtures at High Pressures and Intermediate Temperatures*. Combustion and Flame, vol. 177, pp. 272-290, 1999.

- [72] H. K. Versteeg and W. Malalasekera. *An introductin to Computational Fluid Dynamics*. Longmann Group Limited and John Wiley and Sons Inc, 1995.
- [73] E. Petersen and K. Hanson. *Reduced Kinetics Mechanism for Ram Accelerator Combustion*. Journal of Propulsion and Power, vol. 15, no.4, 1999.
- [74] J. Evans and C. Schexnayder. *Influence of Chemical Kinetics and Unmixedness on Burning in Supersonic Hydrogen Flames*. AIAA Journal., vol. 18, no. 2, pp. 188-193, 1980.
- [75] W. Jones and R. Lindstedt. *Global Reaction Schemes for Hydrocarbon Combustion*. Combustion and Flame,, vol. 73, pp. 233-249, 1998.
- [76] D. Hautmann and F. Dryer. *A Multiple-Step Overall Kinetic Mechanism for the Oxidation of Hydrocarbons*. Combustion Science and Technology, vol. 24, no. 5, pp. 219-249, 1981.
- [77] N. Peters and B. Rogg. *Reduced Kinetic Mechanism for Applications in Combustion System*. Springer Verlag, Berlin, 1993.
- [78] R. Schmehl and J. Steeland. *Computational Analysis of the Oxidizer Preflow in an Upper-Stage Rocket Engine*. Journal of Propulsion and Power, vol. 25, no. 3, 2009.
- [79] Incropera and D. Bergman. *Fundamentals of Heat and Mass Transfer*. John Wiley and Sons,6th Edition, 2006.
- [80] R. Miller and J.Bellan. *Evaluation of equilibrium and non-equilibrium evaporation models for many-droplet gas-liquid flow simulations*. International Journal of Multiphase Flow, 1998.
- [81] NIST. [Online] [Available:<http://webbook.nist.gov/chemistry/fluid/>], [Accessed:4.6.2017].
- [82] E. Oran and J. Boris. *Numerical Simulation of Detonations in Hydrogen-Air and Methan-Air Mixture*. 18th Symposium (International) on Combustion, The Combustion Inst., Pittsburgh, P.A, pp. 1641-1649, 1981.
- [83] L. Clifford and A. Milne. *Numerical Modeling of Chemistry and Gas Dynamics During Shock Induced Ethylene Combustion*. Combustion and Flame, vol. 104, no. 3, pp. 311-327, 1996.
- [84] E. Oran. and J. Boris. *Weak and Strong Ignition II. Sensitivity of the Hydrogen-Oxygen System*. Combustion and Flame, vol. 48, pp. 149-161, 1982.
- [85] M. Frenklach and K. Kailasnath. *Systematic Development of Reduced Reaction Mechanisms for Dynamic Modeling*. AIAA , New York, pp. 365-376, 1986.
- [86] S. Yungsterand M. Rabinowitz. *Computation of Shocked Induced Combustion Using a Detailed Methane Air Mechanism*. Journal of Propulsion and Power, vol. 10, no. 5, pp. 609-617, 1994.
- [87] H. Wang and M. Frenklach. *Detailed Reduction of Reaction Mechanism for Flame Modeling*. Combustion and Flame, vol.87, no. 3, 1991.
- [88] N. Adams. *Script of Lecture of Applied CFD, TU Munich*. WS 15/16.

- [89] N. Adams. *Script of Lecture Numerical Calculation Methods of Turbulent Flows, TU Munich.* WS 16/17.
- [90] O. J. Haidn. *Script of Lecture Raumfahrtantriebe 2, TU Munich.* SS 16.
- [91] G. Mortimer and H. Eyring. *Elementary transition state theory of the soret and dufour effect.* Proceeding National Academy of Science, vol. 77, no. 4, pp. 1728-1731, 1980.
- [92] B. Bird and W. Stewart. *Transport Phenomena.* John Wiley and Sons, New York, 1960.
- [93] V. P. Zhukov and M. Paetz. *On thermal conductivity of gas mixtures containing hydrogen.* Heat and Mass Transfer, vol. 52, no. 12, 2016.
- [94] G. Dixon-Lewis and R. Kee. *A Fortran Computer Code Package for the Evaluation of Gas-Phase, Multicomponent Transport Properties.* Proceedings of the Royal Society, 1986.
- [95] R. J. Kee et al. *CHEMKIN 10112.* Reaction Design, San Diego, 2011.
- [96] L. Monchick and E. Mason. *Transport Properties of Polar Gases.* The Journal of Chemical Physics, vol. 35, pp. 1675-1679, 1961.
- [97] J. Warnatz. *Numerical Methods in Flame Propagation.* Notes on Numerical Fluid Mechanics, vol. 6, Vieweg, Braunschweig, 1982.
- [98] D. Goodwin. *Cantera workshop One Dimensional Flames.* California Institute of Technology: Division of Engineering and Applied Science, 2004.
- [99] G. Rozenchan and L. Zhu. *Outward Propagation, Burning Velocities, and Chemical Effects of Methane Flames Up to 60 atm.* Proceedings of the Combustion Institute, Volume 29, pp. 1461-1469, 2002.
- [100] E. Petersen and D. Davidson. *Ignition Delay Times of Ram Accelerator CH₄/O₂/ Diluent Mixtures.* Combustion and Flame, vol. 177, pp. 272-290, 1999.
- [101] G. Rozenchan and D. Zhu. *Outward Propagation, Burning Velocities, and Chemical Effects of Methane Flames Up to 60 atm.* Proceedings of the Combustion Institute, vol. 29, pp. 1461-1469, 2002.
- [102] M. Sanchez. *script of lecture Rocket Propulsion.* Massachusetts Institute of Technology, 2005.
- [103] M. Burke and M. Chaos. *Comprehensive H₂/O₂ kinetic model for high-pressure combustion.* International Journal of Chemical Kinetics, 2011.
- [104] G. Hagemann and G. Kruelle. *Numerical Flowfield Analysis of the Next Generation Vulcain Nozzle.* Journal of Propulsion and Power, 1996.